Stability analysis of channel flow laden with small particles

by

Joy Klinkenberg

October 2011
Technical Reports from
Royal Institute of Technology
Department of Mechanics
SE-100 44 Stockholm, Sweden

Akademisk avhandling som med tillstånd av Kungliga Tekniska Högskolan i Stockholm framlägges till offentlig granskning för avläggande av teknologie licentiatexamen fredagen den 7 oktober 2011 kl 10.15 i M2, Kungliga Tekniska Högskolan, Brinellvägen 64, Stockholm.

Universitetsservice US–AB, Stockholm 2011

Stability analysis of channel flow laden with small particles

Joy Klinkenberg
Linné FLOW Centre, KTH Mechanics, Royal Institute of Technology
SE-100 44 Stockholm, Sweden

Abstract

This thesis deals with the stability of particle laden flows. Both modal and non-modal linear analyses have been performed on two-way coupled particle-laden flows, where particles are considered spherical, solid and either heavy or light. When heavy particles are considered, only Stokes drag is used as interaction term. Light particles cannot be modeled with Stokes drag alone, therefore added mass and fluid acceleration are used as additional interaction forces.
The modal analysis investigates the asymptotic behavior of disturbances on a base flow, in this thesis a pressure-driven plane channel flow. A critical Reynolds number is found for particle laden flows: heavy particles increase the critical Reynolds number compared to a clean fluid, when particles are not too small or too large. Neutrally buoyant particles, on the other hand, have no influence on the critical Reynolds number.
Non-modal analysis investigates the transient growth of disturbances, before the subsequent exponential behavior takes over. We investigate the kinetic energy growth of a disturbance, which can grow two to three orders of magnitude for clean fluid channel flows. This transient growth is usually the phenomenon that causes transition to turbulence: the energy can grow such that secondary instabilities and turbulence occurs. The total kinetic energy of a flow increases when particles are added to the flow as a function of the particle mass fraction. But instead of only investigating the total energy growth, the non-modal analysis is expanded such that we can differentiate between fluid and particle energy growth. When only the fluid is considered in a particle-laden flow, the transient growth is equal to the transient growth of a clean fluid.
Besides thes Stokes drag, added mass and fluid acceleration, this thesis also discusses the influence of the Basset history term. This term is often neglected in stability analyses due to its arguably weak effect, but also due to difficulties in implementation. To implement the term correctly, the history of the particle has to be known. To overcome this and obtain a tractable problem, the square root in the history term is approximated by an exponential. It is found that the history force as a small effect on the transient growth.
Finally, Direct numerical simulations are performed for flows with heavy particles to investigate the influence of particles on secondary instabilities. The threshold energy for two routes to turbulence is considered to investigate whether the threshold energy changes when particles are included. We show that particles influence secondary instabilities and particles may delay transition.

Descriptors: Transition, modal analysis, non-modal analysis, direct numerical simulations, multi-phase flow, particle-laden, heavy particles, light particles

Preface

This thesis considers particle-laden flows. The first part introduces the particle-laden flows: which models are used and what are the simplifications made in the analysis. Furthermore, both modal and non-modal analysis are presented and their usage with particle-laden flows. Also secondary instabilities are discussed, using results of direct numerical simulations.
The second part contains the following papers.

Paper 1. Joy Klinkenberg, H.C. de Lange and Luca Brandt, 2011
Modal and non-modal stability of particle-laden channel flow,
Physics of Fluids. **23**, 064110 (2011)

Paper 2. Joy Klinkenberg, H.C. de Lange and Luca Brandt, 2011
Modal and non-modal stability analysis of a channel flow seeded with light particles,
submitted to European Journal of Mechanics B/Fluids

Paper 3. Joy Klinkenberg, G. Sardina, H.C. de Lange and Luca Brandt, 2011
Numerical Simulations of laminar-turbulent transition in particle-laden channel flow
Internal report

Division of work between authors
The main advisors of the project are Rick de Lange (RdL) at the Mechanical engineering Department at Technische Universiteit Eindhoven (TU/e), section Energy Technology and Luca Brandt (LB) at KTH Mechanics. The project is a joint project between TU/e and KTH.

Paper 1
The analyses have been performed by Joy Klinkenberg (JK) as well as the writing, with help from LB and RdL. LB provided the initial code that JK extended with the inclusion of particle equations.

Paper 2
JK has done both the analyses and the writing. Both LB and RdL helped with reading, giving comments and structuring the paper.

Paper 3
Gaetano Sardina (GS) and LB provided the numerical code and set up the numerical experiments. JK has done the simulations and writing. LB, RdL and GS read the paper, they gave comments about contents and structure.

Contents

Part I

Introduction

CHAPTER 1

Introduction

Particle laden flows are an important type of flow since many flows contain particles. Examples of such flows are soot in a gas flow or sand in the atmosphere. Because such flows are common, many efforts have been made to better understand the behavior of particles in (turbulent) flow, recent reviews are written by Toschi & Bodenschatz (2009) and Balachandar & Eaton (2009). For turbulent flows, it has been found that adding dust to a turbulent pipe flow reduces drag already in the early '60s by Sproull (1961). Drag reduction is a major issue in increasing the efficiency of fluid transport since it helps minimizing energy losses. Therefore a lot of research is devoted to drag reduction in turbulent flows. Recently, Zhao *et al.* (2010) found numerically that inclusion of small and heavy particles reduces drag. Light particles have been experimentally investigated by McCormick & Bhattacharyya (1973) and Jacob *et al.* (2010) to cite only two. They also found drag reduction for particle laden flows with light particles. Micro bubbles, which can be modeled as rigid spheres when they are small enough, have been numerically investigated by both Ferrante & Elghobashi (2003) and Xu *et al.* (2002) for a turbulent flow. They found that rigid micro-bubbles reduce the drag as well.

Sproull (1961) explains the drag reduction by a reduction of the viscosity of a dusty gas with as much as 40%. Saffman (1962) proposed that dust particles dampens the turbulence structures due to a larger inertia of a dust particle compared to a fluid particle. He also proposes that drag reduction in particle laden flows can be investigated by looking at laminar-turbulent transition. An explanation is that the particle-fluid interaction also dampens the growth of disturbances which might lead to turbulence. Turbulent flow enhances drag and thus, if turbulence is delayed, particles reduce drag.
To investigate the onset of turbulence, a transitional flow has to be considered. To describe such a flow, a laminar flow is considered first. If small, linear, disturbances are added to this laminar flow, these disturbances can either decay or grow in time and space. When the disturbances are damped, the flow stays laminar. When disturbances grow in energy, the disturbances can grow such that secondary (non-linear) effects become important. These secondary effects in turn can lead to a turbulent flow. The transitional flow is the flow state which is neither fully laminar, nor turbulent.
The onset of transition is historically investigated using linear stability analysis.

A perturbation in the form $q = \hat{q}(y)exp(\alpha x - i\omega t)$, with streamwise wavenumber (α) and complex frequency ($\omega = \omega_r + i\omega_i$) is added to a linearized set of equations and the eigenvalues are investigated. These eigenvalues indicate whether perturbations will either grow or decay. A critical Reynolds number exists, above which a flow is unconditionally unstable. Note that this method is suitable to investigate whether the flow is stable for an infinite amount of time, independent of the disturbance amplitude. This method is called modal stability analysis.
The next step is the non-modal analysis. Non-modal analysis is used to investigate short-term behavior of disturbances as opposed to the modal analysis. Some disturbances can grow, before the subsequent exponential behavior becomes the dominant feature (Ellingsen & Palm 1975; Trefethen *et al.* 1993; Reddy & Henningson 1993; Schmid & Henningson 2001*a*). It is found that when modal analysis shows that all eigenmodes are damped, it is possible for some disturbances to grow in a finite amount of time. For a clean fluid channel flow some disturbance energies can grow as much as two to three orders of magnitude. When the initial perturbation is large enough, the energy can grow such that non-linear effects become important and breakdown of the disturbances might occur, which in turn leads to turbulence. The non-modal analysis is used to determine the largest possible energy growth of disturbances in particle-laden flows. The optimal growth of a particle-laden flow is therefore compared to the results of a clean fluid.
The last step performed is the investigation of transition beyond the initial linear disturbances, using Direct Numerical Simulations. Two paths to turbulence are analysed, as defined in Reddy *et al.* (1998*a*). For these paths, the threshold energy is investigated. Above this threshold flows becomes turbulent and below the threshold the flow relaminarizes. We performed numerical simulations with particles and investigated whether this transition threshold shifts. If the threshold shifts to larger amplitudes, the flow has become more stable and vice versa.

Saffman (1962) and Michael (1964) found that heavy particles increase the critical Reynolds number for linear stability, when the particles meet certain criteria: e.g. the particle should not be too small. The equations used by Saffman (1962) are the Navier Stokes equations extended with one extra term, the Stokes drag, which accounts for the coupling between particles and fluid. A two-way coupling model is defined, with a convection equation for the particles including the Stokes drag as interaction term, acting as dissipation. This model is valid for heavy particles only. An extended model for particle laden flows is given by Maxey & Riley (1983): added mass, fluid acceleration, Basset history term and gravity are also modeled. The added mass (or virtual mass) term exists because an accelerating or decelerating particle also accelerates/decelerates fluid from the surroundings. The added mass is therefore modeled as extra fluid moving with the particle, as if the particle were a bit larger, hence the name added mass. The fluid acceleration term, also known

as the pressure correction force, models the pressure of the undisturbed flow. The Basset history term takes the history of the particle into account: the movement of particles depends also on the history of those particles due to the development of a boundary layer on the particles.
For a particle laden flow with heavy particles, only Stokes drag is used. When light particles are considered, particles which have almost equal density as the surrounding fluid, added mass and fluid acceleration term are also considered. The Basset history term is usually not taken into account, for both heavy and light particles. This term might be relevant and is therefore also discussed. Because the history term is not explained in the papers and no results are shown in any of the papers, the Basset history term is explained and discussed in part I. Also, the results including the history term are presented in this part of the thesis.

The aim of the research presented in this thesis is to investigate whether hard, spherical particles affect transition. Both the initial linear stages using stability analysis and the secondary instabilities by means of direct numerical simulations are investigated.
In the following chapter the governing equations are presented and the different interaction terms are shown. An implementation of the the Basset history term is given as well. Chapter 2 also deals with the stability analysis and the implementation of modal and non-modal analysis. Main results from the papers are presented in chapter 3, in which also results from the implementation of the Basset history force are shown. Chapter 4 deals with the numerical simulations. The method is explained and some results are given. In the last chapter some conclusions are presented and an outlook is given for the work that will be performed in the final part of the project.

CHAPTER 2

Theoretical Model

2.1. Particle-Fluid Coupling

To model particle-laden flows, a coupling between the particles and fluid is needed. Three coupling models are used in literature: one-way, two-way and four-way coupling. Figure 2.1 shows the three regimes for turbulent flows with the volume fraction of particles on the horizontal axis and the relative timescale on the vertical axis (Elghobashi 1994). The timescale τ_p is the particle response time, τ_K the Kolmogorov time scale and τ_e the turnover time of large eddy. The Kolmogorov timescale is important in turbulent flows, but not in transitional flow, because transitional flow does not have any turbulent timescales. The turnover time of large eddy is important in transitional flows.
If the particle volume is small, $\Phi < 10^{-6}$, the particles can be modeled through one-way coupling. Particle motion is influenced by the fluid. When the particle volume increases, $10^{-6} < \Phi < 10^{-3}$, a two-way coupling model is sufficient. In this model, the particles also influence the fluid. For an even larger particle volume, $\Phi > 10^{-3}$, a four-way coupling model should be used. In addition to the particle-fluid and fluid-particle interactions, also particle-particle interactions (collisions) are modeled. One should remember that these results are valid for turbulent flows and that we work with laminar flows. Laminar flows might have different bounds on the volume fraction, because the flow is ordered and less chaotic.
The model used throughout this paper is the two-way coupling model.

2.2. Governing Equations

The equations used to model a particle laden flow are described and we explain which interaction terms are present between the flow and particles and how these interaction terms are modeled.

The particle equation described by Maxey & Riley (1983) is the starting point. In the Lagrangian framework the motion of a particle u_{p_i} in a Newtonian fluid

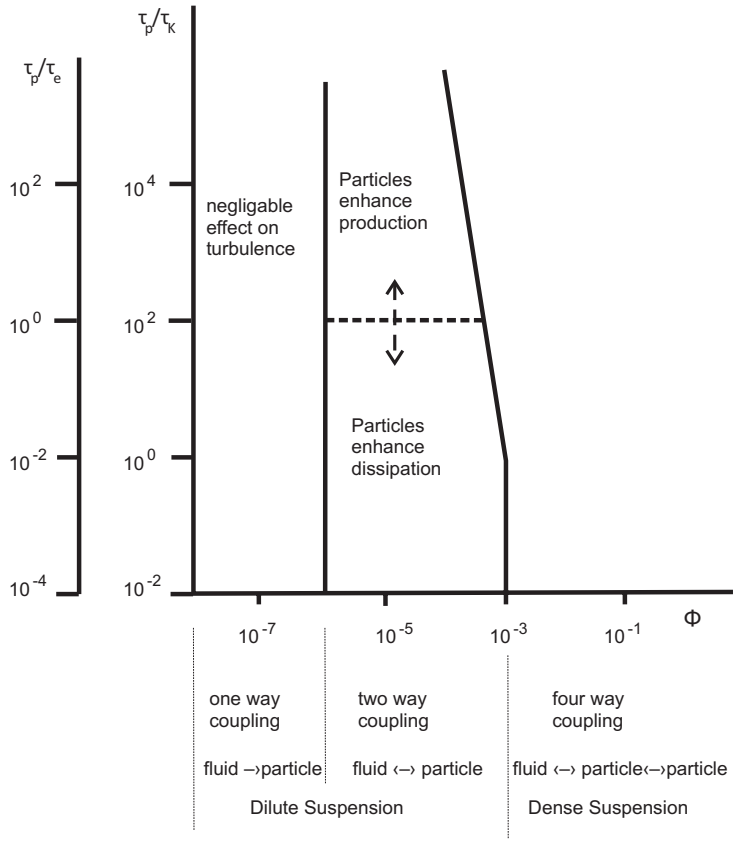

Figure 2.1: A schematic overview of the coupling models used in turbulent flows.

with radius r with its centre at $Y(t)$, particle mass m_p, fluid mass m_f obeys

$$m_p \frac{du_{p_i}}{dt} = m_f \frac{Du_i}{Dt}|_{Y(t)} + \frac{1}{2} m_f \left(\frac{Du_i}{Dt}|_{Y(t)} - \frac{du_{p_i}}{dt} \right) + 6\pi r \mu \left(u_i[Y(t), t] - u_{p_i} \right) + 6\pi r^2 \mu \int_{-\infty}^{t} d\tau \frac{d/d\tau \{u_{p_i}(\tau) - u_i[Y(\tau), \tau]\}}{[\pi \nu (t-\tau)]^{1/2}} + (m_p - m_f) g_i. \tag{2.1}$$

With u_i the fluid velocity, μ the fluid viscosity and g_i the gravitational force. The term d/dt is used for the time derivative following the moving particle, while D/Dt is used for the time derivative following a fluid element. The terms on the right hand side are: the fluid acceleration term, added mass, Stokes drag, the Basset history term and the gravitational force. The fluid acceleration term comes from the undisturbed flow, which is assumed incompressible

Table 2.1: Definition of the non-dimensional numbers used.

ξ	$\frac{\rho_f}{\rho_p}$	Density ratio
f	$\frac{\Phi}{\xi} = \frac{m_p}{m_f}$	Mass fraction
R	$\frac{\rho_f U L}{\mu}$	Reynolds number
S	$\frac{\nu\tau}{L^2} = \frac{2}{9}\frac{r^2}{L^2}\frac{\rho_p}{\rho_f}$	Relaxation time
SR	$\frac{U\tau}{L}$	Stokes number
Φ	$\frac{N_0 \frac{4}{3}\pi r^3}{L^3}$	Volume fraction

and where the term $\nu\nabla^2 u_i$ is neglected. As for the added mass term, it can be seen why it is called like this. If the d/dt term is put on the left hand side, we get: $\left(m_p + \frac{1}{2}m_f\right)\frac{du_{p_i}}{dt}$. Thus a virtual mass, half the mass of the fluid, has been added to the system. The Basset history term takes the development of a boundary layer on the particle into account. The Stokes drag is a drag force induced by the velocity difference between the particle and the fluid.

Stability analysis cannot be performed in the Lagrangian framework, therefore equation 2.1 is rewritten into the Eulerian framework. The Eulerian framework is a valid assumption under the condition that particles are homogeneously distributed.
We consider plane channel flow with a homogeneous particle distribution. In the following, every term is made non-dimensional with the channel half-width L, to be consistent with a clean fluid channel flow, centerline velocity U, fluid density ρ_f and the fluid viscosity μ. The dimensionless numbers used in the equations are defined in Table 2.1, where ρ_p is the particle density, r the particle radius and N_0 the number of particles present in the flow.

The particle momentum equation rewritten into a Eulerian framework reads:

$$\frac{du_{p_i}}{dt} = \xi\frac{Du_i}{Dt} - \frac{1}{2}\xi\left[\frac{du_{p_i}}{dt} - \frac{Du_i}{Dt}\right] + \frac{1}{SR}\left(u_i - u_{p_i}\right). \tag{2.2}$$

The counterpart, the momentum equation for the fluid can be written as

$$\frac{Du_i}{Dt} = -\frac{\partial p}{\partial x_i} + \frac{1}{R}\frac{\partial^2 u_i}{\partial x_j^2} - f\xi\frac{Du_i}{Dt} - \frac{1}{2}f\xi\left[\frac{Du_i}{Dt} - \frac{du_{p_i}}{dt}\right] + \frac{f}{SR}\left(u_{p_i} - u_i\right). \tag{2.3}$$

Two forces described by Maxey & Riley (1983) are discarded here: gravity and the Basset history term. The Basset history term will be discussed later on in more detail. We assume that sedimentation effects do not occur on the timescale we are interested in, therefore gravity is neglected.
The Stokes drag describes the drag force between the fluid and particle velocity, using Stokes number SR. The Stokes drag number consists of two other dimensionless numbers. The Reynolds number R and the particle relaxation

time S. The smaller SR becomes, the smaller the relaxation time and the faster a particle adjusts to the fluid velocity.
Looking closely at these equations one can distinguish two extremes: heavy particles ($\xi \ll 1$) and light particles ($\xi \sim 1$). When heavy particles are considered, the added mass and fluid acceleration terms can be neglected and only Stokes drag remains.

For a full system of equations, we also need the conservation of mass for particles and fluid:

$$\frac{\partial f}{\partial t} = -\frac{\partial}{\partial x_i}(f u_{p_i}) \tag{2.4}$$

$$\frac{\partial u_i}{\partial x_i} = 0 \tag{2.5}$$

Combining these equations with the conservation of momentum and linearizing, we get the following linearized Navier-Stokes equations:

$$\frac{\partial u_i}{\partial t} = -\frac{\partial p}{\partial x_i} - U_j \frac{\partial u_i}{\partial x_j} - u_j \frac{\partial U_i}{\partial x_j} + \frac{1}{SR}\frac{\partial^2 u_i}{\partial x_j^2} + \frac{f}{SR}(u_{p_i} - u_i) + AM_f + FA_f \tag{2.6}$$

$$\frac{\partial u_{p_i}}{\partial t} = -U_j \frac{\partial u_{p_i}}{\partial x_j} - u_{p_j}\frac{\partial U_i}{\partial x_j} + \frac{1}{SR}(u_i - u_{p_i}) + AM_p + FA_p \tag{2.7}$$

$$\frac{\partial f'}{\partial t} = -\frac{\partial}{\partial x_i}(f' U_i + f u_{p_i}) \tag{2.8}$$

$$\frac{\partial u_i}{\partial x_i} = 0. \tag{2.9}$$

With U_i the base velocity and u_i the perturbation velocity and AM and FA the Added Mass and Fluid Acceleration, with subscripts f and p, denoting fluid and particle respectively:

$$\begin{aligned} AM_f &= -\frac{1}{2} f\xi \left(\frac{\partial u_i}{\partial t} + U_j \frac{\partial u_i}{\partial x_j} + u_j \frac{\partial U_i}{\partial x_j} - \frac{\partial u_{p_i}}{\partial t} - U_j \frac{\partial u_{p_i}}{\partial x_j} - u_{p_j}\frac{\partial U_i}{\partial x_j} \right) = \\ &= -\frac{1}{2} f\xi \left(\frac{\partial}{\partial t}(u_i - u_{p_i}) + U_j \frac{\partial}{\partial x_j}(u_i - u_{p_i}) + (u_i - u_{p_i})\frac{\partial U_i}{\partial x_j} \right), \end{aligned} \tag{2.10}$$

$$FA_f = -f\xi \left(\frac{\partial u_i}{\partial t} + U_j \frac{\partial u_i}{\partial x_j} + u_j \frac{\partial U_i}{\partial x_j} \right), \tag{2.11}$$

$$AM_p = -\frac{AM_f}{f}, \tag{2.12}$$

$$FA_p = -\frac{FA_f}{f}. \tag{2.13}$$

The boundary conditions are assumed $u_i = u_{p_i} = 0$ at the walls.
Note that the particle mass conservation is decoupled from the system and can therefore be computed a posteriori.

To perform stability analysis the system is rewritten into an Orr-Sommerfeld-Squire system. The details of the derivations can be found in Part II of this thesis.

2.2.1. *Energy Analysis for Heavy Particles*

For heavy particles it can be shown that when the velocities of particles and fluid are different, this *always* results in a loss in energy in channel flow. The energy equation can be derived by multiplying equation 2.6 with u_i and 2.7 with u_{p_i} and add them using the mass fraction f for the particle momentum equation:

$$\begin{aligned}\frac{\partial E_v}{\partial t} = &-\int_V u_i u_j \frac{\partial U_i}{\partial x_j} dV - \frac{1}{Re}\int_V \frac{\partial u_i}{\partial x_j}\frac{\partial u_i}{\partial x_j} dV \\ &- f\int_V u_{p_i} u_{p_j} \frac{\partial U_i}{\partial x_j} dV - \frac{f}{SR}\int_V \left(u_i - u_{p_i}\right)^2 dV,\end{aligned} \tag{2.14}$$

where the divergence terms disappear owing to periodic boundary conditions and zero velocity at the walls. It is clear from the last term on the right hand side that a velocity difference always induces a loss in energy.

2.3. Basset History Term

The Basset history term has not been used in any of the papers in part II, because the implementation is a recent development. The history term is different than the terms discussed so far. For this term, the total history of the fluid and particle flow has to be known. For Direct Numerical Simulations this is expensive and therefore the total history is usually not taken into account, but only the recent history. Sometimes a model for large times is used(van Hinsberg *et al.* 2011). For stability analysis the intergal in the term is also difficult. Therefore the integral is rewritten into a system which can be implemented in stability analysis.
The Basset history term can be written as convolution:

$$\bar{q}(t) = \frac{1}{Sb}\cdot\int_{-\infty}^{t} d\tau \frac{d/d\tau\{u_{p_i} - u_i\}}{[t-\tau]^{1/2}} = \frac{1}{Sb}\cdot\int_{-\infty}^{t} F(t-\tau)q(\tau)d\tau, \tag{2.15}$$

where we have to approximate $\int_{-\infty}^{t} F(t-\tau)d\tau$ for implementation of this effect in the stability analysis.
The approximation is done using an exponential, because if we have an exponential filter:

$$\bar{q}(t) = \int_{-\infty}^{t} Cexp\left(-\frac{t-\tau}{\Delta}\right) q(\tau)d\tau, \tag{2.16}$$

we can get the differential form:

$$\frac{d\bar{q}(t)}{dt} = Cq - \frac{\bar{q}}{\Delta} \tag{2.17}$$

If we can approximate the history term with an exponential, we are able to solve an eigenvalue problem similar to the case without Basset history term,

but extended with three extra equations for $\bar{q}_i$, similar to equation 2.17 but in all three directions. Sb is a new dimensionless number, similar to the Stokes number SR, but typically larger.

Now we have to approximate the square root dependence of the Basset term into an exponential. Figure 2.2 shows the difficulty with the approximation: either the exponential is more accurate for small times, or for larger times. Several combinations of C and Δ should be tried to investigate whether any combination changes the critical Reynolds number or the transient energy growth.

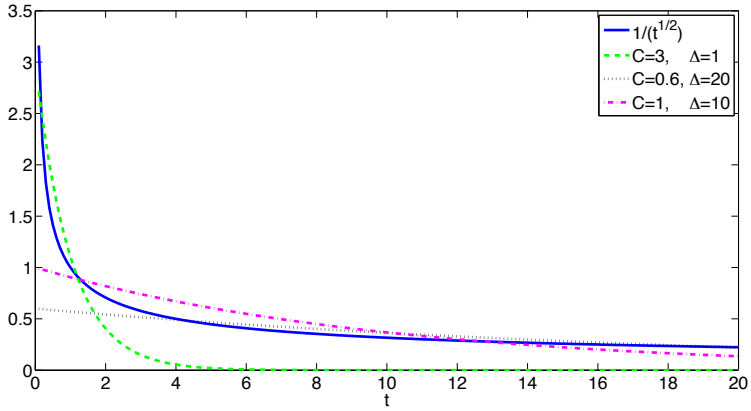

Figure 2.2: The approximation of a $1/\sqrt{(t)}$ by an exponential in the form $C\exp(-t/\Delta)$

2.4. Stability

Both modal and non-modal stability analyses are performed. Modal stability is classical in hydrodynamic stability, where the critical Reynolds number is computed. Below this Reynolds number all disturbances are exponentially damped. At larger Reynolds numbers on the other hand, disturbances exist which exponentially grow. Although this is a very useful tool for predicting transition, it is known that at smaller Reynolds numbers transition to turbulence occurs, due to transient effects. The growth of a perturbation for a limited time, before the exponential modal behavior is most dominant, can induce secondary instabilities and transition to turbulence. The initial growth in energy is investigated using the non-modal analysis.

2.4.1. *Modal analysis*

To study linear stability, we assume wave-like perturbations in the following form:

$$q = \hat{q}(y)e^{i(\alpha x+\beta z-\omega t)},$$

Neglecting the Basset history term for now, $q = (v, \eta, u_p, v_p, w_p)^T$ when the linearized equations are written into an Orr-Sommerfeld-Squire system. In the expression above, α and β define the streamwise and spanwise wavenumber of the perturbation respectively, $\omega = \omega_r + i\omega_i$ is a complex frequency. The temporal problem is considered: when $\omega_i > 0$, the perturbation grows exponentially in time. When $\omega_i) < 0$, the disturbance decays asymptotically. When all complex frequencies have an imaginary part smaller than zero, the flow is stable. The point where $\omega_i = 0$, is called neutrally stable. When computing ω_i in a range of wavenumbers α and Reynolds numbers, a neutral stability curve is obtained. This curve defines the range where exponentially unstable waves can be found.
The neutral stability curve can be computed assuming two-dimensional perturbations, since a modified version of Squire's theorem holds for the modified Orr-Sommerfeld equation (Saffman 1962; Boronin 2008). Squire's theorem states that for every three dimensional disturbance an equivalent two dimensional disturbance exists at smaller Reynolds number (Squire 1933).

2.4.2. *Non-modal analysis*

Non-modal analysis determines the largest possible growth of a perturbation in a finite time interval, also called optimal growth. The initial disturbance yielding optimal growth is called an optimal initial condition.

The governing linear equations can be written in compact form as:

$$\frac{\partial q}{\partial t} = Lq. \tag{2.18}$$

The largest possible growth at time t is the norm of the evolution operator, or propagator, $\mathcal{T} = \exp(tL)$. This propagator takes any initial condition from $t = 0$ to a specified final time t. The maximum amplification is defined as:

$$\max_{q_0} \frac{||q||}{||q_0||} = \max_{q_0} \frac{||\exp(tL)q_0||}{||q_0||} = ||exp(tL)|| \equiv G(t). \tag{2.19}$$

The norm used should be relevant to the problem, therefore the kinetic energy is used.

$$E_{kin} = \frac{1}{2}\left(m_f u_i^2 + m_p u_{p_i}^2\right), \tag{2.20}$$

with m_f and m_p the mass of the fluid and the particles respectively.
A matrix M can be constructed to compute the kinetic energy. This matrix M is applied directly to the vector $q = [v, \eta, u_p, v_p, w_p]^T$ when the full system

is investigated. The kinetic energy integrated over the volume V is

$$E(t) = \frac{1}{2}\int_{\Omega} q^H M q dV. \tag{2.21}$$

With this definition the optimal growth is defined as the 2-norm of a modified propagator, see Schmid & Henningson (2001*b*) and below.
Not only optimisation of the total energy is interesting, but also the investigation of the optimal growth when perturbing only the fluid or particle velocity. In this case, we do not consider the total kinetic energy of the system, but only a part of it, depending on the initial condition and final state chosen. This separation can be achieved by including either fluid or particle energy when computing the optimal growth. The optimisation can be written as

$$\begin{aligned} G(t) &= \frac{||q_{out}(t)||_{E_{out}}}{||q_{in}(0)||_{E_{in}}} = \frac{||\mathcal{T} q_{in}(0)||_{E_{out}}}{||q_{in}(0)||_{E_{in}}} = \frac{||F_{out}\mathcal{T} q_{in}(0)||_2}{||F_{in} q_{in}(0)||_2} = \\ &= \frac{||F_{out}\mathcal{T} F_{in}^{-1} F_{in} q_{in}(0)||_2}{||F_{in} q_{in}(0)||_2} = ||F_{out}\mathcal{T} F_{in}^{-1}||_2. = ||F_{out} C \exp(tL) B F_{in}^{-1}||_2 \end{aligned} \tag{2.22}$$

where F is the Cholesky factorisation of $M = FF^H$.
Here, propagator $\mathcal{T} = C\exp(tL)B$ is rewritten to include input and output operators. The input is $q_{in} = Bq$, while $q_{out} = Cq$ is the output we are interested in. The energy norm must be separated likewise, $M_{in} = F_{in}F_{in}^H$ is applied to q_{in} to measure the input energy while $M_{out} = F_{out}F_{out}^H$ gives the output energy. In the classic non-modal analysis the following applies: $F_{in} = F_{out}$ and $C = B = I$.

2.4.3. *Numerical method*

For the stability computations presented here, the discretization in y-direction of the equations is done using the Chebyshev collocation method. (Reddy *et al.* 1998*b*) Most computations are performed using $n_y = 37$, with n_y the number of collocation points.
For the transient growth computation, we make use of the following energy matrix M (excluding the Basset history term):

$$M = \begin{pmatrix} \left(-\frac{D^2}{k^2} + 1\right) I_w & 0 & 0 & 0 & 0 \\ 0 & \frac{1}{k^2} I_w & 0 & 0 & 0 \\ 0 & 0 & f I_w & 0 & 0 \\ 0 & 0 & 0 & f I_w & 0 \\ 0 & 0 & 0 & 0 & f I_w \end{pmatrix}. \tag{2.23}$$

In the expression above, I_w is the diagonal matrix performing spectral integration in y direction. This matrix can be easily factorized using a singular value

decomposition (SVD): $M = U\Sigma U^H = FF^H$.

When implementing the Basset history term in addition to all other terms, the system is a bit more complicated. The total system then consists of not only fluid and particle velocities, u_i, u_{p_i}, but it includes $\bar{q}_i$, extra terms for the inclusion of the Basset history. The energy computation needed for non-modal analysis is done using the same method of separation as explained previously where only fluid or particles are perturbed.

CHAPTER 3

Stability analysis results

Some results are given in this chapter. More results are reported in Part II, the papers. In part II, the Basset history term is not discussed, therefore the last section in this chapter presents new results using the Basset history term.

3.1. Modal analysis

The modal analysis for heavy particles was already performed by Rudyak *et al.* (1997). For light particles on the other hand, where added mass and fluid acceleration are also important, no results could be found in literature. The main results are the critical Reynolds number as a function of Stokes number and are given in Figure 3.1(a) for several density ratios and a mass fraction of $f = 0.1$. Three regimes can be identified in the figure: small Stokes number, large Stokes number and intermediate values. When the Stokes number is small, particles are also small and have a small relaxation time. The particles react very fast to flow changes. This means that the particles only act as passive tracers in the flow and we call this limit the Lagrangian limit. When the Stokes number is very large, particles are big; too big even to have an influence on the fluid. The relaxation time is such that it takes long time to adjust to the flow. We call this limit the ballistic limit. These limits can be seen in Figure 3.1(a) on the left (Lagrangian limit) and on the right (Ballistic limit). The particles have no influence on the flow stability in these regions. They only result in an effective increase in density of the total flow, for which a modified Reynolds number R_m can be defined:

$$R_m = \frac{(1+f)\,\rho U L}{\mu}.$$

In between the two limits, at moderate Stokes numbers, the particles do have an influence on the stability.
The results for heavy particles are obtained using Stokes drag only as interaction term and are equal to results obtained by Rudyak *et al.* (1997). What is apparent in Figure 3.1(a) is that the lighter the particle, the lower the critical Reynolds number is. Heavy particles obtain the largest critical Reynolds number and this Reynolds number is larger than the critical Reynolds number of a clean fluid flow. When the particles are lighter than the fluid ($\xi > 1$), the critical Reynolds number decreases compared to clean fluid. Neutrally buoyant

particles have no influence, except for a factor of $(1 + f)$, corresponding to an increase in density of the total system. The results show that for a density ratio of $\xi < 1$, the critical Reynolds number increases and therefore the flow is stabilized.

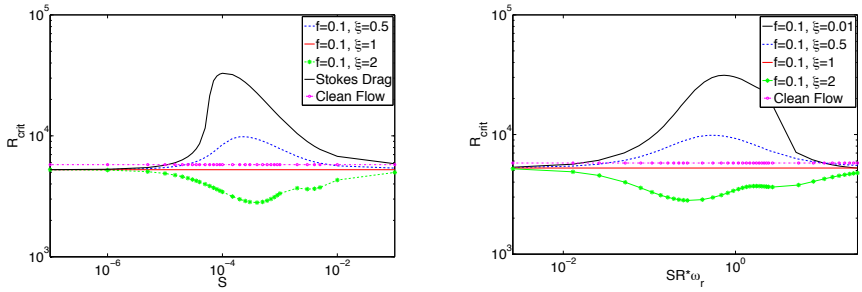

Figure 3.1: Modal analysis for heavy particles (Stokes drag only) and for light particles. Critical Reynolds number as a function of S (left) and $SR\omega_r$ (right)

Instead of investigating the critical Reynolds number as a function of Stokes number, another dimensionless number can be introduced. The Stokes number is a dimensionless scale for the particle relaxation time, which can be related to the time scale of a perturbation. For modal analysis, the time scale of the perturbation is the period of the wave, so we multiply the Stokes number with the frequency of the perturbation. We call this number the stability Stokes number, $SR\omega_r$. Around $SR\omega_r = 1$ the critical Reynolds number is influenced most, Figure 3.1(b). Thus, the particles influence the flow most when the disturbance time is of the same order as the relaxation time.
In the analysis it is important to check the assumptions which have been made. For turbulent flows the two-way coupling model is valid for volume fractions smaller than $\Phi = 10^{-3}$ (Elghobashi 1994). The volume fraction can be written as $\Phi = f\xi$, thus $f\xi < 10^{-3}$. This means that, if we want a valid two-way coupling assumption when we have neutrally buoyant particles, the largest mass fraction with a valid assumption is $f = 0.001$. This is clearly a much smaller mass fraction than the value of f used. But, the assumption by Elghobashi (1994) is true for a turbulent flow and we consider a laminar flow. Because particles have the same base velocity as the fluid and particles are homogeneously distributed, the limit for Φ might be stretched to larger volume fractions.

3.2. Non-modal analysis

A non-modal analysis has been carried out and the optimal growth as a function of spanwise wavenumber β is given in Figure 3.2(a). Here, $fluid \rightarrow fluid$ denotes the system where the fluid has been perturbed and the energy of the

fluid is optimised. $all \rightarrow all$ is the case where the total system is perturbed and the energy of the total system is optimised.
It can be seen that no matter whether added mass and fluid acceleration are taken into account, the growth stays basically the same. For the total system, the energy is increased by $(1+f)^2$. This is, again, the result of an increase in density as shown in the modal analysis. The only difference now, is that this is also valid for larger Stokes numbers and not only at small Stokes numbers. This indicates that the time needed to adjust to the flow (defined using the Stokes number) is less than the time needed for the energy to grow, i.e. the particles still basically act as passive tracers in non-modal analysis.
This finding can also be analyzed using the stability Stokes number. Now, we

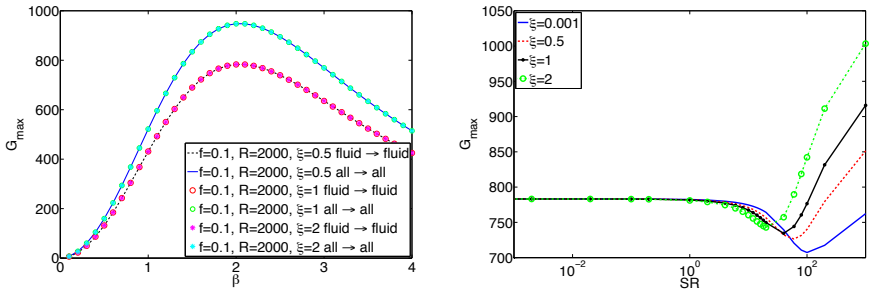

(a) $SR = 1 \cdot 10^{-3}$ (b) $R = 2000$

Figure 3.2: Non-modal analysis of a flow with light particles. (a) $fluid \rightarrow fluid$ equals the clean fluid flow, while $all \rightarrow all$ is larger than a clean fluid flow with a factor of $(1+f)^2$. (b) Optimal growth of $fluid \rightarrow fluid$ as function of SR for heavy ($\xi = 0.001$) and light particles.

do not have a frequency as timescale for the perturbation, but we do have the time needed to reach optimal growth. The time to reach maximum growth is in the order of 100. Thus, the non-modal growth is too slow to be influenced by the particles. This can also be seen in Figure 3.2(b), where we see that at large values of SR the optimal growth is influenced most at SR in the order of 100. But, as already explained in the modal analysis, the volume fraction of light particles can be such that the two-way coupling model is not valid, because particle collisions become more important.

3.3. Basset history term

For heavy particles, only a small difference is found when the history term is used, Figure 3.3(a): The critical Reynolds number is decreased a few percent using $C = 3, \Delta = 1$. In non-modal analysis, Figure 3.3(b), hardly anything changes for all filter parameters investigated. This could be expected due to

the definition of SR and Sb. Sb is $\frac{L\pi^{1/2}}{rR^{1/2}}$ times larger than the Stokes number, thus $1/Sb$ is much smaller than $1/SR$ when $\xi = 0.001$. If we consider $SR = 1$ and $R = 2000$, the size is fixed at $r/L = 0.0015$ and Sb is about 30 times larger than SR; thus the Basset history term is much less important than Stokes drag in this regime.

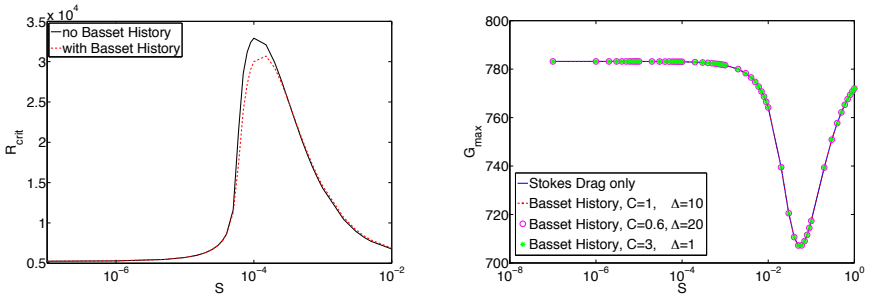

(a) f=0.1, $\xi = 0.001$ (b) f=0.1, R=2000, $\xi = 0.001$

Figure 3.3: Basset History with heavy particle approximation (only Stokes drag as interaction term apart from the Basset History term). Left: critical Reynolds number as a function of S. Right: Maximum transient growth as a function of S.

When light particles are considered, the Basset history term might have an effect because the density ratio changes to $\xi \sim 1$. Indeed, when we investigate at the critical Reynolds number in Figure 3.4(a), one can see that the history term has an effect. For neutrally buoyant particles, the results are the same, while for the $\xi = 2$ and $\xi = 0.5$, the critical Reynolds number shifts. In both cases, the particles have less influence on the critical Reynolds number compared to the case when light particles without Basset History are considered. The model used for the Basset history in this case is $\Delta = 1$ and $C = 3$.
At a certain relaxation time, our method in finding the eigenmodes fails. Although we only have a model up to a certain value of S, we can see the trend in critical Reynolds number. We see that the history term makes the particles less relevant. The history term increases the critical Reynolds number for $\xi = 2$ and it decreases the critical Reynolds number for $\xi = 0.5$.
Figure 3.4(b) shows the transient growth for light particles both with and without the Basset history term. A small decrease in maximal growth at small values of SR is present, although this is hardly visible on this scale. In the figure only one set of filter parameters is used ($\Delta = 1, C = 3$), more data with different filters is given in Table 3.1 for three density ratios. The value given is the optimal growth at a Stokes number $SR = 1 \cdot 10^{-3}$ compared to the optimal growth of a clean fluid. We see that all filters reduce the optimal growth, although only up to 2% for neutrally buoyant particles. The effect of

the history term is more profound when the filter for long times is used. This indicates that when the original square root is used, the optimal growth might be reduced even more, because the square root is effective for even larger times. All exponential filters and the square root reach zero asymptotically, however the exponential filters approach zero faster than the original square root.
These results imply that the Basset history does affect both modal and non-modal stability for light particles, but the effects are small. For heavy particles, the Basset history term has no significant influence on flow stability.

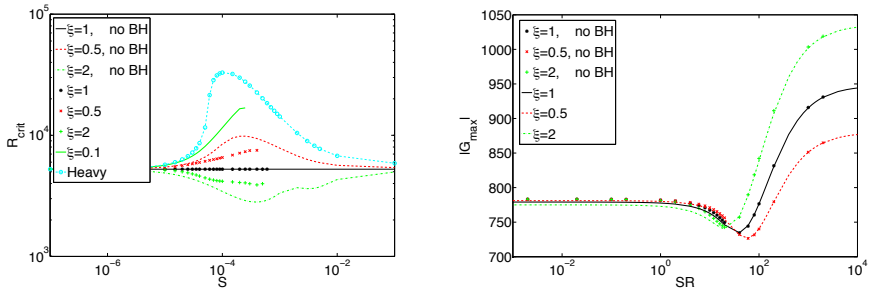

(a) f=0.1 (b) f=0.1, R=2000

Figure 3.4: Basset History with light particles. Left: critical Reynolds number as a function of S. Right: Maximum transient growth as a function of SR.

Table 3.1: Normalized transient growth for different filter parameters C and Δ at Stokes number $SR = 1 \cdot 10^{-3}$ and a mass fraction of $f = 0.1$. The value 1 represents the growth of a clean fluid

	$\xi = 0.5$	$\xi = 1$	$\xi = 2$
$\Delta = 1, C = 3$	0.997	0.995	0.990
$\Delta = 10, C = 1$	0.991	0.983	0.967
$\Delta = 20, C = 0.6$	0.990	0.980	0.963

CHAPTER 4

Direct Numerical Simulations

In the previous chapters, the linear stability of particle-laden flows is discussed. The linear stability analysis provides information about the initial, linear stages of transition, but not about breakdown of the perturbations and non-linear effects. To investigate transition beyond the initial stages, we performed direct numerical simulations of a flow laden with heavy particles, i.e. only Stokes drag is accounted for as interaction term. By means of numerical simulations, we investigate the behavior of a finite energy perturbation. We investigate how the threshold energy for transition, the minimum initial disturbance energy necessary to reach the turbulent state, varies in the presence of heavy particles. This provides information about the non-linear behavior of streaks and it shows whether the secondary instabilities might be damped by the presence of particles.
In relation to transition thresholds several researchers have considered the idea of 'edge of chaos' (Schneider *et al.* 2007); this is the asymptotic state reached by perturbations neither decaying or evolving into the turbulent regime. It is charachterized by a complex dynamics where unstable solutions (such as travelling waves, periodic orbits) may play a relevant role. A review about this edge state is given by Eckhardt *et al.* (2007).

We examine the two transition scenarios previously analysed by Reddy *et al.* (1998*a*). First transition initiated by streamwise vortices is considered, without streamwise dependence. The streamwise vortices initiate largest linear transient growth and they are common in many shear flows (Trefethen *et al.* 1993; Reddy & Henningson 1993; Schmid & Henningson 2001*a*). Schematically the transition process as given by Reddy *et al.* (1998*a*) reads:

streamwise vortices $\Rightarrow$ streamwise streaks $\Rightarrow$ streak breakdown $\Rightarrow$ transition.

Transition cannot take place without streamwise dependent structures, therefore an extra streamwise perturbations is added to get streak breakdown and transition. The extra perturbation can be either random noise, or a well-defined disturbance. We have chosen for one perturbation, an oblique mode with streamwise wavenumber $\alpha = 1$ and spanwise wavenumber $\beta = 1$.
In the second route to turbulence as discussed by Reddy *et al.* (1998*a*), a pair of symmetrical oblique optimal waves is considered. Each of these waves grows via the transient growth mechanism. The nonlinear interaction of these modes

forces streamwise independent structures which, in turn, induce streamwise streaks by the lift-up effect. The scenario is thus similar to the previously discussed scenario of streamwise vortices, but with one extra step:

$$\text{oblique waves} \Rightarrow \text{streamwise vortices} \Rightarrow \text{streamwise streaks} \Rightarrow$$
$$\Rightarrow \text{streak breakdown} \Rightarrow \text{transition}.$$

This scenario has been extensively investigated in the past for a single phase fluid, see e.g. Schmid & Henningson (1992); Berlin *et al.* (1994).

4.1. Numerical implementation

The equations of motion for the fluid and particles are the same as used previously for the heavy particle approximation. One difference is that the particles are now solved in a Lagrangian framework and the fluid in an Eulerian grid. In stability analysis both were solved in a Eulerian framework. The numerical code is a pseudo-spectral solver where we used a plane Poiseuille flow as base velocity, $u = 1 - y^2$. The velocity perturbations are expanded in both x (streamwise) and z (spanwise) direction with Fourier modes and with Chebyshev polynomials in the wall-normal, or y-direction. For time-advancement, we use a fourth order Runge-Kutta algorithm. Boundary conditions in x and z are periodic and no-slip is assumed at both walls, $y = \pm 1$. More details about this code are given in Chevalier *et al.* (2007).
The coupling from the Eulerian grid to the Lagrangian particles, to compute the Stokes drag, is implemented using tri-linear interpolation. The time advancement of the particle uses the same Runge-Kutta algorithm as the time-advancement of the fluid. Because a two-way coupling model is used, the Stokes drag has to be extrapolated back onto the Eulerian grid. For this the same tri-linear scheme of the interpolation step is used.
The streamwise and spanwise dimensions of the domain are $L_x = 2\pi$ and $L_z = 2\pi$. The Reynolds number used in all computations is $Re = 2000$ and Stokes number $SR = 5$. The resolution used is $64 \times 65 \times 64$ for streamwise, wall-normal and spanwise directions respectively. More resolutions have been used to investigate the convergence of the solution.

A bisection algorithm is used to find the energy threshold (Toh & Itano 2003; Duguet *et al.* 2008, 2010). In this algorithm, a lower and upper bound of initial amplitudes are specified of which we are certain they evolve into a laminar state and into a turbulent state respectively. The algorithm starts with an amplitude in between these bounds. We investigate whether this amplitude triggers turbulence or evolves into a laminar state. In the following step either the lower or upper bound is replaced with the amplitude from the previous step, depending on the result. This process is repeated, until the energy threshold is reached. Convergence of the energy threshold is assumed when

$$2\frac{A_u - A_l}{A_u + A_l} < 1 \cdot 10^{-5},$$

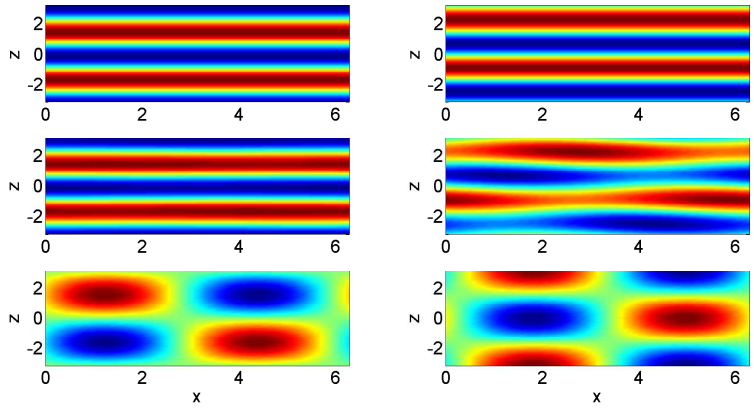

Figure 4.1: Initial conditions of streamwise vortices (top), streamwise vortices with an additional oblique mode (middle) and two oblique modes (bottom). On the left, v-velocity and on the right w-velocity. Horizontal axis is the streamwise direction, vertical axis the spanwise direction at the channel center. Positive velocities are colored in red and negative velocities in blue.

with A_u the amplitude of the upper bound and A_l the amplitude of the lower bound.

4.2. Results

The bisection results for both the streamwise vortices and the oblique waves are presented in this section. The initial conditions of these cases are given in Figure 4.1, consisting of a slice of the domain in streamwise (horizontal axis) and spanwise (vertical axis) direction at the center of the channel. On the left, wall-normal velocity v is given and on the right spanwise velocity w. The top figure presents the initial condition when only streamwise vortices are implemented, no streamwise dependence is present. The perturbation in the middle consists of the same streamwise vortices, but with an added streamwise dependence, an oblique mode. This streamwise dependency is necessary for turbulence as explained in the introduction. The bottom figure shows the initial perturbation of two oblique modes. The 'checkerboard' is clearly visible. The bisection algorithm is used with the latter two initial conditions.

The results of the bisection algorithm for the first case, with streamwise vortices as initial condition ($\alpha = 0, \beta = 2$), are given in Figure 4.2. Here, the initial condition is perturbed with an extra oblique wave ($\alpha = 1, \beta = 1$) with as initial energy 1/9 of the initial energy of the streamwise vortices. The figure

shows that the threshold energy for small particle mass fractions slightly decreases. This decay can be attributed to the forcing from the particles on the fluid. There are few particles present and they act locally and induce streamwise modulations. Large particle mass fractions result in a small increase in threshold energy, compared to a clean fluid. All changes to threshold energy are small, indicating that particles do not have a significant influence on this transition scenario.

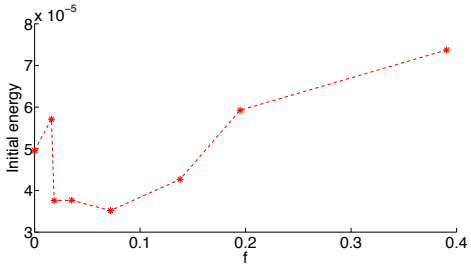

Figure 4.2: The critical threshold energy as a function of mass fraction particles f.

For the second case, with two symmetrical oblique waves ($\alpha = 1, \beta = \pm 1$) both given the same energy initially, the bisection results are given in Figure 4.3. What can be seen here, is that again for small particle mass fractions, the threshold energy decreases. At large particle mass fractions on the other hand, particles significantly increase the threshold energy, with a factor up to 4, compared to the clean fluid.

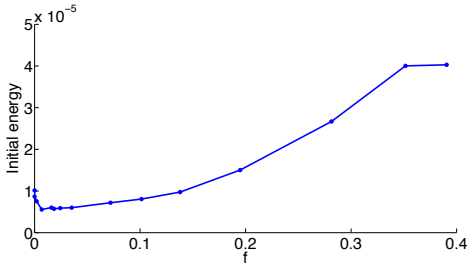

Figure 4.3: The critical threshold energy of two symmetrical oblique waves ($\alpha = 1, \beta = \pm 1$) as a function of mass fraction particles f.

CHAPTER 5

Summary of the papers

Paper 1

Modal and non-modal stability of particle-laden channel flow

Both modal and non-modal analyses of flows laden with heavy particles are performed. The non-modal analysis is expanded such that the fluid and particle energies can be separated.
Modal analysis confirms what was already known in literature: particles with moderate Stokes number increase the critical Reynolds number. For a small Stokes number, the critical Reynolds number is decreased with a factor of $(1 + f)$, with f the mass fraction particles. For large Stokes numbers, the particles are so large that they have no influence on the fluid anymore. We show that the energy production in the system is equal for all Stokes numbers, but that Stokes drag dissipates energy, causing stabilization.
In non-modal analysis mostly spanwise waves are considered, as these cause the largest growth. When the total system is considered, the energy growth increases with $(1+f)^2$. When only the fluid is investigated, the growth rates of clean fluid flow and particle laden flow are equal. The explanation for $(1 + f)^2$ in the total system is that particles increase the density of the total flow with $(1 + f)$. The transient growth is a function of Reynolds squared, hence the square dependence on the mass fraction.
Instead of the Stokes number another dimensionless number is defined, the Stability Stokes number. The stability Stokes number is the ratio of the dimensionless relaxation time to the timescale of the disturbance, for modal analysis the period of the wave. The most stabilizing effect can be seen when the stability Stokes number is in the order of one. The timescale of transient growth is large, the process is slow. Therefore, particles have ample time to adapt to the flow and thus, the particles have hardly an effect on the transient growth.
Overall, this paper shows that although modal analysis shows an increase in critical Reynolds number, non-modal shows that heavy particles hardly have an effect on stability.

Paper 2

Modal and non-modal stability analysis of a channel flow seeded with light particles

The same method for modal and non-modal analysis is used as in Paper 1, but with added mass and fluid acceleration terms included in the system. Neutrally buoyant particles do not affect the critical Reynolds number, except a decrease by $(1 + f)$, which can be seen as an increase in density due to the particles. When particles are lighter than the fluid, the critical Reynolds number even decreases. The conclusion is that particles lighter than the fluid decrease the critical Reynolds number and particles heavier than the fluid increase the critical Reynolds number.
Non-modal analysis shows the same behavior for light particles as for heavy particles: there is no change in transient growth. With light particles one has to be careful about the size and number of particles. For neutrally buoyant particles and a mass fraction of $f = 0.1$, the volume fraction $\Phi = 0.1$. When we have such a volume fraction, the model might not be valid anymore: particle collisions become important and the particles get too big to use the Eulerian framework. This is discussed in the paper.

Paper 3

Numerical Simulations of laminar-turbulent transition in particle-laden channel flow

Direct numerical simulations of particle-laden channel flow laden with heavy particles are performed. Two scenarios have been examined: streamwise vortices and two symmetric oblique waves.
First, streamwise vortices have been implemented as disturbance with a small initial amplitude. The amplitude is small such that streaks are formed after which the flow relaminarizes. It is shown that the energy gain of a particle laden flow is similar to the optimal growth shown in paper 1.
The next step was adding an extra oblique wave with small initial energy compared to the streamwise vortices. With this set-up an analysis of the threshold energy is performed. The influence of particles on the threshold energy is investigated and particles are found to have a small influence on the secondary instabilities. Large particle mass fractions slightly increase the threshold energy. Also, at a certain initial disturbance energy, the time needed to reach the turbulent state is investigated. Also shown is that particles increase the time for transition for disturbances of equal initial energy.
The second scenario consisted of two symmetric oblique waves as disturbance. The oblique waves interact non-linearly and form streamwise vortices which leads to streaks and, depending on amplitude, streak breakdown. It is found that particles enhance the transition threshold for this scenario at large particle mass fractions.

The results from these two classical scenarios indicate that, although linear stability analysis predicts that particles hardly have an influence on optimal growth, particles do influence the secondary instabilities and streak breakdown.

Conclusions & Outlook

The first conclusion that can be drawn from the work done is that although modal analysis shows that flows laden with heavy particles are more stable, non-modal shows particles hardly have any effect. For neutrally buoyant particles, both the modal and non-modal analysis shows that particles have a small influence. When the Basset history term is taken into account, small changes to the optimal growth are present at small particle relaxation times.
When investigating the energy gain of the fluid with initial condition a fluid perturbation, small differences can be found only at large Stokes number. At these values, the stability Stokes number is of order one, as is the case when most stabilization is seen in modal analysis. The Stokes number is that large though, that some assumptions for the particles are not valid anymore: particles become too large and particle collisions should be taken into account.
Direct Numerical Simulations show that particles do influence the secondary instabilities. For the case with two symmetrical oblique waves, small particle mass fractions reduce the energy threshold and large particle mass fractions enhance the energy threshold. Streamwise vortices show the same behavior, except that the increase in threshold energy is less than with the oblique waves. The results of the Direct Numerical Simulations shows that, although particles hardly have an effect on the initial linear stages of transition, particles influence secondary instabilities and streak breakdown.

Outlook

The project will continue for another two years, in which two major paths will be explored: DNS with finite sized particles as well as experiments in a water channel.
The DNS computations will be performed with a code developed by Breugem (2010) from Delft university, based on a code by Uhlmann (2005). With this numerical model we are able to investigate channel flows with the inclusion of neutrally buoyant particles. The stability analysis for neutrally buoyant particles showed that particles affect the flow most when the stability Stokes number is of order one. To reach this number, the particles have to have a diameter of 1-10% of the channel height. The numerical code by Breugem (2010) models such particles using the Immersed Boundary Method. Because both the particles and the volume fraction of particles is large, a collision model is present to

account for the particle-particle and particle-wall interactions.
Experiments will be performed in the same set-up as Mans (2007) has performed stability experiments several years ago. Instead of channel flow investigated in this thesis, a boundary layer flow is considered where we investigate bypass transition. Two examples of breakdown scenarios as observed by Mans (2007) are given in Figure 5.1. To investigate the effect on transition of a boundary layer flow, we will insert (almost) neutrally buoyant particles into the flow with size of 1-10% of the boundary layer thickness. One might think of changes to the distance from the leading edge where such breakdown occurs, or how particles influence the transition scenario: do particles change something to the sinuous and varicose modes? Some difficulties that we have to overcome are the injection of the particles into the flow to have a homogeneous distribution in the boundary layer.

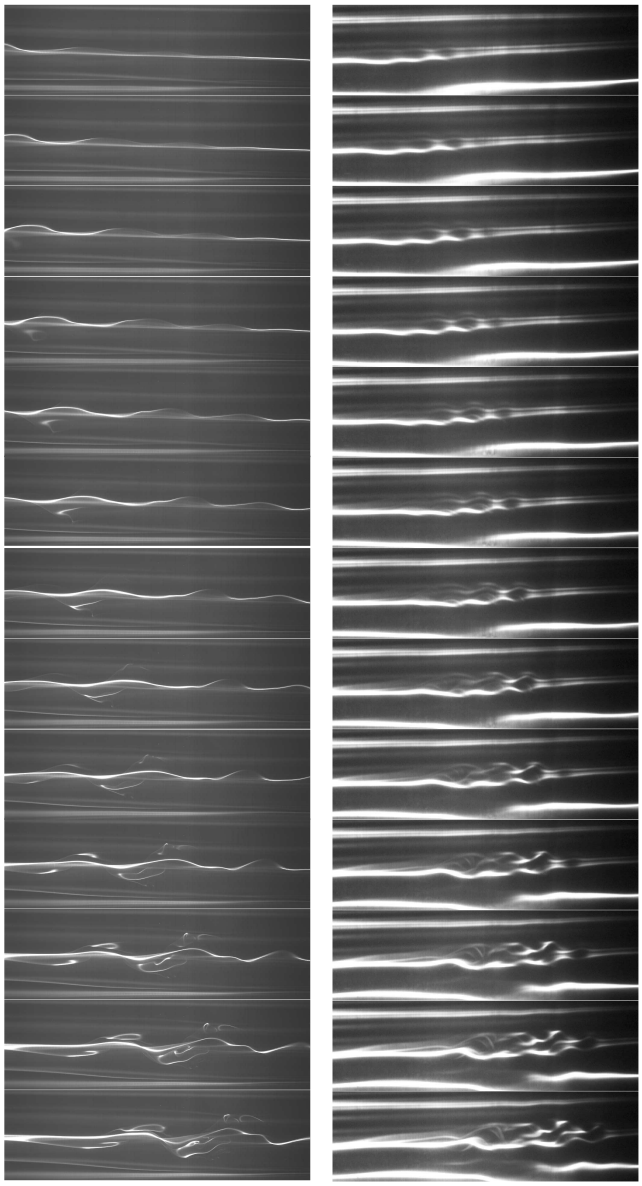

Figure 5.1: Examples of two breakdown scenarios as observed by Mans (2007).
A sinuous instability mode and a varicose mode.

Acknowledgements

I would like to acknowledge both my supervisors Dr. ir. Rick de Lange and Dr. Luca Brandt for their support, guidance, enthusiasm and encouraging inspirations. Thanks Luca, for all our discussions and your patience with me. Not only in real life, but also via Skype and e-mail during my time in Eindhoven. Thank you Rick, for our weekly discussions when I am in Eindhoven which are great for generating new ideas and directions.
I would also like to thank Prof. Anton van Steenhoven, for the interest in the project and interesting questions asked during our meetings. It helps me to step back and look at the total picture.
This thesis has been read by Geert Brethouwer, whom I would like to thank for the feedback and comments provided. It is very much appreciated.
Furthermore, I would like to thank my officemates, both in Eindhoven and in Stockholm. You are making it a pleasure to come to work everyday. I would like to specially name: Eldhose Iype and Dr. Erik Arlemark for guarding the office when I am in Stockholm, Junghan Kim, Zhipeng Liu, Kiran Kumar, Dr. Ilhan Yildirim, Konstantin Ermakov, Dr. Pieter van den Akker and Dr. Henk Ouwerkerk for the coffee breaks and all nice events. I would like to thank Linda Essink and Marianne Meves for the small talks whenever I am at the coffee machine. In Stockholm, floor 8 is a great floor to work on, thanks Armin Hosseini, Iman Lashgari, Solmaz Akbaripur, Miriam LaVecchia, Bram van de Sande, Gerardo Del Guercio, Dr. Ruth Lambert, Azad Noorani, Yoann Prigent, Dr. Gaetano Sardina and more. Furthermore I would like to thank all people for nice fika-times, lunches and discussions, thank you Johan Malm, Enrico Deusebio, Onofrio Semararo, Florian von Stillfried, Dr. Antonios Monokrousos, David Tempelmann, Qiang Li, Lailai Zhu, Dr. Miloş Ilak, Dr. Lars-Uve Schrader, Reza Dadfar, Dr. Outi Tammisola, Peter Lenaers, Werner Lazeroms, Steven van Wyk, Bernhard Semlitsch, Amin Rasam, Zeinab Pouransari and many more.
I would also like to thank my family, especially my mom & dad, Lucienne & Martin, Don and my nephew Dimar. Thank you for your care, support and encouragements. Finally, most important of all, I would like to thank my girlfriend Yvette, for her love and endless support, continuing while I am living in Stockholm.

Bibliography

Balachandar, S. & Eaton, J. K. 2009 Turbulent Dispersed Multiphase Flow. *Ann. Rev. of Fluid Mech.* **42**, 111–133.

Berlin, S., Lundbladh, A. & Henningson, D. S. 1994 Spatial simulations of oblique transition. *Phys. Fluids* **6**, 1949–1951.

Boronin, S. A. 2008 Investigation of the stability of a plane-channel suspension flow with account for finite particle volume fraction . *Fluid Dynamics* **43**, 873–884.

Breugem, W.-P. 2010 A combined soft-sphere collision/immersed boundary method for resolved simulations of particulate flows. *ASME Conference Proceedings* **2010** (49484), 2381–2392.

Chevalier, M., Schlatter, P., Lundbladh, A. & Henningson, D. S. 2007 A Pseudo-Spectral Solver for Incompressible Boundary Layer Flows. *Tech. Rep* TRITA-MEK 2007:07. Royal Institute of Technology (KTH), Dept. of Mechanics, Stockholm.

Duguet, Y., Brandt, L. & Larsson, B. R. J. 2010 Towards minimal perturbations in transitional plane couette flow. *Phys. Rev. E* **82**, 026316.

Duguet, Y., Willis, A. P. & Kerswell, R. R. 2008 Transition in pipe flow: the saddle structure on the boundary of turbulence. *Journal of Fluid Mechanics* **613**, 255–274.

Eckhardt, B., Schneider, T. M., Hof, B. & Westerweel, J. 2007 Turbulence transition in pipe flow. *Annual Review of Fluid Mechanics* **39**, 447–468.

Elghobashi, S. 1994 On predicting particle-laden turbulent flows. *Applied Scientific Research* **52**, 309–329.

Ellingsen, T. & Palm, E. 1975 Stability of linear flow. *Phys. Fluids* **18**, 487–488.

Ferrante, A. & Elghobashi, S. 2003 On the physical mechanisms of two-way coupling in particle-laden isotropic turbulence. *Phys. Fluids* **15**, 315–329.

van Hinsberg, M., ten Thije Boonkkamp, J. & Clercx, H. 2011 An efficient, second order method for the approximation of the basset history force. *Journal of Computational Physics* **230** (4), 1465 – 1478.

Jacob, B., Olivieri, A., Miozzi, M., Campana, E. F. & Piva, R. 2010 Drag reduction by microbubbles in a turbulent boundary layer. *Phys. Fluids* **22** (11), 115104.

Mans, J. 2007 Streak development and breakdown during bypass transition. PhD thesis, Technische Universiteit Eindhoven, The Netherlands.

Maxey, M. R. & Riley, J. J. 1983 Equation of motion for a small rigid sphere in a nonuniform flow. *Phys. Fluids* **26**, 883–889.

McCormick, M. E. & Bhattacharyya, R. 1973 Drag reduction of a submersible hull by electrolysis. *Naval Engineers Journal* **85** (2), 11–16.

Michael, D. H. 1964 The stability of plane Poiseuille flow of a dusty gas. *J. Fluid Mech.* **18**, 19–32.

Reddy, S. C. & Henningson, D. S. 1993 Energy growth in viscous channel flows. *J. Fluid Mech.* **252**, 209–238.

Reddy, S. C., Schmid, P. J., Baggett, J. S. & Henningson, D. S. 1998*a* On stability of streamwise streaks and transition thresholds in plane channel flows. **365**, 269–303.

Reddy, S. C., Schmid, P. J., Baggett, J. S. & Henningson, D. S. 1998*b* On the stability of streamwise streaks and transition thresholds in plane channel flows. *J. Fluid Mech.* **365**, 269–303.

Rudyak, V., Isakov, E. & Bord, E. 1997 Hydrodynamic stability of the poiseuille flow of dispersed fluid. *J. Aerosol Sc.* **82**, 53–66.

Saffman, P. G. 1962 On the stability of laminar flow of a dusty gas. *J. Fluid Mech.* **13**, 120–128.

Schmid, P. J. & Henningson, D. S. 1992 A new mechanism for rapid transition involving a pair of oblique waves. *Physics of Fluids* **4**, 1986–1989.

Schmid, P. J. & Henningson, D. S. 2001*a* *Stability and transition in shear flows*. Springer.

Schmid, P. J. & Henningson, D. S. 2001*b* *Stability and Transition in Shear Flows*. New York: Springer.

Schneider, T. M., Eckhardt, B. & Yorke, J. A. 2007 Turbulence transition and the edge of chaos in pipe flow. *Phys. Rev. Lett.* **99**, 034502.

Sproull, W. T. 1961 Viscosity of Dusty Gases. *Nature* **190**, 976–978.

Squire, H. B. 1933 On the stability of three-dimensional disturbances of viscous flow between parallel walls. In *Proc. Roy. Soc. Lond. A*, , vol. 142, pp. 621–628.

Toh, S. & Itano, T. 2003 A periodic-like solution in channel flow. *Journal of Fluid Mechanics* **481**, 67–76.

Toschi, F. & Bodenschatz, E. 2009 Lagrangian properties of particles in turbulence. *Ann. Rev. of Fluid Mech.* **41**, 375–404.

Trefethen, L. N., Trefethen, A. E., Reddy, S. C. & Driscoll, T. A. 1993 Hydrodynamic stability without eigenvalues. *Science* **261**, 578–584.

Uhlmann, M. 2005 An immersed boundary method with direct forcing for the simulation of particulate flows. *Journal of Computational Physics* **209** (2), 448 – 476.

Xu, J., Maxey, M. R. & Karniadakis, G. E. 2002 Numerical simulation of turbulent drag reduction using micro-bubbles. *J. Fluid Mech* **468**, 271–281.

Zhao, L. H., Andersson, H. I. & Gillissen, J. J. J. 2010 turbulence modulation and drag reduction by spherical particles. *Phys. Fluids* **22**, 081702.

Part II

Papers

1

Paper 1

Modal and non-modal stability of particle-laden channel flow

By Joy Klinkenberg[1,2], H.C. de Lange[1] and Luca Brandt[2]

[1]TU/e, Mechanical Engineering, 5600 MB, Eindhoven, The Netherlands

[2]Linné FLOW Centre, KTH Mechanics
SE-100 44 Stockholm, Sweden

Physics of Fluids **23** (064110)

Modal and non-modal linear stability analysis of channel flow with a dilute particle suspension is presented where particles are assumed to be solid, spherical and heavy. The two-way coupling between particle and fluid flow is therefore modeled by the Stokes drag only. The results are presented as function of the particle relaxation time and mass fraction. First, we consider exponentially growing perturbations and extend previous findings showing the potential for a significant increase of the critical Reynolds number. The largest stabilization is observed when the ratio between the particle relaxation time and the oscillation period of the wave is of order one. By examining the energy budget we show that this stabilization is due to the increase of the dissipation caused by the Stokes drag. The observed stabilization has led to the hypothesis that dusty flows can be more stable. However, transition to turbulence is most often subcritical in canonical shear flows where non-modal growth mechanisms are responsible for the initial growth of external disturbances. The non-modal analysis of the particle-laden flow, presented here for the first time, reveals that the transient energy growth is, surprisingly, increased by the presence of particles, in proportion to the particle mass fraction. The generation of streamwise streaks via the lift-up mechanism is still the dominant disturbance-growth mechanism in the particle laden flow: the length scales of the most dangerous disturbances are unaffected while the initial disturbance growth can be delayed. These results are explained in terms of a dimensionless parameter relating the particle relaxation time to the time scale of the instability. The presence of a dilute solid phase therefore may not always work as a flow-control strategy for maintaining the flow as laminar. Despite the stabilizing effect on modal instabilities, non-modal mechanisms are still strong in internal flows seeded with heavy particles. Our results indicate that the initial stages of transition in dilute suspensions of small particles are similar to the stages in a single phase flow.

1. Introduction

The dynamics of small inertial particles transported in a flow is crucial in many engineering and environmental applications. It is a long known fact that adding dust to a fluid may reduce the drag in pipe flows (Sproull 1961). To explain this phenomenon it has been suggested that the dust delays transition and dampens the formation of turbulent structures. More recently, drag reduction has been demonstrated by direct numerical simulations in plane channel flow using heavy spherical particles (Zhao *et al.* 2010), similarly to what has been observed with polymer or fibrous additives. Motivated by these results, we investigate whether the transition from laminar to turbulent flow might also be delayed, i.e. whether particles make the flow more stable. As a first step in this direction, the stability of a dusty-laminar flow is discussed in this paper.

The stability problem for a dusty gas was already formulated by Saffman (1962). He considered a plane parallel flow, where the base laminar profile is the same for the two phases considered, and an Eulerian description for the particle field; the coupling between fluid and solid phase is defined only through Stokes drag. In addition, a homogeneous distribution of particles is assumed and classic modal stability analysis performed. The particle perturbation velocities are expressed in terms of the fluid velocities and the stability problem reduces to solving a modified complex Orr-Sommerfeld equation. Saffman (1962) distinguishes two different cases: fine and coarse dust. For fine dust, the particle relaxation time is small and the dust adjusts quickly to the gas flow. Therefore, the added particles only lead to an increase in density and consequently a decrease of the critical Reynolds number. Coarse dust, conversely, increases the critical Reynolds number and thus stabilizes the flow. In a later investigation, Michael (1964) considers Poiseuille flow and presents neutral stability curves for several relaxation times. The results confirm that fine particles indeed decrease the critical Reynolds number whereas coarser particles increase it. Furthermore, Michael shows that very large/heavy particles have almost no effect on flow stability: the neutral stability curves retreats to the curve for the clean fluid when particles are too heavy to be affected by the fluid (ballistic limit).

The work by Michael (1964) was extended by Rudyak *et al.* (1997) using an improved numerical accuracy. These authors (Rudyak *et al.* 1997) again considered the linear modal stability of plane Poiseuille flow seeded with small heavy particles. Besides the fact that they propose to change the dimensionless numbers to some having more relevant physical meaning, the general results stay the same: small particles decrease stability, while larger particles increase the stability of the flow. In this study, inhomogeneous particle concentration is also examined and it is shown that stability is modified, both enhanced and reduced, when increasing the particle concentration in two layers near the walls while keeping the total number of particles constant.

The stability of the flat-plate boundary-layer flow is studied by Asmolov & Manuilovich (1998). These authors adopt the same model as introduced by Saffman (1962); in this case, however, the base flow differs from the case of single phase fluid in the presence of particles. For large particles and long relaxation times, the numerical analysis of Michael (1964) becomes inaccurate, the neutral stability curves become irregular, and integration of the stability equation needs to be performed in the complex plane, as done also by Rudyak *et al.* (1997). The dust suppresses the instability waves for a wide range of the particle size. The most efficient suppression takes place when the relaxation length of the particle velocity is close to the wavelength α of the Tollmien–Schlichting wave. The analysis by Asmolov & Manuilovich (1998) is also extended to a polydisperse dust. The growth rate of disturbances does not differ much from the monodisperse dust, only discontinuities arise in the (α, R)-plane for damped disturbances (with R the Reynolds number). The number of discontinuities equals the number of different particle sizes present.

These investigations only used Stokes drag as coupling term between the two phases: however, more recent studies discuss also additional coupling terms, mostly in the context of turbulent flows, e.g. Calzavarini *et al.* (2009). The paper by Maxey & Riley (1983) introduces the description of several forces arising between fluid and particles for different density ratios, namely the added mass term, a pressure gradient term, buoyancy and the Basset history term. The starting point of their analysis is the equation of motion proposed by Tchen (1947) and modified by Corrsin & Lumley (1956). Boronin & Osiptsov (2008) investigated the influence of the Saffman lift force (Saffman 1965) and a non-uniform particle distribution on the flow stability. The Saffman lift force itself has been investigated by several authors (Dandy & Dwyer 1990; Mei 1992; McLaughlin 1991). Furthermore the effect of the finite particle volume fraction is investigated by Vreman (2007) and Boronin (2008).

All investigations mentioned so far have considered only modal stability analysis. However, it is now understood that perturbation in wall-bounded shear flow can experience significant transient energy growth (Ellingsen & Palm 1975; Trefethen *et al.* 1993; Reddy & Henningson 1993; Schmid & Henningson 2001); the latter is responsible for the initial linear amplification of external disturbances which lead to subcritical transition to turbulence. As example, the critical Reynolds number for channel flow is $R = 5772$, while experiments show transition at Reynolds numbers as low as $R \approx 1000$. From a mathematical point of view, this transient energy growth is related to the non-normality of the governing linear stability operator: non-orthogonal eigenfunctions can be linearly combined to yield a low energy initial condition. However, owing to the different decay rates, the initial cancellation is later lost and the perturbation energy increases before eventually decaying to zero in a stable system. From a physical point of view, transient growth is associated to the generation of elongated spanwise-periodic streamwise velocity perturbations. These streaks are induced by pairs of counter-rotating streamwise vortices via the so-called

lift-up effect (Landahl 1980). In such a context, modal stability analysis is only relevant to study the asymptotic behavior of the system at large times: non-modal input-output analysis is necessary to explore the possibility of transient energy growth. In this case, one wishes to know the largest possible energy amplification that can be obtained over a finite time. The initial condition leading to the largest possible growth is denoted *optimal disturbance* and it is indeed found to consist of streamwise vortices in shear flows. The growth of the streaks, induced by these streamwise vortices, can be such that disturbances reach significant amplitudes and non-linear effects become important. In particular, it has been observed that streaks of high amplitude become susceptible to secondary inflectional instability leading to breakdown to turbulence (Reddy *et al.* 1998; Elofsson *et al.* 1999; Brandt & Henningson 2002).

The aim of this paper is therefore to investigate for the first time the non-modal stability of particle-laden channel flows for different particle mass fraction and relaxation time. Although modal stability analysis shows a stabilization of the flow in the presence of particles, an effective delay of the turbulent onset in channel flows requires also damping of non-modal growth mechanisms.

2. Governing equations and stability analysis

2.1. *Equations for particle-laden flows*

We consider a channel flow seeded with solid spherical particles whose size is smaller than the characteristic scale of the flow. To perform our analysis, we adopt the continuous, or Eulerian, model introduced by Saffman (1962): the particles are assumed to be under the action of Stokes drag only; lift force, buoyancy and added mass are neglected. While the continuous approach is bound to fail in turbulent flows, owing to particle clustering and singularities in the particles field, it can still be retained valid for laminar flow and perturbation of it, such as in linear stability calculations (Boffetta *et al.* 2007). In the following, p is the pressure, ρ the density of the fluid, N the number of particles per unit volume, r the radius of the particle and μ the dynamic viscosity. mN is the mass of the particles per volume with $m = \frac{4}{3}\pi r^3 \rho_p$ the mass of one particle, using the density of the particle ρ_p. Furthermore, K is the Stokes drag per relative velocity and defined as $K = 6\pi r\mu$. The governing equations for incompressible flow can be written as follows where u_i and u_{p_i} are the fluid and particle velocity respectively,

$$\rho\frac{\partial u_i}{\partial t} = -\frac{\partial p}{\partial x_i} - \rho u_j\frac{\partial u_i}{\partial x_j} + \mu\frac{\partial^2 u_i}{\partial x_j^2} + KN\left(u_{p_i} - u_i\right) \tag{1}$$

$$mN\frac{\partial u_{p_i}}{\partial t} = -mNu_{p_j}\frac{\partial u_{p_i}}{\partial x_j} + KN\left(u_i - u_{p_i}\right), \tag{2}$$

$$\frac{\partial N}{\partial t} = -\frac{\partial}{\partial x_i}\left(Nu_{p_i}\right) \tag{3}$$

$$\frac{\partial u_i}{\partial x_i} = 0. \tag{4}$$

The stability of this flow is investigated by considering a small perturbation u' to the base flow U. The base flow considered is Poiseuille flow driven by a constant pressure gradient. In the presence of a dispersed phase, the steady mean flow for both fluid and particles takes the form $U(y) = 1-y^2$, $y \in [-1, 1]$, independent of the number of particles. Substituting $u = U + u'$, $u_p = U + u'_p$, $p = P + p'$ and $N = N_0 + N'$ in equations(1-4), linearized stability equations are derived in a standard way (Schmid & Henningson 2001). These read (primes are omitted):

$$\frac{\partial u_i}{\partial t} = -\frac{\partial p}{\partial x_i} - U_j \frac{\partial u_i}{\partial x_j} - u_j \frac{\partial U_i}{\partial x_j} + \nu \frac{\partial^2 u_i}{\partial x_j^2} + \frac{K N_0}{\rho} \left(u_{p_i} - u_i\right) \tag{5}$$

$$\frac{\partial u_{p_i}}{\partial t} = -U_j \frac{\partial u_{p_i}}{\partial x_j} - u_{p_j} \frac{\partial U_i}{\partial x_j} + \frac{K}{m} \left(u_i - u_{p_i}\right) \tag{6}$$

$$\frac{\partial N}{\partial t} = -\frac{\partial}{\partial x_i} \left(NU + N_0 u_{p_i}\right) \tag{7}$$

$$\frac{\partial u_i}{\partial x_i} = 0. \tag{8}$$

The dimensional parameters used are reported in table 1 for clarity. Three non-dimensional parameters can be defined for this problem and they are given in table 2 where we follow the notation by Saffman (1962). They are the mass concentration f, defined as the mass of particles divided by the mass of the fluid per unit volume, the Reynolds number R, using channel half height L, and the Stokes number S defined as the particle relaxation time over the viscous time scale. Note however that S appears in the equations multiplied by R: SR can be seen as a Stokes number based on the convective time scale of the flow.

Table 1: Physical parameters defining the particle laden flows under consideration.

N		m^{-3}	Number density of particles
K	$6\ \pi r \mu$	$\mathrm{kg\ s}^{-1}$	For sphere with radius r, constant
mN		$\mathrm{kg\ m}^{-3}$	Mass of dust per unit volume
s	$\frac{KN_0}{\rho_f}$	s^{-1}	Constant, dimension of frequency
τ	$\frac{m}{K} = \frac{f}{s} (= \frac{2}{9} \frac{r^2}{\nu} \frac{\rho_p}{\rho_f})$	s	Relaxation time

For the particular configuration considered, the equation for the particle distribution N_0 (equation 7) is decoupled from the rest of the system. As a consequence, Squire's theorem can be extended to this case and a complex Orr-Sommerfeld equation can be derived for the stability of the flow (Saffman 1962; Michael 1964), which has been considered in the past. However, we are also interested in the non-modal stability of the full three-dimensional problem and introduce therefore the initial value problem for the particle velocities

Table 2: Definition of the non-dimensional numbers used.

f	$\frac{m_p}{m_f}$	-	Mass concentration
R	$\frac{\rho U L}{\mu}$	-	Reynolds Number
S	$\frac{\nu\tau}{L^2} = \frac{2}{9}\frac{r^2}{L^2}\frac{\rho_p}{\rho_f}$	-	Dimensionless relaxation time

and for the wall-normal velocity v and wall-normal vorticity $\eta = \frac{\partial u}{\partial z} - \frac{\partial w}{\partial x}$ of the fluid, analogous to the standard Orr-Sommerfeld-Squire system used for parallel single phase flows. The corresponding system of linearized equations in dimensionless form is given by:

$$
\begin{aligned}
-\frac{\partial}{\partial t}\nabla^2 v &= \left[\left(U\frac{\partial}{\partial x} + \frac{f}{SR}\right)\nabla^2 - U''\frac{\partial}{\partial x} - \frac{1}{R}\nabla^4\right] v + \\
&\quad + \frac{f}{SR}\left(\frac{\partial^2 u_p}{\partial x \partial y} + \frac{\partial^2 w_p}{\partial y \partial z} - \frac{\partial^2 v_p}{\partial x^2} - \frac{\partial^2 v_p}{\partial z^2}\right) && (9)\\
\frac{\partial \eta}{\partial t} &= \left[-U\frac{\partial}{\partial x} + \frac{1}{R}\nabla^2 - \frac{f}{SR}\right]\eta + \frac{f}{SR}\left(\frac{\partial u_p}{\partial z} - \frac{\partial w_p}{\partial x}\right) - \frac{\partial v}{\partial z}U' && (10)\\
\frac{\partial u_p}{\partial t} &= -U\frac{\partial u_p}{\partial x} - v_p\frac{\partial U}{\partial y} + \frac{1}{SR}(u - u_p) && (11)\\
\frac{\partial v_p}{\partial t} &= -U\frac{\partial v_p}{\partial x} + \frac{1}{SR}(v - v_p) && (12)\\
\frac{\partial w_p}{\partial t} &= -U\frac{\partial w_p}{\partial x} + \frac{1}{SR}(w - w_p) && (13)
\end{aligned}
$$

The boundary conditions of this system are $v = \eta = u_p = v_p = w_p = 0$ at both walls.

In the limit of $SR \to 0$, Lagrangian limit ($r \ll L$), the coupling between the fluid and particle motion is very strong and particles behave as passive tracers. The particles have a very small relaxation time and will adjust to the fluid almost immediately. This results in an effective increase in density of the total flow, for which a modified Reynolds number R_m can be defined:

$$R_m = \frac{(1+f)\,\rho U L}{\mu}.$$

In the limit $SR \to \infty$, ballistic limit ($\rho_p \ll \rho_f$), the equation describing the particles motion is decoupled from the particle velocity. Particles are too heavy to be affected by the fluid and perturbations in the particle velocity are simply advected by the base flow.

2.2. *Modal Stability*

To study modal linear stability, we assume wave-like perturbations

$$q = \hat{q}(y)e^{i(\alpha x+\beta z-\omega t)},$$

with $q = (v, \eta, u_p, v_p, w_p)^T$. In the expression above, α and β define the streamwise and spanwise wavenumber of the perturbation, respectively, while ω is a complex frequency: $\Im(\omega) > 0$ indicates solutions exponentially growing in time. Here we will mainly focus on the onset of the instability, $\Im(\omega)$ equals zero, and report neutral stability curves. As mentioned above, the neutral stability curve can be computed assuming two-dimensional perturbations since a modified version of Squire's theorem holds for the complex Orr-Sommerfeld equation (Saffman 1962) derived from equations (9, 11, 12).

2.3. *Non-modal Stability*

As discussed in the introduction, when the eigenvectors of the system are non-orthogonal, transient growth is possible even in asymptotically stable systems. Input-output or non-modal analysis is then necessary. The aim of such analysis is to determine the largest possible growth that can be achieved during a finite time interval; this is called optimal growth. The initial condition yielding optimal growth is denoted as optimal initial condition. If we indicate the discretized governing linear equations (9-13) in compact form as

$$\frac{\partial q}{\partial t} = Lq, \tag{14}$$

the largest possible energy growth at time t is the norm of the evolution operator, or propagator, $\mathcal{T} = \exp(tL)$. To quantify the energy growth, we use the kinetic energy of the full system defined as the kinetic energy of the fluid and of the particles

$$E_{kin} = \frac{1}{2}\left(m_f u_i^2 + m_p u_{p_i}^2\right), \tag{15}$$

with m_f and m_p the mass of the fluid and the particles respectively.
A matrix M can be associated with the energy norm. This is applied directly to the vector $q = [v, \eta, u_p, v_p, w_p]^T$ to give the kinetic energy integrated over the volume V

$$E(t) = \frac{1}{2}\int_V q^H M q dV. \tag{16}$$

In this study, we are not only interested in optimizing the total energy of the system. We wish also to investigate the optimal way to excite a response in the fluid/particles by an initial condition consisting only of perturbations in the fluid/particle velocity. To this aim we introduce the input disturbance q_{in}, the output q_{out} and corresponding input and output operators B and C. The input q_{in} consists of those quantities we wish to optimize for at time $t = 0$, while q_{out} defines the quantities we want to have amplified at time t. The dynamics of the system is still described by (14); to restrict the initial condition to q_{in}

we need to define the input operator B such that $q = Bq_{in}$. In analogy, to study only the response q_{out}, C is defined such that $q_{out} = Cq$. The evolution operator from $q_{in}(t = 0)$ to $q_{out}(t)$ becomes therefore

$$\mathcal{T} = C \exp(tL)B. \tag{17}$$

Finally we define the input and output energy matrix with $M_{in} = F_{in}F_{in}^H$ and $M_{out} = F_{out}F_{out}^H$ and the corresponding norms as $||q_{in}||_{E_{in}} = ||F_{in}q_{in}||_2$, $||q_{out}||_{E_{out}} = ||F_{out}q_{out}||_2$.

Using the definition for optimal growth (Schmid & Henningson 2001) one can show that the optimal growth corresponds to the 2-norm of the matrix

$$G(t) = \frac{||q_{out}(t)||_{E_{out}}}{||q_{in}(0)||_{E_{in}}} = \frac{||\mathcal{T}q_{in}(0)||_{E_{out}}}{||q_{in}(0)||_{E_{in}}} = \frac{||F_{out}\mathcal{T}q_{in}(0)||_2}{||F_{in}q_{in}(0)||_2} =$$
$$= \frac{||F_{out}\mathcal{T}F_{in}^{-1}F_{in}q_{in}(0)||_2}{||F_{in}q_{in}(0)||_2} = ||F_{out}\mathcal{T}F_{in}^{-1}||_2 = ||F_{out}C\exp(tL)BF_{in}^{-1}||_2. \tag{18}$$

The classic computation of the optimal growth is retrieved when $F_{in} = F_{out}$ and $C = B = I$.

2.4. *Energy analysis*

An equation for the evolution of the kinetic energy of the system can be derived by multiplying equation (5) with u_i and equation (6) by u_{p_i}. Adding the two energies using a factor f to account for the particle mass and integrating over the total volume of the system V gives

$$\frac{\partial E_v}{\partial t} = -\int_V u_i u_j \frac{\partial U_i}{\partial x_j} dV - \frac{1}{Re}\int_V \frac{\partial u_i}{\partial x_j}\frac{\partial u_i}{\partial x_j} dV$$
$$- f\int_V u_{p_i} u_{p_j}\frac{\partial U_i}{\partial x_j} dV - \frac{f}{SR}\int_V (u_i - u_{p_i})^2\, dV \tag{19}$$

where the divergence terms disappear owing to periodic boundary conditions and zero velocity at the walls.

The first two terms in (19) represent production of kinetic energy of the perturbation due to the work of the Reynolds stress u_iu_j against the shear of the base flow and viscous dissipation in the fluid. The third term, appearing in the presence of particles, accounts for the production of particle kinetic energy against the mean shear of the particle base motion. The last term accounts for fluid/particle interactions and it is always negative. The fluid-particle interaction always introduces a loss in energy. One can therefore expect that, as a results of the optimization, particles and fluid will tend to have the same velocity in order to reduce losses. When $u_{p_i} = u_i$ the dissipative term equals zero and the production of kinetic energy is enhanced by the presence of the particles, by a factor proportional to their mass fraction. When examining the energy gain of particles only,

$$\frac{\partial E_{v_p}}{\partial t} = -f\int_V u_{p_i} u_{p_j}\frac{\partial U_i}{\partial x_j} dV + \frac{f}{SR}\int_V (u_i u_{pi} - u_{p_i} u_{p_i})\, dV, \tag{20}$$

we see that when $SR \to \infty$, the coupling between the particle and fluid velocities becomes negligible and the last term in equation (20) vanishes. This results in a particle energy equation without dissipation, which then can result in unbounded growth of the particle energy, the inviscid Orr-Mechanism (Orr 1907).

The production and dissipation terms in equation (19) can be computed separately to gain insight into the instability mechanisms (Cossu & Brandt 2004). Assuming normal mode expansion, $(E, D, D_s, T_y, T_{p_y}) = (\hat{E}, \hat{D}, \hat{D}_s, \hat{T}_y, \hat{T}_{p_y})e^{2\omega_i t}$, with T_y and T_{p_y} the energy production terms, D the viscous dissipation, D_s the losses induced by the coupling Stokes drag and E the total perturbation kinetic energy. These terms become of the form (in 2 dimensions)

$$\hat{E} = \int_{-1}^{1} (\hat{u}\hat{u}^* + \hat{v}\hat{v}^*)\, dy \tag{21}$$

$$\hat{T}_y = \int_{-1}^{1} -(\hat{u}\hat{v}^* + \hat{u}^*\hat{v})\frac{dU}{dy}dy \qquad \hat{T}_{p_y} = \int_{-1}^{1} -(\hat{u_p}\hat{v_p}^* + \hat{u_p}^*\hat{v_p})\frac{dU}{dy}dy \tag{22}$$

$$\hat{D} = \int_{-1}^{1} 2\left(\frac{\partial \hat{u}_i}{\partial x_j}\cdot\frac{\partial \hat{u}_i}{\partial x_j}^*\right)dy \qquad \hat{D}_s = \int_{-1}^{1} \left((\hat{u}_i - \hat{u}_{p_i})(\hat{u}_i - \hat{u}_{p_i})^*\right)dy \tag{23}$$

where * indicates the complex conjugate.
Using equation (20) one can show that

$$\omega_i = \frac{\hat{T}_y}{2\hat{E}} + \frac{\hat{T}_{p_y}}{2\hat{E}} - \frac{\hat{D}}{2\hat{E}} - \frac{\hat{D}_s}{2\hat{E}}. \tag{24}$$

The different terms in this equation can be evaluated using the eigenvector from the stability analysis $(\hat{u}, \hat{v}, \hat{u}_p, \hat{v}_p)$.Variation of the production terms and of the Stokes drag is used to understand how modal stability is affected by the presence of particles. Note that the different terms should add to the growth rate ω_i, the imaginary part of the eigenmode. Eq. (24) therefore represents an a posteriori validation of the numerics.

2.5. *Numerical method*

Discretization of the equations is done using a Chebyshev collocation method in y-direction (Reddy *et al.* 1998). For most of the computations presented we used $n_y = 37$, with n_y being the number of collocations points. Tests were performed with $n_y = 67, 167$ to validate the accuracy of the results.

For the computation of the neutral stability, integration in the complex $y-$plane is performed to remove singularity in the limit of $SR \to \infty$ (Asmolov & Manuilovich 1998; Rudyak *et al.* 1997). To validate our implementation we report in Figure 1 a comparison with the results of Rudyak *et al.* (1997).

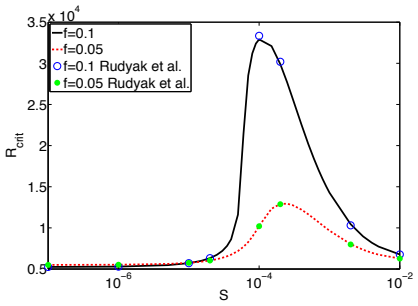

Figure 1: The critical Reynolds number as a function of dimensionless relaxation time S. A comparison between the present results and those in Rudyak *et al.* (1997)

For the computation of transient growth, the energy matrix M is built to compute the kinetic energy of the fluid and particles

$$M = \begin{pmatrix} \left(-\frac{D^2}{k^2}+1\right) I_w & 0 & 0 & 0 & 0 \\ 0 & \frac{1}{k^2} I_w & 0 & 0 & 0 \\ 0 & 0 & f I_w & 0 & 0 \\ 0 & 0 & 0 & f I_w & 0 \\ 0 & 0 & 0 & 0 & f I_w \end{pmatrix}, \tag{25}$$

where I_w is a diagonal matrix performing spectral integration in y direction. As M is diagonal, this can be easily factorized $M = U\Sigma U^H$ using Singular Value Decomposition (SVD). This can be done for M_{in} as well as M_{out} to define F_{in}, F_{in}^{-1},F_{out} and F_{out}^{-1}: given $M = U\Sigma U^H$, $F = U\Sigma^{1/2}$.

3. Results

3.1. *Modal analysis*

Considering the least stable eigenvalue of our system of equations, the neutral stability curves for different values of S are given in figure 2. The critical Reynolds number is seen to decrease for small $S(S = 1 \cdot 10^{-7})$, to increase for intermediate S, while for larger S it returns to the value found in Poiseuille flow without particles.

When S is very small, the particles are very small and just follow the fluid: relaxation time is fast and the particles adjust almost immediately to the fluid velocity. Therefore, the particles just act as to increase the total density of the system, thus lowering the critical Reynolds number by a factor $(1 + f)$. The neutral stability curves would coincide when instead of R, the Reynolds number of the mixture, R_m, is taken into account. For large values of S, however, the heavy and large particles are not able to interact with the fluid, thus they have no effect on the flow stability. In between these two extremes,

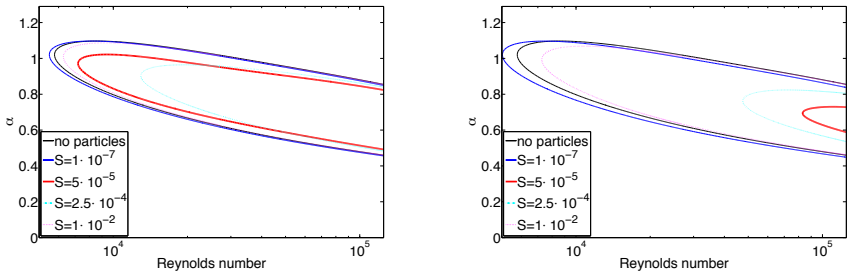

(a) $f = 0.05$ (b) $f = 0.15$

Figure 2: (Color online) Neutral stability curves for a particle laden flow with $S = [1 \cdot 10^{-7}, 5 \cdot 10^{-5}, 2.5 \cdot 10^{-4}, 1 \cdot 10^{-2}]$ and $f = 0.05$ (a), $f = 0.15$ (b). As reference, also the curve for a single phase flow is given.

the particles do interact with the flow and they have a positive effect on the flow stability; the critical Reynolds number increases with respect to the single phase channel flow. On the other hand, both the wavenumber and the phase velocity corresponding to the critical Reynolds number decreases. Our results are in agreement with the results of Saffman (1962), Rudyak *et al.* (1997) and Michael (1964), obtained using the complex Orr-Sommerfeld equation.

It can be noted that the mass fraction f affects the value of the critical Reynolds number: more particles have larger stabilizing effect. For mass fraction $f = 0.15$, R_{crit} can grow to as much as 10^5, i.e. almost two order of magnitude. When increasing f, a second effect is that the value of S yielding the largest critical Reynolds number decreases.

In figure 3 we display the critical Reynolds number versus $St_\omega = SR\omega_r$; this is the ratio of the particle relaxation time to the period of the wave and can be interpreted as stability Stokes number. With this scaling, the largest reduction of the growth rate is observed for $St_\omega = \mathcal{O}(1)$ for all values of the mass fraction f. In other words, particles have a stabilizing effect on the flow when their relaxation time is close to the pulsation of the least stable waves.

To better understand this behavior, we consider the energy budget given in equation (19), where the expressions in (21-23) are used to compute the production and dissipation terms. Table 3 shows the results of these computations using $R = 1.25 \cdot 10^4$, $\alpha = 1$, $f = [0\ 0.05]$ and $SR = [0.001\ 1\ 5\ 10\ 100]$ In the last column we report the difference between the system eigenvalue and the growth rate estimated by the energy balance as further validation of our implementation. Figure 4 shows the production and dissipation terms versus the particle relaxation time SR. It can be noted that the total energy production, $\hat{T}_y + \hat{T}_{y_p}$, and the viscous dissipation are almost constant with SR. The energy losses induced by the Stokes drag are initially very low but increase significantly when

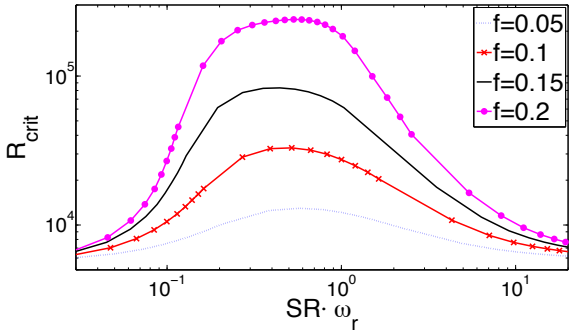

Figure 3: (Color online) Critical Reynolds number as a function of $St_\omega = SR\omega_r$ for $f = [0.05, 0.1, 0.15, 0.2]$, where $SR\omega_r$ is the ratio of the particle relaxation time to the period of the wave. The larger the f, the larger the critical Reynolds number R_{crit}.

$SR \approx 1$. The large increase of $\hat{D}_s$ is therefore responsible for the stabilization documented above.

SR	$\frac{\hat{T}_y}{2\hat{E}} \cdot 10^3$	$\frac{\hat{T}_{py}}{2\hat{E}} \cdot 10^3$	$\frac{\hat{D}}{2\hat{E}} \cdot 10^3$	$\frac{\hat{D}_s}{2\hat{E}} \cdot 10^3$	$\Sigma(\hat{T} - \hat{D}) \cdot 10^3$	$\omega_i \cdot 10^3$	Δ_ϵ
(f=0)	9.9442	0	5.7273	0	4.2169	4.2046	0.0123
0.001	9.4227	0.4790	5.6611	0.0074	4.2331	4.2206	0.0125
1	4.7140	5.7205	5.5637	5.5503	-0.6794	-0.6915	0.0121
5	5.9511	4.9145	5.4490	6.7058	-1.2892	-1.3006	0.0114
10	7.6115	3.9600	5.4401	5.7641	0.3673	0.3558	0.0115
100	8.5340	1.6584	5.0170	1.6262	3.5492	3.5382	0.0110

Table 3: Production and dissipation terms for modal stability with $\alpha = 1$, $f = 0.05$ and $R = 1.25 \cdot 10^4$. Production terms T_y and T_{p_y} are positive, while D and D_s are negative. The difference Δ_ϵ between the computed eigenvalue and the growth rate estimated by the energy budget is reported in the rightmost column.

Finally, the eigenfunctions of the most unstable mode for $\alpha = 1$ and Reynolds number 10^4 are given in figure 5, both for a clean fluid and for a particle-laden flow. The single phase fluid has an unstable mode, while the particle laden flow with $f = 0.15$ is stable. The streamwise u- and wall-normal v-velocities, depicted in figure 5(a) are similar for single phase and particle laden flow. For particle laden flow, the maximum u-velocity is larger for the same kinetic energy of the disturbance, although this value is reached further away from the walls. The fluid and particle velocities for the case of particle laden flow are shown in figure 5(b). The disturbance particle velocity u_p is larger

than that of the fluid, while the wall-normal particle velocity, v_p, is smaller. The difference in the u_i and u_{p_i} velocities are responsible for the increase of the critical Reynolds number, as the difference between these values stabilizes the flow by introducing extra dissipation in the system (cf. equation 19).

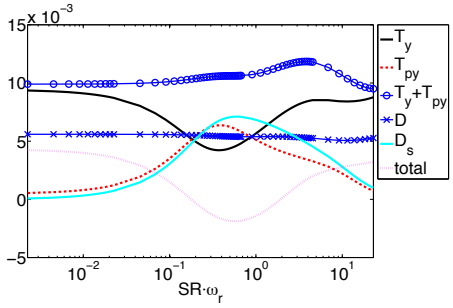

Figure 4: (Color online) Energy as a function of $St_\omega = SR\omega_r$ for $f = 0.05$, $R = 12500$ and $\alpha = 1$. The total production is also shown.

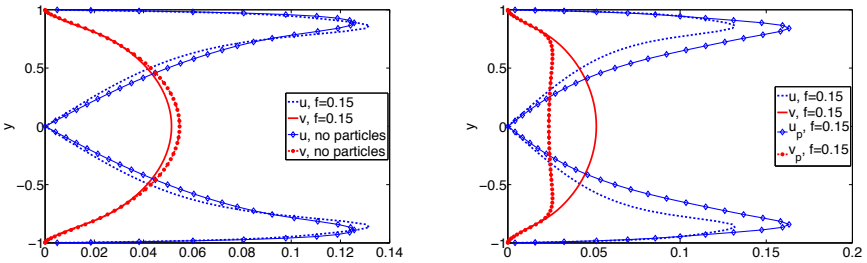

(a) u, v for $f = [0\ 0.15]$

(b) u, u_p, v and v_p for $f = 0.15$

Figure 5: (Color online) Eigenfunctions at $R = 10^4$, $\alpha = 1$, using $S = 2.5 \cdot 10^{-4}$ and particle concentration $f = 0.15$. (a) shows the absolute velocities u and v for flow with and without particles. (b) shows absolute particle and fluid velocities for a particle laden flow.

3.2. *Non-modal analysis*

As discussed earlier, non-modal growth mechanisms are responsible for sub-critical transition to turbulence in shear flows. We wish to investigate, therefore, whether these are affected by the presence of the particles in the same way

as the linear modal stability. This would imply that particles may induce significant transition delay. First, we introduce the quantities that will be considered in the following. The transient growth for a perturbation with wavenumbers $(\alpha, \beta) = (0, 2)$ in a single phase flow with $R = 2000$ is given in figure 6. In this example, pertaining to the wavenumber pair yielding the largest amplification in Poiseuille flow, the optimal growth is given as a function of time, as defined in equation (18). The curve is the envelope of the amplification curves of all initial conditions, in other words the maximum response to each optimal initial condition $q_0(t; Re, \alpha, \beta, f, S)$ is used to define this curve. The maximum growth, G_{max}, presented in figure 6, is an interesting parameter to be used to investigate the influence of particles on fluid flow as this is the global maximum in time of possible energy growth,

$$G_{max} = \max_t G(t) .$$

Preliminary calculations indicate that, in agreement to the case without particles, the largest non-modal amplification is attained by streamwise independent perturbations, where $\alpha = 0$. Therefore, in the following, we will present results of the non-modal analyses as curves of G_{max} versus α or β in which β and α are in turn set to zero. The case $\beta = 0$ will also be considered, in analogy to previous investigations in single phase shear flows (Farrell 1988), to examine the effect of particles on the Orr-mechanism and the optimal triggering of modal disturbances.

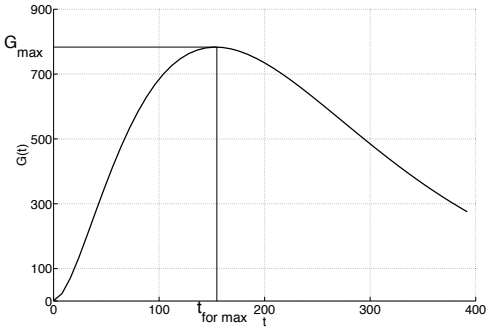

Figure 6: Transient growth for (α, β)=(0,2) and $R = 2000$ for a clean fluid. G_{max} indicates the largest growth in energy while $t_{for\ max}$ indicates the time needed to reach this maximum

As already mentioned, results for nine different cases will be presented. In addition to these, results for the single phase flow, or reference flow, will also be displayed in each plot. All these cases are given in figure 7 for $S = 5 \cdot 10^{-5}$, $R = 2000$ and $f = 0.15$. Results are reported both for spanwise waves, $\alpha = 0$ in 7(a-b), and streamwise waves, $\beta = 0$ in 7(c-d). The cases displayed

are denoted as *initial* $\rightarrow$ *final* with reference to the quantities used in the definitions of input and output energy norms; when both the particle and fluid kinetic energy are considered in the input/output norm, the case is denoted as *all*.

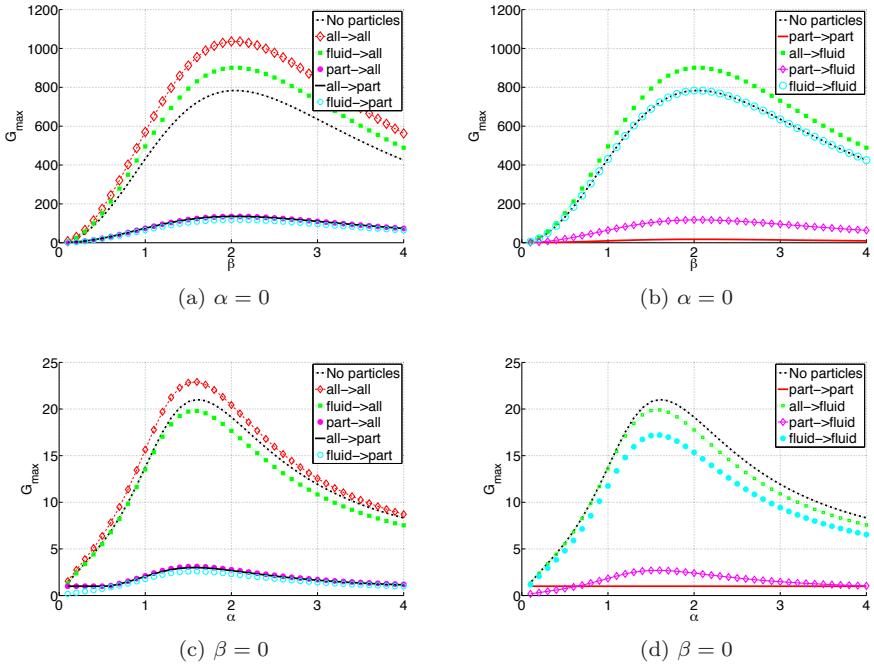

(a) $\alpha = 0$ (b) $\alpha = 0$

(c) $\beta = 0$ (d) $\beta = 0$

Figure 7: (Color online) Optimal growth for all 9 cases using $S = 5 \cdot 10^{-5}$, $R = 2000$ and $f = 0.15$, for spanwise (top) and streamwise (bottom) disturbances. As reference, also the single phase optimal growth is displayed. For clarity, the nine cases are divided into two figures (left and right).

Comparing the results for streamwise (α) and spanwise (β) perturbations, it is obvious that spanwise perturbations lead to higher energy gain than streamwise perturbations. This result is in agreement to results of single phase flow, as already presented in Butler & Farrell (1992), Gustavsson (1991) and Henningson *et al.* (1993). The spanwise perturbations consist of counter-rotating streamwise vortices, which induce high- and low-speed streaks owing to the lift-up effect.

3.2.1. *Spanwise-dependent disturbances*

The results for streamwise-independent spanwise-periodic disturbances are first discussed referring to the results shown in figure 7(a-b). The energy gain for

the case $all \rightarrow all$ provides the largest possible energy growth, the amplification is augmented by a factor $(1+f)^2$ with respect to the flow without particles. The optimal energy growth for the total system is thus larger for particle-laden flows. The optimal gain in the case of a non-zero initial fluid velocity only ($fluid \rightarrow all$) also gives response larger than that in the clean flow, which may be expected since the particles contribute to the final energy as well. The growth is however smaller than for $all \rightarrow all$. The level of perturbation induced by perturbations in the particle motion, induced by stirring the particles with some external force, $part \rightarrow all$, is much lower in comparison to the previous cases; this indicates that initial particle disturbances are less effective to excite the flow. This can be explained by the low mass fraction of the solid phase in our model.

Considering the final particle velocity only ($initial \rightarrow part$) indicates the possibility to induce mixing in the density distribution. The values of the possible energy amplification are small, about $1/f$ lower than for the fluid velocity. However, the particle velocity is the same as the fluid velocity, and the gain is small only because the mass fraction is small, $f = 0.15$. The cases $all \rightarrow part$ and $fluid \rightarrow part$ are close to each other, suggesting a small amplification $part \rightarrow part$, which is indeed the case.

The final three cases examined deal with the optimal growth of the fluid flow perturbations (figure 7b). The fluid is able to gain more energy from the system when particles are present, compare $all \rightarrow fluid$ to no-particles. The fluid, however, is not able to gain much energy from the particles only ($part \rightarrow fluid$), while the $fluid \rightarrow fluid$ case is very close to the single phase optimal growth. This may indicate that losses due to the particle-fluid interactions are weak for the parameters in figure 7. As shown below, however, we observe a more complicated interplay between initial losses induced by interaction with the particles and the larger amplification observed in the case $all \rightarrow fluid$.

As seen above when considering the total energy of the system (equation 19), the dissipation of energy due to fluid/particle interactions vanishes when the fluid and particle velocity are equal. It is therefore not surprising that the optimal initial condition has the same velocity for fluid and particles in the case $all \rightarrow all$. For the values of S allowed by our model, moderate SR, also in the case of zero initial particle velocity, the difference (and thus the Stokes drag) becomes small and eventually zero for relatively long optimization intervals. In figure 8 we report the optimal initial condition (a) and the optimal response (b) for the case $fluid \rightarrow fluid$ with $\beta = 2, S = 5 \cdot 10^{-5}, f = 0.15$ and $R = 5000$. The initial condition consists of a pair of counter-rotating streamwise vortices spanning the full channel height. The particles have no initial disturbance velocity. The perturbation at the final time is composed mainly of streamwise velocity, with two streaks antisymmetric with respect to the centerline, for both the fluid and particles. The lift-up effect is clearly at work also in particle-laden flows. Note that the particle velocity adjusts to the fluid velocity, although only

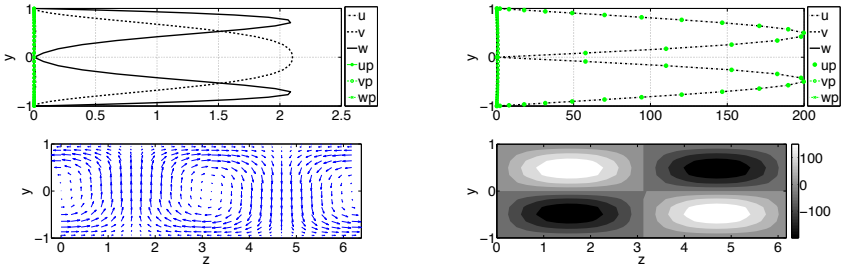

(a) Initial condition (b) Response

Figure 8: (Color online) Optimal initial condition and response for the case $fluid \rightarrow fluid$ with $\beta = 2, S = 5 \cdot 10^{-5}, f = 0.15$ and $R = 5000$. On top the absolute velocities of fluid and particles are displayed. On the bottom figures the velocity vectors of the fluid (a) or the u-velocity contours are given (b). Initial condition consists of streamwise vortices of the fluid (a), while the disturbance velocity of the particles is zero. For the response (b), low- and high-speed streaks can be clearly recognized.

the response of the fluid perturbation is considered. These equal velocities reduce the dissipation of energy due to fluid/particle interaction.

We now investigate the effect of S and f. In figure 9(a) the optimal growth is given for five different cases and a value of $S = 2.5 \cdot 10^{-3}$, larger than that in figure 7. The difference between the single phase flow and the case $fluid \rightarrow fluid$ is small, although present. It is interesting to note that, at this value of S, very large variations in the asymptotic stability of the two-phase flow are already observed, see figure 3. The presence of particles has therefore a completely different impact on modal and non-modal stability.

While the maximum gain of the fluid kinetic energy is hardly affected by the particles, the time at which the optimal growth is reached varies. To document this, the optimal growth is displayed as a function of time for $(\alpha, \beta) = (0, 2)$ and $R = 2000$ in figure 9(b) for $fluid \rightarrow fluid$. Here results for two values of f and two values of S are compared to the case without particles. The results indicate that the delay induced by the particles increases with increasing f, but that this delay is not affected by the value of S.

Figure 10 shows the optimal growth and the time to reach the optimal growth as a function of mass fraction f using $S = 2.5 \cdot 10^{-3}$ and $R = 2000$. The optimal growth increases by a factor $(1 + f)^2$ for the case $all \rightarrow all$ compared to the single phase flow, while for the cases $all \rightarrow fluid$ and $fluid \rightarrow all$ the optimal growth is enhanced only with a factor $(1 + f)$. The time needed to reach the optimal growth on the other hand increases by $(1 + f)$ for all cases, figure 10(b).

Two competing mechanisms appear to be present in this case. Losses are induced by the initial difference between fluid and particle velocity. These are proportional to the mass fraction f and cause a slower initial growth of the perturbation (figure 9b). Losses decrease faster for lower S, indicating shorter relaxation time, but this effect appears negligible. At the same time, once particles move at the fluid velocity, larger amplifications are observed (see $all \rightarrow fluid$ in figure 7 and figure 10). In conclusion, the amplification of the fluid kinetic energy in the presence of particles is slower because of the losses due to the initial difference between fluid and particle velocity but the potential growth is larger. *These two effects compensate and the total energy gain is similar in laden and unladen flow.*

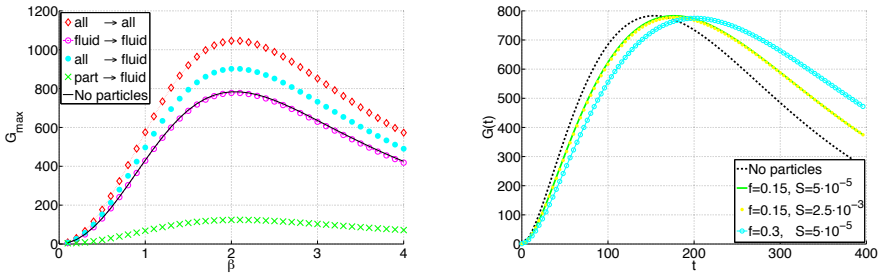

(a) Optimal growth (b) Transient growth

Figure 9: (Color online) (a): Optimal growth for 5 different cases, including the clean fluid flow, using $\alpha = 0$, $f = 0.15$, $S = 2.5 \cdot 10^{-3}$ and $R = 2000$. (b): Transient growth for the case $fluid \rightarrow fluid$ with $\beta = 2$, $\alpha = 0$ and $R = 2000$, using $f = 0.3$ and 0.15 as well as $S = 2.5 \cdot 10^{-3}$ and $5 \cdot 10^{-5}$.

The optimal growth versus Reynolds number is given for spanwise perturbations in figure 11(a). The growth for spanwise waves is found to be proportional to R^2, as in the case of flows without particles. The results also confirm that non-modal growth is enhanced in the presence of particles, and, as shown by the inset in the figure, the energy gain for the case $all \rightarrow all$ is $(1 + f)^2$ times that for the single phase flow. The transient growth appears to be proportional to the effective Reynolds number based on the total density of the medium $\rho_t = (1 + f)\,\rho_{fluid}$ as in the case of modal stability at low values of S. In this case, however, the effect is observed also at large values of S. This again suggests that a different definition of the Stokes number may be more relevant for stability problems. We therefore consider again the stability Stokes number St_ω, introduced above as the ratio of the particle relaxation time and the instability time scale. This parameter St_ω assumes low values for non-modal growth since the latter is occurring on a time scale longer than the characteristic particle relaxation time. The effect of particles on modal and non-modal

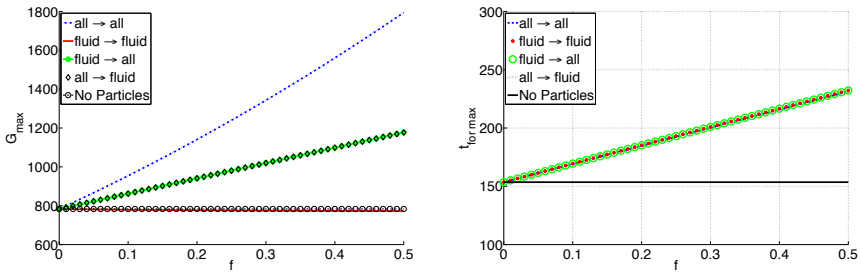

(a) $G_{max}(f)$ (b) $t_{for\ max}(f)$

Figure 10: (Color online) (a): G_{max} as a function of mass fraction f for several cases denoted in the legend using $S = 2.5 \cdot 10^{-3}$ and $R = 2000$. (b): $t_{for\ max}$ as a function of mass fraction f for the same cases as (a) using $S = 2.5 \cdot 10^{-3}$ and $R = 2000$.

stability can therefore be explained by this new parameter: at low values of St_ω, the solid phase acts only to increase the total density and therefore the effective Reynolds number. Significant energy losses having a stabilizing effect are found only when $St_\omega \approx 1$.

The optimal growth as a function of S is displayed in figure 11(b). The figure shows the flow behavior in the ballistic limit, when particles are not affected by the fluid, and quantifies when these effects become relevant. As shown by equations (5-8), for large SR the motion of fluid and particles are decoupled. Particles behave as the fluid but the particle velocity field is not required to be divergence free and there is no dissipation. In absence of dissipation, we observe that the particle perturbation velocity can grow significantly. This observation is in line width the inviscid algebraic instability first examined in Ellingsen & Palm (1975) for streamwise-independent modes The same behavior is observed also for streamwise-dependent modes: here it can be seen as the inviscid Orr mechanism. The computations become grid-dependent and the optimal initial conditions for the particle velocity become as narrow as possible in the wall-normal direction, limited to non-zero values in the grid point associated to highest shear of the base flow. This is allowed since the velocity field for the particles does not need to be solenoidal and is in agreement with the inviscid limit of the Orr-Sommerfeld equation. Note however that the validity of our model is questionable for large particles, i.e. large S.

The case $fluid \rightarrow fluid$ does not show increased growth at large S, which indicates that indeed the large growth in the case $all \rightarrow all$ is associated to the energy of the particles. The value of S does not have a very large effect on the optimal gain: the optimal growth between $S = 1 \cdot 10^{-5}$ and $S = 1 \cdot 10^{-2}$ is hardly changing. This confirms that particle relaxation time has little effect on

non-modal stability since St_ω is low in the range considered; the main effect is from the mass fraction f that increases the fluid density.

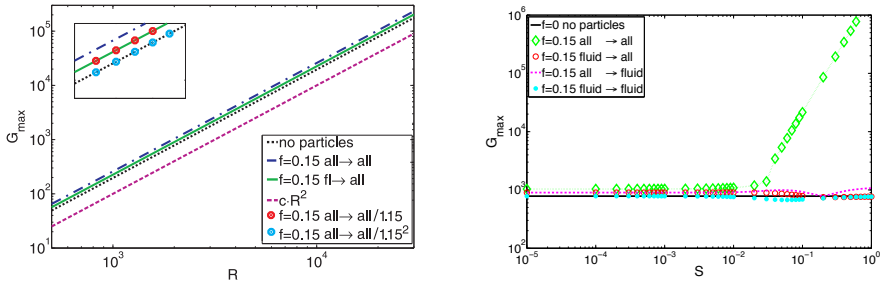

(a) $\beta = 2, \alpha = 0, S = 5 \cdot 10^{-5}$ (b) $\beta = 2, \alpha = 0, R = 2000$

Figure 11: (Color online) (a): optimal growth versus Reynolds number. In the large figure the cases for a clean fluid, the $all \rightarrow all$ and $fl \rightarrow all$ are given, in which the dependence of R^2 can be clearly recognized. As reference, a function of a constant times R^2 has been given as well, the blue line. In the insert the $all \rightarrow all$-case has been given, but then divided by $(1 + f)$(●) and $(1 + f)^2$(●). (b): the optimal growth versus S is displayed, for the same cases as in the left figure including $fluid \rightarrow fluid$.

3.2.2. *Two-dimensional streamwise-dependent waves*

The results for streamwise-dependent disturbances are first discussed referring to the results shown in figure 7(c-d). The energy gain for the case $all \rightarrow all$ is responsible for the largest possible energy gain, as for spanwise disturbances. For streamwise disturbances the increase with respect to the case of single phase flow is$(1 + f)$ for small values of S. For the cases where the initial condition consists of fluid velocity only, $fluid \rightarrow all$, its response in energy growth is less compared to the clean fluid flow. When only the particles are disturbed, $part \rightarrow all$, the response is even less at these low values of the particle relaxation time.

Investigating the response of the particles reflects the ability to produce mixing. The possible energy growth of the particles is small; all cases $initial \rightarrow part$ are small compared to the cases just presented. As already discussed for spanwise disturbances, this difference is of order f^{-1}. Furthermore, for $part \rightarrow part$ the maximum gain is always equal to one, i.e. no growth.

The final three cases discussed deal with the optimal energy growth of the fluid. The fluid gains less energy compared to the single phase flow. Even for a disturbance of the total system, $all \rightarrow fluid$, the energy gain is less compared to the single phase flow. The case $fluid \rightarrow fluid$ shows a decrease of the transient growth by more than a factor of $(1 + f)$. This indicates that for streamwise

disturbances the particles introduce extra dissipation of the disturbance energy. An initial disturbance of the particles results in a small response to the fluid, $part \rightarrow fluid$, which again can be explained by the relative low density of the particles.

The initial condition and optimal response for a streamwise disturbance with $\alpha = 1.6, S = 5 \cdot 10^{-5}, f = 0.15$ and $R = 5000$ for the case $fluid \rightarrow fluid$ is displayed in figure 12. The initial condition consists of flow patterns opposing the mean shear direction. As time evolves, they tilt into the mean shear direction, which introduces the transient growth. This process is similar to the Orr-mechanism in fluid alone (Orr 1907). Note that at the final optimization time, the fluid and particle velocities are not exactly equal to each other, unlike for spanwise disturbances at the same value of S.

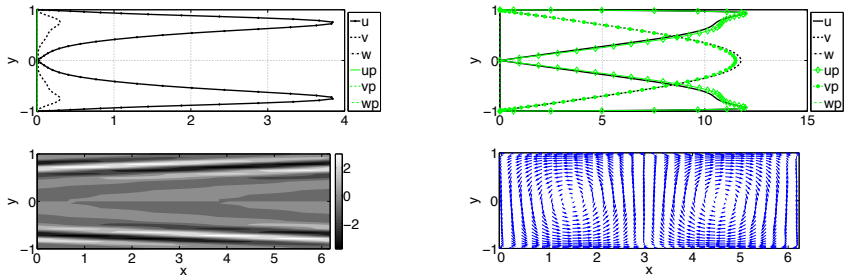

(a) Initial condition (b) Response

Figure 12: (Color online) Optimal initial condition and response for the case $fluid \rightarrow fluid$ with $\alpha = 1.6, S = 5 \cdot 10^{-5}, f = 0.15$ and $R = 5000$. On top the absolute velocities of fluid and particles are displayed. The bottom figures represent the u-velocity contours (a) and the velocity vectors of the fluid (b). Initial condition can be seen as flow patterns opposing the mean shear (a). The disturbance velocity of the particles is zero. In the response (b), the disturbance is changed into the the mean shear direction. The Orr-mechanism can be recognized.

In figure 13(a) the optimal growth as function of α is displayed for particles with $S = 2.5 \cdot 10^{-3}$, a value larger than that used in figure 7. One notices a growth larger than in single phase fluid in three different cases, namely $all \rightarrow all$, $all \rightarrow fluid$ and $part \rightarrow fluid$. In other words, in all the cases with large energy growth, the initial condition consists of particle disturbance velocity. This can be either as particles alone or as the total system, which includes particle velocity.

To investigate the effect of S on the growth of two-dimensional disturbances, figure 13(b) shows the optimal growth as a function of S. For small values

of S, the results are as in figure 7(c). The energy gain is enhanced by a factor $(1+f)$ in the case $all \rightarrow all$ with respect to the single phase flow, unlike spanwise disturbances where the growth in the laden flow is enhanced by a factor $(1+f)^2$. When considering an initial disturbance consisting only of fluid velocity, $fluid \rightarrow fluid$ and $fluid \rightarrow all$, the energy gain is always smaller in the presence of particles. The particles induce therefore an energy loss. For the case of perturbation induced by the particle motion, $part \rightarrow fluid$, one observes that for values of $SR = \mathcal{O}(1)$ the transient growth increases significantly and reaches asymptotic values for the largest S considered. Larger values of the energy gain in the case of two-dimensional disturbances can therefore be observed when the particle relaxation time is longer than the typical convective time scale of the flow. Comparing the amplification with the case $all \rightarrow all$, one can see that this effect is associated to the growth of the particle perturbation kinetic energy in the ballistic limit. This was discussed before for spanwise-periodic modes.

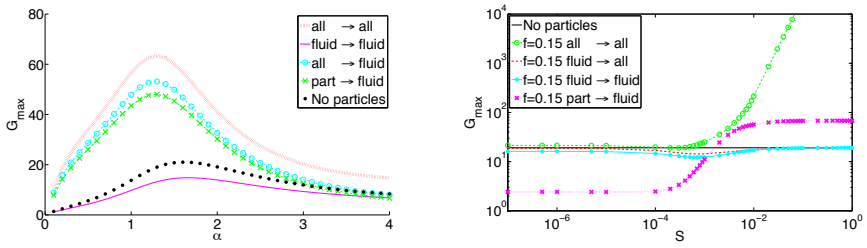

(a) $\beta = 0, S = 2.5 \cdot 10^{-3}$ and $R = 2000$ (b) $\beta = 0, \alpha = 2$ and $R = 2000$

Figure 13: (Color online) (a): optimal growth for streamwise waves for 5 different cases, including the single phase flow. (b): optimal growth versus S, for same cases as in the figure on the left. Note that $all \rightarrow all$ diverges from the other results at $S \sim 10^{-3}$

4. Conclusions

We perform modal and non-modal stability analysis of channel flow seeded with small, heavy, spherical particles. The interaction between the two phases is modeled solely by Stokes drag. We present results for different values of the particle relaxation time and volume fraction. The particle relaxation time is limited by the fact that particle are assumed to be much smaller than the flow length scale, while the mass fraction is assumed small since particle-particle collisions are not included in our model.

We show that the presence of particles has a very different effect on the exponential and transient growth of external perturbations. The differences are explained in terms of the different characteristic time scale of the two instability

mechanisms. As shown in previous investigations, particles can increase the critical Reynolds number by at least one order of magnitude. However, we demonstrate here that particles increase the non-modal energy growth. The presence of a dilute solid phase therefore will not work as a flow-control strategy for maintaining laminar flow.

Modal stability is influenced by the dimensionless relaxation time, S. At small values (small particles) the critical Reynolds number decreases proportionally to the density of the solution, as $(1 + f)$. Intermediate values of S yield the largest increase of the critical Reynolds number, where the increase is proportional to the volume fraction of the solid phase. In the ballistic limit, the neutral curves approach again the results for. The largest stabilization is obtained for $St_\omega = SR\omega_r \approx 1$, that is for waves whose period of pulsation is of the order of the particle relaxation time. To gain further insight into the stabilizing mechanisms we consider the evolution of the disturbance kinetic energy and show that the resonance between particle and instability characteristic times gives the maximum dissipation associated to the work of Stokes' drag.

The generation of streamwise streaks via the lift-up mechanism is still the dominant disturbance-growth mechanism in subcritical particle laden flows: the length scales of the most dangerous disturbances are unaffected while the disturbance growth can be initially delayed. The increase by a factor $(1 + f)^2$ of the non-modal gain can also be explained in terms of the stability Stokes number St_ω. This dimensionless parameter assumes very low values in the case of the low-frequency non-modal growth ($St_\omega \approx SR/t_{max}$, with $t_{max} \approx \mathcal{O}(100)$) and therefore the effect of particles is just that of altering the fluid density. Particles have the time necessary to follow the slow formation of the streaks. Indeed particles increase the solution density and the Reynolds number of the laden fluid becomes then $R_m = (1 + f)\, R$. As the optimal growth in unladen flows is proportional to R^2, the presence of the particles increases the energy gain by $(1 + f)^2$.

To summarize, the effect of particles on the modal and non-modal stability of channel flows can be explained by the stability Stokes number St_ω. Low values of this parameter indicate that the particles follow passively the fluid instability and their effect is only that of increasing the total density of the suspension. Significant energy losses that can have a stabilizing effect are observed only when $St_\omega = \mathcal{O}(1)$.

A method for investigating the response of different flow quantities to different input disturbances has been introduced. Instead of optimizing the energy of the total system, we optimize for fluid and particles separately as well. When examining a disturbance in the fluid alone and the corresponding fluid energy at final time, we find that the optimal growth for a particle laden flow is close to that of the clean fluid and a noticeable difference is seen only for the largest values of S. The energy that the fluid can extract by an initial perturbation of the particle velocity is proportional to the mass fraction f.

The work presented in this paper could be extended in a number of non-trivial and interesting ways. First, we have here focussed on heavy particles, neglecting contributions from added mass and pressure forces. The effect of light particles on the flow stability should be addressed. Second, one may consider finite-size particles of different shapes. Finally, our results indicate that the initial stages of transition in dilute suspensions of small particles should follow a similar path as in a single phase flow. However, to be able to estimate the effect of the solid phase on the laminar/turbulent transition full nonlinear simulations will be necessary. Indeed, while little changing the initial formation of the streamwise elongated streaks, particles may accumulate and affect the self-sustaining cycle of turbulence (Waleffe 1995). The recent results in turbulent channel flow (Zhao *et al.* 2010) indicate that this may be the case.

References

Asmolov, E. S. & Manuilovich, S. V. 1998 Stability of a dusty-gas laminar boundary layer on a flat plate. *J. Fluid Mech.* **365**, 137–170.

Boffetta, G., Celanu, A., De Lillo, F. & Musacchio, S. 2007 The eulerian description of dilute collisionless suspension. *Europhysics Letters* **78**, 14001.

Boronin, S. A. 2008 Investigation of the stability of a plane-channel suspension flow with account for finite particle volume fraction . *Fluid Dynamics* **43**, 873–884.

Boronin, S. A. & Osiptsov, A. N. 2008 Stability of a Disperse-Mixture Flow in a Boundary Layer. *Fluid Dynamics* **43**, 66–76.

Brandt, L. & Henningson, D. S. 2002 Transition of streamwise streaks in zero-pressure-gradient boundary layers. *J. Fluid Mech.* **472**, 229–261.

Butler, K. M. & Farrell, B. F. 1992 Three-dimensional optimal perturbations in viscous shear flow. *Phys. Fluids A* **4**, 1637–1650.

Calzavarini, E., Volk, R., Bourgoin, M., Lévêque, E., Pinton, J. & Toschi, F. 2009 Acceleration statistics of finite-sized particles in turbulent flow: the role of Faxén forces. *J. Fluid Mech.* **630**, 179–189.

Corrsin, S. & Lumley, J. 1956 On the equation of motion for a particle in turbulent fluid. *Appl. Sci. Res.* **A6**, 114–116.

Cossu, C. & Brandt, L. 2004 On Tollmien-Schlichting-like waves in streaky boundary layers. *Eur. J. Mech./B Fluids* **23**, 815–833.

Dandy, D. S. & Dwyer, H. A. 1990 A sphere in shear flow at finite reynolds number: effect of shear on particle lift, drag, and heat transfer. *J. Fluid Mech.* **216**, 381–400.

Ellingsen, T. & Palm, E. 1975 Stability of linear flow. *Phys. Fluids* **18**, 487–488.

Elofsson, P. A., Kawakami, M. & Alfredsson, P. H. 1999 Experiments on the stability of streamwise streaks in plane Poiseuille flow. *Phys. Fluids* **11**, 915–930.

Farrell, B. F. 1988 Optimal excitation of perturbation in viscous shear flow. *Phys. Fluids* **32**, 2093–2102.

Gustavsson, L. H. 1991 Energy growth of three-dimenisonal disturbances in plane Poiseuille flow. *J. Fluid Mech.* **224**, 241–260.

Henningson, D. S., Lundbladh, A. & Johansson, A. V. 1993 A mechanism for bypass transition from localized disturbances in wall-bounded shear flows. *J. Fluid Mech.* **250**, 169–207.

Landahl, M. T. 1980 A note on an algebraic instability of inviscid parallel shear flows. *J. Fluid Mech.* **98, part 2**, 243–251.

Maxey, M. R. & Riley, J. J. 1983 Equation of motion for a small rigid sphere in a nonuniform flow. *Phys. Fluids* **26**, 883–889.

McLaughlin, J. B. 1991 Inertial migration of a small sphere in linear shear flows. *J. Fluid Mech.* **224**, 262–274.

Mei, R. 1992 An approximate expression for the shear lift force on a spherical particle at finite reynolds number. *Int. J. Multiphase Flow* **18**, 145–147.

Michael, D. H. 1964 The stability of plane Poiseuille flow of a dusty gas. *J. Fluid Mech.* **18**, 19–32.

Orr, W. M. F. 1907 The stability or instability of the steady motions of a perfect

liquid and of a viscous liquid. Part I: A perfect liquid. Part II: A viscous liquid. In *Proc. Roy. Irish Acad. A*, , vol. 27, pp. 9–138.

Reddy, S. C. & Henningson, D. S. 1993 Energy growth in viscous channel flows. *J. Fluid Mech.* **252**, 209–238.

Reddy, S. C., Schmid, P. J., Baggett, J. S. & Henningson, D. S. 1998 On the stability of streamwise streaks and transition thresholds in plane channel flows. *J. Fluid Mech.* **365**, 269–303.

Rudyak, V., Isakov, E. & Bord, E. 1997 Hydrodynamic stability of the poiseuille flow of dispersed fluid. *J. Aerosol Sc.* **82**, 53–66.

Saffman, P. G. 1962 On the stability of laminar flow of a dusty gas. *J. Fluid Mech.* **13**, 120–128.

Saffman, P. G. 1965 The lift on a small sphere in a slow shear flow. *J. Fluid Mech.* **22**, 385–400.

Schmid, P. J. & Henningson, D. S. 2001 *Stability and transition in shear flows*. Springer.

Sproull, W. T. 1961 Viscosity of Dusty Gases. *Nature* **190**, 976–978.

Tchen, C. M. 1947 Mean value and correlation problems connected with the motion of small particles suspended in a turbulent fluid. PhD thesis, Delft.

Trefethen, L. N., Trefethen, A. E., Reddy, S. C. & Driscoll, T. A. 1993 Hydrodynamic stability without eigenvalues. *Science* **261**, 578–584.

Vreman, A. W. 2007 Macroscopic theory of multicomponent flows: Irreversibility and well-posed equations. *Physica D* **225**, 94–111.

Waleffe, F. 1995 Hydrodynamic stability and turbulence: Beyond transients to a self-sustaining process. *Stud. Appl. Math.* **95**, 319–343.

Zhao, L. H., Andersson, H. I. & Gillissen, J. J. J. 2010 turbulence modulation and drag reduction by spherical particles. *Phys. Fluids* **22**, 081702.

2

Paper 2

Modal and non-modal stability analysis of a channel flow seeded with light particles

By Joy Klinkenberg[1,2], H.C. de Lange[1] and Luca Brandt[2]

[1]TU/e, Mechanical Engineering, 5600 MB, Eindhoven, The Netherlands

[2]Linné FLOW Centre, KTH Mechanics
SE-100 44 Stockholm, Sweden

Submitted to: European Journal of Mechanics B/Fluids

Both modal and non-modal stability analysis of a channel flow laden with light particles is presented. The particles are assumed spherical and solid and their presence modeled using two-way coupling, with Stokes drag, added mass and fluid acceleration as coupling terms. The Stokes drag is a function of particle relaxation time and mass fraction, while added mass and fluid acceleration are a function of mass fraction and density ratio. When the particles considered have a density ratio of order one, all three terms are important. Modal analysis shows a decrease in critical Reynolds number proportional to the mass fraction for all particle relaxation times at a density ratio of one. Lighter particles decrease the critical Reynolds number further, whereas heavier particles might increase the critical Reynolds number. Most effect is found when the stability Stokes number is of order one. Non-modal analysis shows that the transient growth of the total system is enhanced in proportion to the particle mass fraction, as observed in flows laden with heavy particles. The generation of streamwise streaks is still the most dominant disturbance-growth mechanism in particle laden flows with light particles. Thus, the presence of particles may not work to delay the transition.

1. Introduction

Particle laden flows are found in our environment and many applications deal with these, such as turbines. Indeed, significant efforts have been recently devoted to the study of particles in turbulence as reviewed by Toschi & Bodenschatz (2009) and Balachandar & Eaton (2009). In the early '60, it has been shown that adding dust to a pipe flow reduces the drag (Sproull 1961). As an explanation for this phenomenon, it has been proposed that the interaction between fluid and particles dampens the initiation and growth of disturbances which then leads to turbulent structures. Turbulent structures enhance drag, thus, if turbulence is delayed, drag can be reduced. Drag reduction in turbulent

flow has been found more recently in a channel flow seeded with heavy particles, using Direct Numerical Simulations (Zhao *et al.* 2010). Drag reduction in flows with light particles, e.g. bubbles in a liquid, has been demonstrated in experimental work (McCormick & Bhattacharyya 1973; Jacob *et al.* 2010). Micro-bubbles, which can be modeled as rigid spheres when the bubbles are small enough, have been numerically investigated by Ferrante & Elghobashi (2003) and Xu *et al.* (2002) for a turbulent flow. These found that rigid micro-bubbles reduce the drag.

These findings motivated us to investigate whether the laminar-turbulent transition can be delayed using particles. In a previous paper (Klinkenberg *et al.* 2011) we discussed the case of heavy particles. The interaction term between fluid and particles consisted of Stokes Drag only. This simplification was justified for heavy particles, whose density is much larger than the fluid density. Modal analysis showed stabilization, the critical Reynolds number increased for a large range of particle sizes. The stabilization effect was shown to arise when the ratio of particle relaxation time and the period of the instability, the stability Stokes number, is of order one.
The non-modal analysis showed no sign of stabilization: the energy gain of perturbations of the total system increased with a factor of $(1+f)^2$ for streamwise-independent spanwise-periodic waves, where f is the particle mass fraction. This effect can again be explained using the stability Stokes number: non-modal growth is a slow process, thus the particle relaxation time is much smaller than the disturbance time scale. Therefore, the stability Stokes number is small and the particle has less influence on the non-modal growth. The present study investigates the effect of the other interaction terms, which are important when the densities of fluid and particles are of the same order.

Stability analysis of particle laden flows was first by Saffman (1962). He showed theoretically that adding dust to a gas might stabilize the flow(Saffman 1962). This analysis was used by Michael (1964) to show neutral stability curves for several particle sizes. The particle sizes are described using a relaxation time, the time for a particle to adjust to the flow velocity. Both Saffman and Michael considered a plane parallel Poiseuille flow in which the base flow of particles equals the base flow of the fluid. Both the fluid and the particles are modeled in a Eulerian framework. Besides this, particles are considered spherical and homogeneously distributed.

The neutral stability curves given by Michael confirm the previous analysis by Saffman. He noticed that even larger particles have less effect in the stability. Therefore, an optimal particle relaxation time exists for stabilization. To perform stability analysis for large relaxation times, Rudyak *et al.* (1997) and Asmolov & Manuilovich (1998) extended the research done by Michael. They improved numerical accuracy in channel flow and boundary layer flow using

a different technique based on integration in the complex plane. The general results stay the same: small particles destabilize the flow due to increased density while intermediate-size particles enhance stability. In addition to modal analysis, the more recent paper by Klinkenberg *et al.* (2011) also discusses non modal analysis of the particle laden flow. These authors found that non modal analysis shows that heavy particles have no effect on flow stability, as mentioned above.

Non-modal analysis is a relatively new, but an important tool to predict instabilities. Nowadays it is understood that a perturbation in a shear flow can experience significant transient energy growth (Ellingsen & Palm 1975; Trefethen *et al.* 1993; Reddy & Henningson 1993; Schmid & Henningson 2001). This growth is responsible for the initial linear amplification of disturbances which leads to subcritical transition to turbulence. Non-modal effects can therefore explain the discrepancy observed between the critical Reynolds number for linear instability and the experimental observations of transition in wall-bounded shear flows. We therefore need to use non-modal analysis to gain insight into the stability of flows seeded with light particles.

To perform stability analysis on particle laden flows with light particles, some interaction terms cannot be neglected, which can be with heavy particles. Maxey & Riley (1983)give an overview of the interaction forces in particle laden flows. These forces consist of the Stokes drag, the added mass, the fluid acceleration force (also known as pressure correction force), buoyancy and the Basset history term. The starting point of their analysis is the equation of motion proposed by Tchen (1947) and modified by Corrsin & Lumley (1956). Besides these interaction forces, the Saffman lift force (Saffman 1992) is present, as discussed by several authors (Dandy & Dwyer 1990; Mei 1992; McLaughlin 1991) and more recently by Boronin & Osiptsov (2008). In addition to these different interaction terms, the effect of finite particle volume, the volume the particles have, is investigated by Vreman (2007) and Boronin (2008).

Although the different forces between fluid and particles have been known for a long time and have been discussed for turbulent flows in several papers, e.g. Calzavarini *et al.* (2009), transitional flows with light particles have not been considered much in literature. Relevant work on transition with the inclusion of particles is done by Matas *et al.* (2003*b*) and Matas *et al.* (2003*a*). They performed experiments on particle laden flows using light particles in a pipe flow, with a density ratio of exactly one. To control transition to start at $Re \approx 2100$ for a clean flow, they inserted a ring at the pipe entrance. Particles of four different sizes were injected into the flow and the Reynolds number at which transition starts, the transitional Reynolds number investigated. These authors found that for large concentrations all particle sizes stabilized the flow, i.e. the transitional Reynolds number increased. For smaller concentrations (volume fraction ≤ 0.2), large particles destabilized the flow, while the smaller

Table 1: Definition of the non-dimensional numbers used.

Φ	$\frac{N_0 \frac{4}{3}\pi r^3}{L^3}$	Volume fraction
ξ	$\frac{\rho_f}{\rho_p}$	Density ratio
f	$\frac{\Phi}{\xi} = \frac{m_p}{m_f}$	Mass fraction
R	$\frac{\rho_f U L}{\mu}$	Reynolds number
S	$\frac{\nu\tau}{L^2} = \frac{2}{9}\frac{r^2}{L^2}\frac{\rho_p}{\rho_f}$	Relaxation time
SR	$\frac{U\tau}{L}$	Stokes number

particles ($d/D \leq 70$) stabilized the flow. Interestingly, in the range of small particles, the results became independent of the particle diameter.

The aim of this paper is to investigate the linear stability for flows laden with light particles using both modal and non-modal analysis. We consider several interaction terms between fluid and particles and show how these terms influence the stability of the flow. The interaction terms considered in this paper are the Stokes drag, the added mass and the fluid acceleration. To perform our analysis, we adopt the model introduced by Maxey & Riley (1983), rewritten into a Eulerian framework. While this continuous approach is likely to fail in turbulent flows, due to particle clustering and singularities in the particle field, it can still be used for laminar flow with a perturbation, such as in linear stability calculations (Boffetta *et al.* 2007).

2. Flow model and analysis

A numerical stability analysis is performed in which a channel flow is considered seeded with small, spherical particles.

2.1. *Governing equations*

The equations used are the Navier Stokes Equations with the addition of several interaction terms, written in a Eulerian framework. In the following, every term is made non-dimensional with the channel half-width L, centerline velocity U, fluid density ρ_f and the fluid viscosity μ. The dimensionless numbers used throughout this paper are defined in Table 1, where ρ_p is the particle density, r the particle radius and N_0 the number of particles present in the flow.
The Reynolds number and the non-dimensional relaxation time S are both used; these two can also be combined into the Stokes number SR. The momentum equations finally read:

$$\frac{du_{p_i}}{dt} = \xi \frac{Du_i}{Dt} - \frac{1}{2}\xi\left[\frac{du_{p_i}}{dt} - \frac{Du_i}{Dt}\right] + \frac{1}{SR}\left(u_i - u_{p_i}\right), \tag{1}$$

$$\frac{Du_i}{Dt} = -\frac{\partial p}{\partial x_i} + \mu\frac{\partial^2 u_i}{\partial x_j^2} - f\xi\frac{Du_i}{Dt} - \frac{1}{2}f\xi\left[\frac{Du_i}{Dt} - \frac{du_{p_i}}{dt}\right] + \frac{f}{SR}\left(u_{p_i} - u_i\right). \quad (2)$$

The terms on the right hand side of the particle momentum, equation (1), are the fluid acceleration term, added mass and Stokes drag, respectively. All these terms can also be found in the momentum equation of the fluid. The derivative D/Dt is used for the total derivative following a fluid element, while d/dt is used for the total derivative following a moving particle. In addition to the momentum equations, conservation of mass is necessary to close the system; for particles and fluid these read

$$\frac{\partial f}{\partial t} = -div(fu_{p_i}) \quad (3)$$

$$\frac{\partial u_i}{\partial x_i} = 0 \quad (4)$$

A small perturbation (u') to a base flow (U) is introduced, where the base flow is considered to be a parallel Poiseuille flow, $U = U(y) = 1 - y^2$, with $y \in [-1, 1]$. The particle base flow is equal to the fluid base flow, independent of the number of particles. Substituting $u_i = U + u_i'$, $u_{p_i} = U + u_{p_i}'$, $p = P + p'$ and $f = f' + f$ in equations(2-4), linearized stability equations are derived in a standard way (Schmid & Henningson 2001). These read (primes are omitted):

$$\frac{\partial u_i}{\partial t} = -\frac{\partial p}{\partial x_i} - U_j\frac{\partial u_i}{\partial x_j} - u_j\frac{\partial U_i}{\partial x_j} + \frac{1}{SR}\frac{\partial^2 u_i}{\partial x_j^2} + \frac{f}{SR}\left(u_{p_i} - u_i\right) + AM_f + FA_f \quad (5)$$

$$\frac{\partial u_{p_i}}{\partial t} = -U_j\frac{\partial u_{p_i}}{\partial x_j} - u_{p_j}\frac{\partial U_i}{\partial x_j} + \frac{1}{SR}\left(u_i - u_{p_i}\right) + AM_p + FA_p \quad (6)$$

$$\frac{\partial f'}{\partial t} = -div(f'U + fu_{p_i}) \quad (7)$$

$$\frac{\partial u_i}{\partial x_i} = 0. \quad (8)$$

with AM and FA the Added Mass and Fluid Acceleration, with subscripts $_f$ and $_p$, denoting fluid and particle respectively:

$$AM_f = -\frac{1}{2}f\xi\left(\frac{\partial u_i}{\partial t} + U_j\frac{\partial u_i}{\partial x_j} + u_j\frac{\partial U_i}{\partial x_j} - \frac{\partial u_{p_i}}{\partial t} - U_j\frac{\partial u_{p_i}}{\partial x_j} - u_{p_j}\frac{\partial U_i}{\partial x_j}\right) =$$

$$= -\frac{1}{2}f\xi\left(\frac{\partial}{\partial t}\left(u_i - u_{p_i}\right) + U_j\frac{\partial}{\partial x_j}\left(u_i - u_{p_i}\right) + \left(u_i - u_{p_i}\right)\frac{\partial U_i}{\partial x_j}\right), \quad (9)$$

$$FA_f = -f\xi\left(\frac{\partial u_i}{\partial t} + U_j\frac{\partial u_i}{\partial x_j} + u_j\frac{\partial U_i}{\partial x_j}\right), \quad (10)$$

$$AM_p = -\frac{AM_f}{f}, \quad (11)$$

$$FA_p = -\frac{FA_f}{f}. \quad (12)$$

For the configuration considered, the equation for the particle mass fraction f (equation 7) is decoupled from the rest of the system. As a consequence, Squires theorem can be extended to this case and a complex Orr-Sommerfeld equation can be derived. (Boronin 2008) This has been done by Saffman (1962) and Michael (1964) for heavy particles, but the approach cen be extended to incorporate the added mass and fluid acceleration. However, we are also interested in non-modal stability of the full three-dimensional problem and therefore consider the corresponding initial value problem. The fluid velocities are rewritten into wall-normal velocity v and wall-normal vorticity $\eta = \frac{\partial u}{\partial z} - \frac{\partial w}{\partial x}$, analogous to the standard Orr-Sommerfeld-Squire system used for parallel monophase flows. This is done by eliminating the pressure from Equation 5 and by solving $\frac{\partial u}{\partial z} - \frac{\partial w}{\partial x}$. The corresponding total system of particle and fluid equations then reads:

$$\begin{aligned}
&\left(1+\frac{3}{2}f\xi\right)\frac{\partial}{\partial t}\bigtriangledown^2 v - \frac{1}{2}f\xi\frac{\partial}{\partial t}Q = \\
&= \left\{-\left(1+\frac{3}{2}f\xi\right)\left[U\frac{\partial}{\partial x}\bigtriangledown^2 - U''\frac{\partial}{\partial x}\right] - \frac{f}{SR}\bigtriangledown^2 + \frac{1}{R}\bigtriangledown^4\right\} v + \\
&+ \frac{1}{2}f\xi\left[-U''\frac{\partial v_p}{\partial x} - U'\frac{\partial}{\partial x}\bigtriangledown\cdot\vec{u}_p + U\frac{\partial}{\partial x}Q\right] + \frac{f}{SR}Q
\end{aligned} \tag{13}$$

$$\begin{aligned}
&\left(1+\frac{3}{2}f\xi\right)\frac{\partial\eta}{\partial t} - \frac{1}{2}f\xi\frac{\partial}{\partial t}\left(\frac{\partial u_p}{\partial z} - \frac{\partial w_p}{\partial x}\right) = \\
&= -\left(1+\frac{3}{2}f\xi\right)\left(U\frac{\partial\eta}{\partial x} + U'\frac{\partial v}{\partial z}\right) + \frac{1}{2}f\xi\left(U'\frac{\partial v_p}{\partial z} + U\frac{\partial}{\partial x}\left(\frac{\partial u_p}{\partial z} - \frac{\partial w_p}{\partial x}\right)\right) + \\
&+ \frac{f}{SR}\left(\frac{\partial u_p}{\partial z} - \frac{\partial w_p}{\partial x} - \eta\right) + \frac{1}{R}\bigtriangledown^2\eta
\end{aligned} \tag{14}$$

with

$$Q = \frac{\partial^2 v_p}{\partial x^2} + \frac{\partial^2 v_p}{\partial z^2} - \frac{\partial^2 u_p}{\partial x \partial y} - \frac{\partial^2 w_p}{\partial z \partial y} \tag{15}$$

The boundary conditions of this system are $v = \eta = u_p = v_p = w_p = 0$ at top and bottom walls.

2.2. *Modal analysis*

To study linear stability, we assume wave-like perturbations in the following form:

$$q = \hat{q}(y)e^{i(\alpha x + \beta z - \omega t)},$$

with $q = (v, \eta, u_p, v_p, w_p)^T$. In the expression above, α and β define the streamwise and spanwise wavenumber of the perturbation respectively and ω is a complex frequency. The temporal problem is considered here: when $\Im(\omega) > 0$, the perturbation will grow exponentially in time. Conversely, when all $\Im(\omega) < 0$, all disturbances decay asymptotically, i.e. the flow is stable. The point where

$\omega_i = 0$, is called neutrally stable. When computing ω_i in a range of wavenumbers α and Reynolds numbers, a neutral stability curve can be obtained. This curve defines the range where exponentially unstable waves can be found. As mentioned earlier, the neutral stability curve can be computed assuming two-dimensional perturbations, since a modified version of Squire's theorem holds for the modified Orr-Sommerfeld equation (Saffman 1962; Boronin 2008).

2.3. *Non-modal analysis*

Transient growth exists when the eigenvectors of the system are non-normal. This is also the case in systems which are asymptotically stable. To investigate transient growth, non-modal analysis is necessary. Non-modal analysis determines the largest possible growth of a perturbation in a finite time interval, also called optimal growth. The initial disturbance yielding optimal growth is called an optimal initial condition.

The governing linear equations can be written in compact form as:

$$\frac{\partial q}{\partial t} = Lq. \tag{16}$$

The largest possible growth at time t is the norm of the evolution operator, or propagator, $\mathcal{T} = \exp(tL)$. This propagator takes any initial condition from $t = 0$ to a specified final time t. The maximum amplification is defined as:

$$\max_{q_0} \frac{||q||}{||q_0||} = \max_{q_0} \frac{||\exp(tL)q_0||}{||q_0||} = ||exp(tL)|| \equiv G(t). \tag{17}$$

The norm used should be relevant to our problem. Therefore we use the kinetic energy of the full system defined as the kinetic energy of the fluid and of the particles together:

$$E_{kin} = \frac{1}{2}\left(m_f u_i^2 + m_p u_{p_i}^2\right), \tag{18}$$

with m_f and m_p the mass of the fluid and the particles respectively.
A matrix M can be constructed to compute the kinetic energy. This matrix M is applied directly to the vector $q = [v, \eta, u_p, v_p, w_p]^T$ to give the kinetic energy integrated over the volume V

$$E(t) = \frac{1}{2}\int_\Omega q^H M q dV. \tag{19}$$

With this definition the optimal growth is defined as the 2-norm of the modified propagator

$$\max_{q_0} \frac{||q||_E}{||q_0||_E} = \max_{q_0} \frac{||Fq||_2}{||Fq_0||_2} = \max_{q_0} \frac{||F\exp(tL)F^{-1}Fq_0||_2}{||Fq_0||_2} = ||Fexp(tL)F^{-1}||_2 \equiv G(t) \tag{20}$$

where F is the Cholesky factorization of $M = FF^H$.

As in our previous study, we are not only interested in optimizing the total energy of the system, but also wish to investigate the optimal growth when perturbing only the fluid or particle velocity. In this case, we do not consider the total kinetic energy of the system, but only a part of it, depending on the initial condition and final state chosen. This separation can be achieved by including either fluid or particle energy when computing the optimal growth (Klinkenberg *et al.* 2011). The optimizarion can be written as

$$G(t) = \frac{||q_{out}(t)||_{E_{out}}}{||q_{in}(0)||_{E_{in}}} = \frac{||\mathcal{T} q_{in}(0)||_{E_{out}}}{||q_{in}(0)||_{E_{in}}} = \frac{||F_{out}\mathcal{T} q_{in}(0)||_2}{||F_{in} q_{in}(0)||_2} =$$
$$= \frac{||F_{out}\mathcal{T} F_{in}^{-1} F_{in} q_{in}(0)||_2}{||F_{in} q_{in}(0)||_2} = ||F_{out}\mathcal{T} F_{in}^{-1}||_2. = ||F_{out} C \exp(tL) B F_{in}^{-1}||_2 \quad (21)$$

Here, propagator $\mathcal{T} = C\exp(tL)B$ is rewritten to include the input and output operators. The input is $q_{in} = Bq$, while $q_{out} = Cq$ is the output we are interested in. The energy norm must be separated likewise, $M_{in} = F_{in}F_{in}^H$ is applied to q_{in} to measure the input energy while $M_{out} = F_{out}F_{out}^H$ gives the output energy. In the classic non-modal analysis discussed, $F_{in} = F_{out}$ and $C = B = I$.

2.4. *Numerical method*

The discretization in y-direction of the equations is done using the Chebyshev collocation method (Reddy *et al.* 1998). Most computations are performed using $n_y = 37$, with n_y the number of collocation points. Several cases have also been computed with $n_y = 67$ to validate the accuracy of the results.

For the transient growth computation, we made use of the following energy matrix M:

$$M = \begin{pmatrix} \left(-\frac{D^2}{k^2} + 1\right) I_w & 0 & 0 & 0 & 0 \\ 0 & \frac{1}{k^2} I_w & 0 & 0 & 0 \\ 0 & 0 & f I_w & 0 & 0 \\ 0 & 0 & 0 & f I_w & 0 \\ 0 & 0 & 0 & 0 & f I_w \end{pmatrix}. \quad (22)$$

In the expression above, I_w is the diagonal matrix performing spectral integration in y direction. This matrix can be easily factorized using a singular value decomposition (SVD): $M = U\Sigma U^H = FF^H$.

3. Results

3.1. *Modal analysis*

The results for modal stability analysis are given in Figure 1, where we display the critical Reynolds number versus the particle relaxation time. When the density ratio $\xi = 1$, the particles act as a passive tracer: no change is found in the critical Reynolds number, except for a shift corresponding to the mass

the particles add to the system $(1 + f)$. When the particles are heavier than the fluid, the critical Reynolds number is enhanced. The largest stabilization is found when considering heavy particles and the only relevant interaction term is the Stokes drag. Particles lighter than the fluid ($\xi > 1$ and still rigid in our model) behave oppositely to heavy particles and decrease the critical Reynolds number. The results in Figure 1(b) shows that the largest is found when the stability Stokes number $SR\omega_r \approx 1$. The stability Stokes number is defined as the Stokes number times the period of the disturbance wave. The stability Stokes number therefore, is the ratio between the particle relaxation time and the timescale of the disturbance.

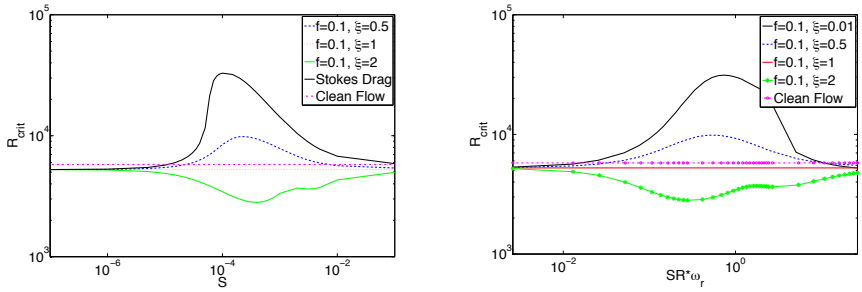

Figure 1: Critical Reynolds number as a function of S and $SR\omega_r$ for light particles using both added mass and fluid acceleration: ξ=[0.5, 1, 2], $f = 0.1$.

To gain further understanding on the modal stability, we examine the critical Reynolds number as a function of density ratio in Figure 2(a and b). The size of the particles is prescribed together with the volume fraction in panel (a) and the mass fraction in panel (b). When fixing the particle volume fraction, three different regimes can be distinguished. For small values of ξ ($\xi < 0.02$) the critical Reynolds number is only a function of r/L and ξ, not of Φ: this is the case of heavy particles. For large values of ξ ($\xi > 0.6$) the particles are so light that they have basically no influence on the flow. When $\xi > 1$, the critical Reynolds number decreases $R_{crit,clean}/(1+f)$. In the region in between those two extremes, particles do have an effect on the stability and the critical Reynolds number is increased.

When prescribing the mass fraction (fig. 2b), we can clearly distinguish between the three values used: the larger the mass fraction, the larger the critical Reynolds number. On the other hand, when the particle size is larger the maximum critical Reynolds number is lower. Also, with larger particles the maximum stabilization is reached for larger values of ξ. The latter finding can be explained by the definition of S, which is a function of the particle size.

The largest stabilization is is indeed for stability Stokes number of order one, as shown above.

In figure 2(c) we display the critical Reynold snumber versus the particle size normalized with the channel half width, r/L. If we consider small particles, the critical Reynolds number is not increasing. Since S is too small, we only see the effect of increasing density: the critical Reynolds number is decreased by a factor $(1+f)$. When particle size increases, on the other hand, we see the largest critical Reynolds number for values in the range $r/L = 0.001 < r/L < 0.01$. The size at which the critical Reynolds number is maximum is related to the density ratio: the particle relaxation time S depends linearly on $\xi = \Phi/f$. The data for heavy particles are obtained using Stokes drag only; fixing the same volume and mass fraction as for light particles $\xi = \Phi/f$ and the size is defined by $r/L = \sqrt{9/2S\xi}$ as a function of S. The forces important at lower density ratio decrease the critical Reynolds number of the system as seen in 2(d), where the critical Reynolds number is given as a function of SR with prescribed size and mass fraction (cf. fig.2 b). We can see that heavy particles induce a larger critical Reynolds number than light particles. Also, a sharp edge is present at $SR \sim 10$: the ballistic limit. In this region the particles are heavy and we can use the heavy particle approximation.

The effect of added mass and fluid acceleration on the critical Reynolds number is examined in Figure 3. The added mass term shows the same trend as obtained with Stokes drag only: the critical Reynolds number is enhanced, see Figure 3(a). When the particles become heavier, the stability curve computed with added mass overlaps with that for heavy particles. The figure indicates that the lighter the particle, the lower the critical Reynolds number when considering only added mass. Figure 3(b) shows the results obtained considering fluid acceleration and Stokes drag: particles seems not to affect the flow when they are neutrally buoyant; only the density of the system increases by a factor $(1 + f)$. Lighter particles destabilize the flow and reduce the critical Reynolds number, as shown for $\xi = 2$.
The results obtained including the fluid accelaration are similar to those shown before when all terms are used. Apparently, the fluid acceleration term is the most dominant force in the system.

3.2. *Non-modal analysis*

Results of the non-modal analysis are presented in Figure 4. The only cases presented are $fluid \rightarrow fluid$ and $all \rightarrow all$. The first case only investigates the transient growth of the fluid energy when the initial condition consists of fluid perturbation only; the optimal growth of the fluid disturbance velocity is studied. The particles are in the system and can gain energy, but this is not apparent. In the case $all \rightarrow all$, the total energy of the two-phase system is investigated and particles may also have some initial disturbance velocity.

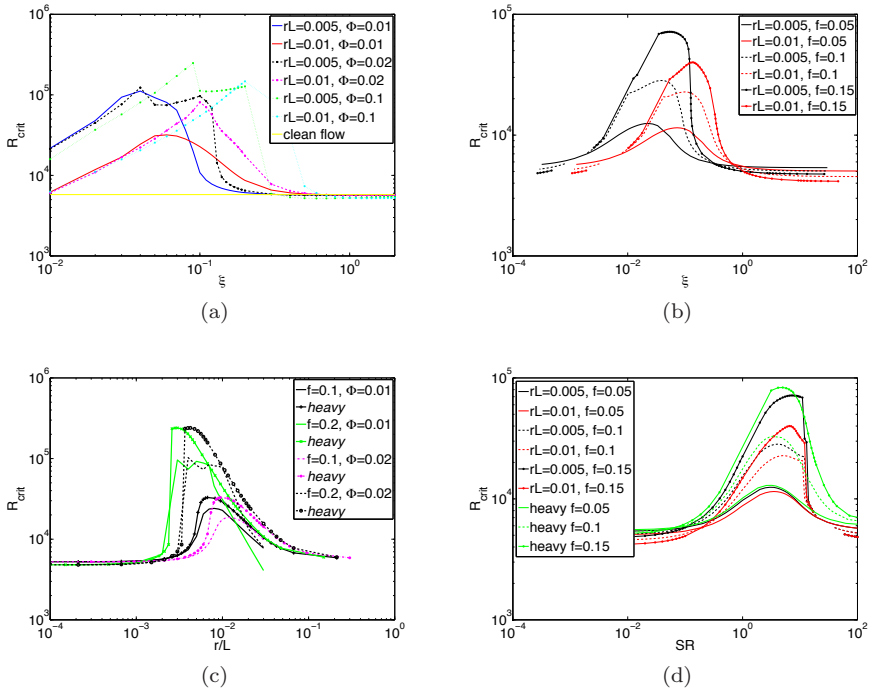

Figure 2: Critical Reynolds number as a function of the density ratioξ (a-b), the particle size r/L and the Stokes number SR(d). In (c) and (d) we report also the results for heavy particles. Note that the data in (b) and (d) pertain the same particle sizes and mass fractions.

In Figure 4(a), we display the optimal growth as a function of spanwise wave-number β, the streamwise wave-number α is set to zero. The data represent the maximum over the final optimization time. The computations are performed for 2D waves as well; since the transient growth of these streamwise waves is two orders smaller than for spanwise waves the results will be presented later. The density ratios under consideration are those used also in the modal analysis, $\xi = [0.5,\ 1,\ 2]$. The results with all extra forces included are similar to those of heavy particles, namely there is no significant effect of particles on the streak transient growth. The optimal growth is equal, irrespective of whether only Stokes drag is used, or whether the system includes added mass and fluid acceleration. In the second figure, Figure 4(b), the particle size and total volume is set, while the density ratio is changed along the horizontal axis. For small values of ξ, the mass fraction is very high and thus the growth for the case *all* $\rightarrow$ *all* is higher. As shown in Klinkenberg *et al.* (2011) for heavy particles, the maximum possible amplification is proportional to $(1+f)^2$. The

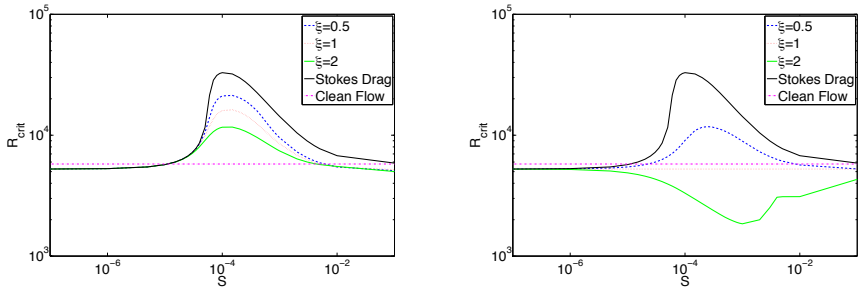

(a) Added mass (b) Fluid acceleration

Figure 3: Critical Reynolds number vs. relaxation time S for particles of density ratio ξ=[0.5, 1, 2] and mass fraction $f = 0.1$. As reference, we display the results for clean flow and heavy particles (Stokes drag only).

larger ξ gets, the smaller the mass fraction and therefore the smaller the optimal growth, approaching the case of clean fluid.

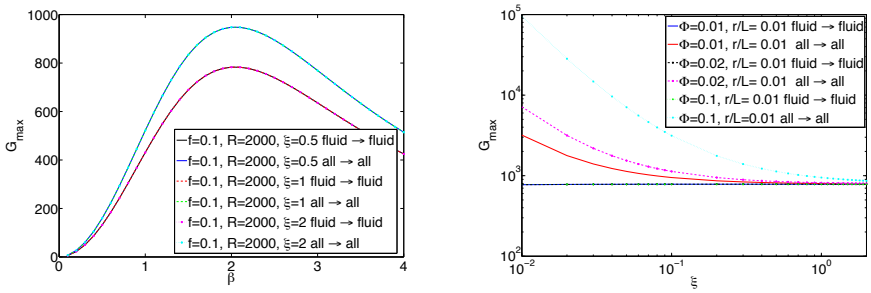

(a) (b)

Figure 4: a: Optimal growth (G_{max}) as a function of spanwise wave-number β at $S = 5 \cdot 10^{-5}$, $f = 0.1$ and $R = 2000$. The cases $fluid \rightarrow fluid$ and $all \rightarrow all$ are presented for $\xi = [0.5,\ 1,\ 2]$. b: Optimal growth as a function of ξ using $\beta = 2$ at $S = 5 \cdot 10^{-5}$ and $R = 2000$

The effect of the added mass and fluid acceleration on the streak transient growth is further investigated for several values of S using $\beta = 2$, where the optimal growth is at a maximum. These results can be found in Figure 5. The case $all \rightarrow all$ with $f = 0.1$ starts to deviate considerably from $S = 1 \cdot 10^{-2}$; this is due to the decoupling of particle and fluid behavior as discussed for heavy particles (Klinkenberg *et al.* 2011). Apparently the two extra terms do not have

much influence on the growth at large values of S and the results are consistent with those for heavy particles. One can note that the energy amplification is larger when considering both fluid and particle energy ($all \rightarrow all$) than for fluid alone ($fluid \rightarrow fluid$). Finally, figure 5(a) shows that at fixed mass fraction, the energy growth for the $fluid \rightarrow fluid$ case is almost equal to that for clean fluid and heavy particle flow. Only at very large values of S the optimal growth deviates a few percent in the presence of particles, as shown later in more detail. If we prescribe the volume fraction and particle size, the maximum growth goes as $(1+f)^2$ as displayed in Figure 5(b) where the largest values of f occur at large S. This could be seen if plotting $G/(1+f)^2$ instead of G.

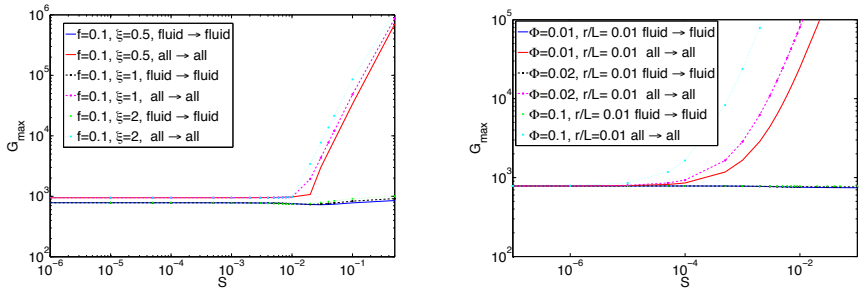

(a) f and ξ (b) r/L and Φ

Figure 5: Optimal growth (G_{max}) as a function of S, using $\beta = 2$, $R = 2000$ and (a) $f = 0.1$, $\xi = [0.5,\ 1,\ 2]$ and (b) $\Phi = [0.01,\ 0.1,\ 0.2]$, $r/L = [0.005,\ 0.01]$. The cases $fluid \rightarrow fluid$ and $all \rightarrow all$ are presented

To investigate the structures of the disturbances, we display the optimal initial condition and response in Figure 6 for the case $fluid \rightarrow fluid$, $S = 1{\cdot}10^{-2}$. The velocity field at final time of particles and fluid are almost identical to each other and to the case of clean fluid (not shown here). Since differences in velocity induce a loss in energy, particles and fluid have similar velocity in optimal configurations; light particles do not induce any additional gain or loss in disturbance energy.

We therefore demonstrated how light particles have no effect on the non-modal stability of spanwise waves, confirming the results previously obtained for heavy particles; we now investigate streamwise and oblique disturbances. Even though these disturbances grow less than purely spanwise disturbances, they might be important for transition in real configurations, e.g. when transition is initiated by localized disturbances. The effect of particles on these is therefore worth investigation. Figure 7 shows the results for several streamwise α and spanwise wavenumbers β. When both are nonzero, the waves are oblique. The values of the maximum possible amplification are reported in the table, while the plots display the relative variation with respect to the case of clean

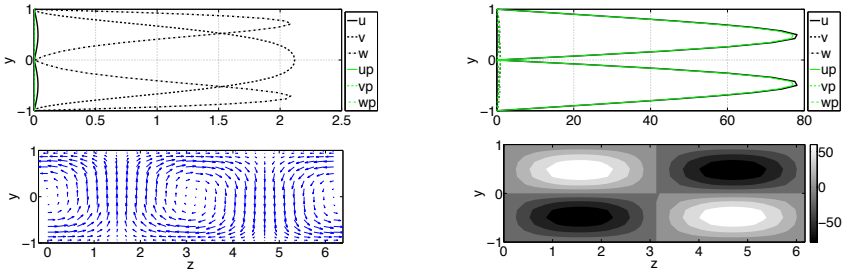

(a) Initial condition (b) Response

Figure 6: Initial condition and response for $S = 1 \cdot 10^{-2}$. Case $fluid \rightarrow fluid$ with $\xi = 1$, $\beta = 2$, $R = 2000$ and $f = 0.1$

fluid. We first consider small values of SR: for streamwise waves, particles induce a decrease in transient growth of order $(1+f)$ (case $fluid \rightarrow fluid$), while spanwise waves show no difference between laden and unladen flow. For oblique waves, the results lie in between these two extremes. For slightly oblique waves ($\beta = 2, \alpha = 0.1$), we observe the lowest relative loss of energy growth. The magnitude of this loss increases for larger values of α.

When increasing the Stokes number, we see a clear decrease of transient growth when compared to the case of single phase fluid. This occurs at lower SR for two-dimensional and at larger values of SR for disturbances approaching spanwise waves. This stabilization effect is observed for values of the stability Stokes number, defined by the time giving the largest amplification, of order one; so at lower Stokes for modes with $\beta = 0$ for which the transient growth is faster, and at higher Stokes for modes with $\alpha = 0$ for which the transient growth is a slower process. This stabilization is the counterpart of the increase of critical Reynolds number shown by the modal analysis. Note however, as discussed in the next section, that the values of the Stokes number necessary to observe this stabilization can be related to parameters outside the range of validity of our model. When farther increasing the particle relaxation time, we observe an increase of the transient growth (values larger than 1 in the figure). Again, we note that this is however happening for particle size too large for our model to be valid. The relative increment of the transient growth can be explained by the fluid acceleration term; the Stokes drag goes to zero as SR tends to infinity.

4. Discussion

The modal analysis reveals differences between light and heavy particles: the different interaction terms may have a large influence on the computed critical

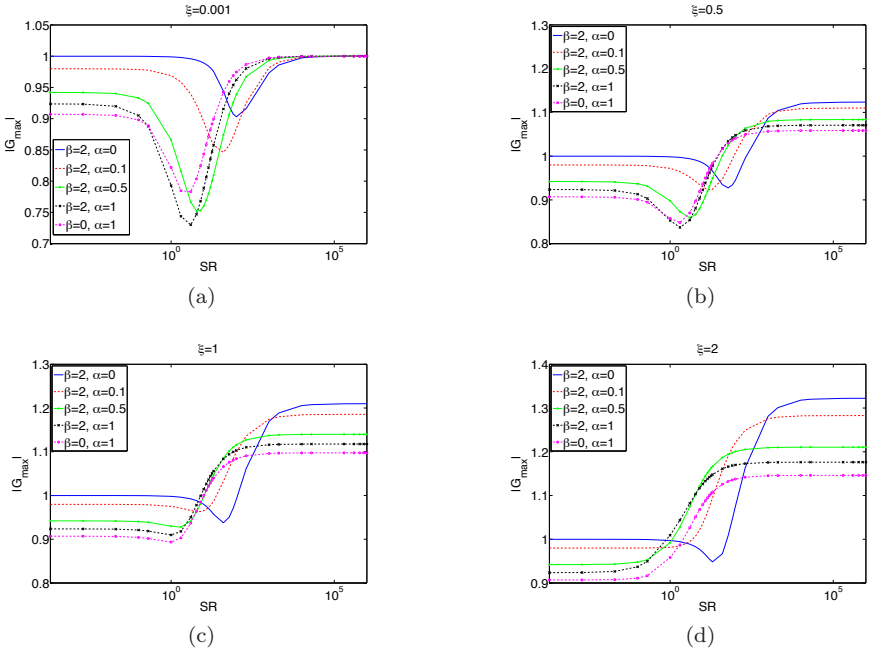

Case	Clean flow growth
$\beta = 2,\ \alpha = 0$	783.24
$\beta = 2,\ \alpha = 0.1$	664.14
$\beta = 2,\ \alpha = 0.5$	346.71
$\beta = 2,\ \alpha = 1$	193.87
$\beta = 0,\ \alpha = 1$	13.76

Figure 7: Transient growth of oblique waves normalised with the growth rate of a clean flow as a function of SR for $fluid \rightarrow fluid$ and $f = 0.1$. The values of the amplification for a single phase fluid are reported in the table.

Reynolds number. As shown in previous studeis, Stokes drag can induce a significant delay of the instability onset for certain particle relaxation times. The added mass term has the least influence on the critical Reynolds number when used in combination with the Stokes Drag. The fluid acceleration has a more complicated effect. When $\xi = 1$, neutrally buoyant particles, the additional mass of the particles reduces the critical Reynolds number. This is similar to the effect at small values of S when heavy particles are considered (Klinkenberg *et al.* 2011) where it can be explained by looking at the total energy budget. Particles lighter than the fluid destabilize the flow, while heavier particles induce lower stabilization when acceleration term is considered. When taking the added mass and fluid acceleration into account, the fluid acceleration term has

most influence. The particles can be seen more as a passive tracer within the fluid, and the stabilizing effect on the critical Reynolds number decreases.

Non-modal analysis gives a different result than modal analysis. For heavy particles, when Stokes drag is used as only interaction term, the total transient growth for spanwise waves is larger with a factor of $(1+f)^2$ for the case $all \rightarrow all$ with respect to a clean fluid flow, up to large values of S. This can be explained by the increased Reynolds number due to the increased density of the total system. The optimal condition is that particles and fluid have equal velocities in order to minimize energy losses. When implementing extra interaction terms, this result is still true. Independent of which interaction forces one takes into account, the optimal growth is equal up to $S = 10^{-2}$. At larger values of S, the equations decouple and the particle energy can grow infinitely in the linear model, because the only dissipative terms in the particle momentum equation stems from the forces exchanged with the fluid.
When we look at streamwise-dependent disturbances, for which modal analysis reveals an increase of the critical Reynolds number, the optimal growth $fluid \rightarrow fluid$ is smaller by a factor of $(1+f)$ when compared to that in a clean fluid flow. Table 2 shows the relation of the optimal growth of particle laden flows versus clean fluid for both spanwise and streamwise waves for small values of S. We recall that the transient growth is at least one order of magnitude larger for spanwise-periodic streamwise-independent modes. The extra

Table 2: Dependence of the optimal growth on mass fraction f for streamwise and spanwise disturbances.

case	spanwise	streamwise
$all \rightarrow all$	$(1+f)^2$	$(1+f)^1$
$all \rightarrow fluid$	$(1+f)^1$	$(1+f)^0$
$fl \rightarrow fl$	$(1+f)^0$	$(1+f)^{-1}$

interaction terms have no influence on the non-modal stability and this appears less obvious than for heavy particles. The energy analysis of heavy particles shows that particle-fluid interaction always induces a loss in kinetic energy. To optimize energy, both the fluid and particles should have equal velocities, which then results in an $(1+f)^2$ increase of the energy gain when the particles act as passive tracers and increase the fluid density. In non-modal analysis the particles act basically as passive tracer up to large values of S because transient growth is a slow process. Therefore, the stability Stokes number is small indicating that particles react to the flow faster than the time needed for the streaks to grow.

So far we reported data for wide variations of the different parameters defining the particle laden channel flow. Now, we discuss the range of validity

of the model we use and the limitations of the results. With the help of figure 8 we consider the size of the particles, the number of particles, the density ratio and the volume fraction of the particles. Investigating these, we see that we have to be careful in choosing S; the system should be physically feasible. The density ratio and the size of the particle are related through $S = \frac{2}{9}\frac{r^2}{L^2}\frac{1}{\xi}$. This means that, if the density ratio is known, we can relate dimensionless relaxation time S to the dimensionless radius of the particle, r/L, where L is the channel half width. Figure 8 (a) shows the values of S for sizes of the particles small enough for the model to apply and for different particle density. The lighter the particles, the larger the particles should be to have the same value of S. Because most particle-fluid interaction occurs at a stability Stokes number of order one, we need larger particles to obtain relevant stability Stokes number for lower density ratios. A problem that might occur is that particles are too big for solely two-way coupling: particle-particle and particle-wall interactions become more important.

Figure 8 (b) shows the volume fraction of the particles, Φ, as a function of the number of particles for different particle sizes. When particles are larger, the amount of particles needed for a certain volume fraction decreases. The amount of particle has to be large enough to have a valid assumption for the Eulerian approach: if we have too few particles, the particles cannot be described by avaraged particle parameters. For example, with a volume fraction $\Phi = 0.1$ and a minimum number of $N = 1000$ particles, the size of the particles becomes $r/L = 0.03$, a particle diameter of 6% of the channel half-width. This diameter is not consistent with our analysis. Or, if the size of the particle is $r/L = 0.01$ and the density ratio of $\xi = 1$, the value of S is small enough that particles only act as in increase in density: no interaction between the particles and fluid can cause a delay in transition.

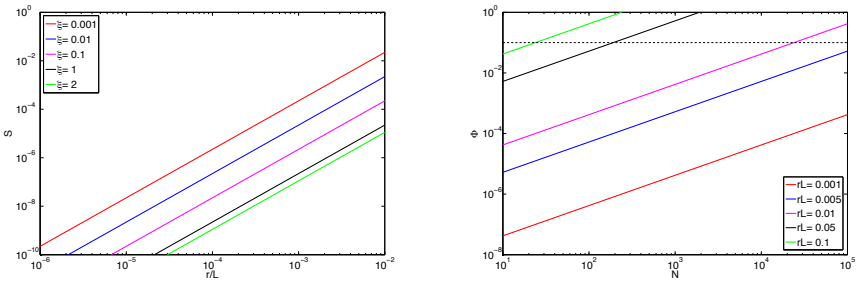

(a) S as a function of r/L

(b) N as a function of Φ

Figure 8: Particle parameters for different values of ξ (a) and for different size of particles r/L (b). N is the number of particles per volume l^3

5. Conclusion

We presented results for linear modal and non-modal stability of channel flow laden with particles of varying density. Light particle behaves differently from heavy particle as concerns the modal growth. Neutrally buoyant particles have almost no effect when taking the fluid acceleration term into account: the particles only act as to increase the density of the suspension. This increase in density then results in a decrease of the critical Reynolds number. The added mass term has less effect on the modal stability than fluid acceleration force, although the added mass decreases the critical Reynolds number. The particles do stabilize the flow compared to the clean fluid flow when the particle relaxation time is of the order of the period of oscillations of the instability. This stabilization decreasing when increasing the ratio between fluid density and particle density.

Non-modal analysis on the other hand does not show a significant difference between light and heavy particles. Streamwise-independent modes can undergo large non-modal growth; this is associated to the amplification of streamwise velocity streaks induced by counter-rotating streamwise vortices. The optimal energy growth is found when the particle and fluid velocity are equal, resulting in an increase of the transient energy growth by a factor $(1 + f)^2$ compared to a clean fluid when considering the total energy of the system. The interaction terms added for light particles do appear in the energy budget but do not affect the whole process; this can be explained by the long time scale associated to the streak lift-up which allows particles to follow the fluid structures.

Finally, we discuss the limitation of the current model and the values of particle relaxation times for which S the results are valid. Although some stabilization may be seen also for transient growth at large values of S, this may happen when the model used might not be valid. Considering also the first part of this investigation (Klinkenberg *et al.* 2011), we see that the presence of a solid phase has no significant effect on the non-modal growth responsible for subcritical transition in channel flows, especially in the case of elongated structures. As a next step, a non-linear model should be used to investigated which shows the effect of particles on secondary instabilities and final breakdown.

References

Asmolov, E. S. & Manuilovich, S. V. 1998 Stability of a dusty-gas laminar boundary layer on a flat plate. *J. Fluid Mech.* **365**, 137–170.

Balachandar, S. & Eaton, J. K. 2009 Turbulent Dispersed Multiphase Flow. *Ann. Rev. of Fluid Mech.* **42**, 111–133.

Boffetta, G., Celanu, A., De Lillo, F. & Musacchio, S. 2007 The eulerian description of dilute collisionless suspension. *Europhysics Letters* **78**, 14001.

Boronin, S. A. 2008 Investigation of the stability of a plane-channel suspension flow with account for finite particle volume fraction . *Fluid Dynamics* **43**, 873–884.

Boronin, S. A. & Osiptsov, A. N. 2008 Stability of a Disperse-Mixture Flow in a Boundary Layer. *Fluid Dynamics* **43**, 66–76.

Calzavarini, E., Volk, R., Bourgoin, M., Lévêque, E., Pinton, J. & Toschi, F. 2009 Acceleration statistics of finite-sized particles in turbulent flow: the role of Faxén forces. *J. Fluid Mech.* **630**, 179–189.

Corrsin, S. & Lumley, J. 1956 On the equation of motion for a particle in turbulent fluid. *Appl. Sci. Res.* **A6**, 114–116.

Dandy, D. S. & Dwyer, H. A. 1990 A sphere in shear flow at finite reynolds number: effect of shear on particle lift, drag, and heat transfer. *J. Fluid Mech.* **216**, 381–400.

Ellingsen, T. & Palm, E. 1975 Stability of linear flow. *Phys. Fluids* **18**, 487–488.

Ferrante, A. & Elghobashi, S. 2003 On the physical mechanisms of two-way coupling in particle-laden isotropic turbulence. *Phys. Fluids* **15**, 315–329.

Jacob, B., Olivieri, A., Miozzi, M., Campana, E. F. & Piva, R. 2010 Drag reduction by microbubbles in a turbulent boundary layer. *Phys. Fluids* **22** (11), 115104.

Klinkenberg, J., de Lange, H. C. & Brandt, L. 2011 Modal and non-modal stability of particle laden channel flow. *Phys. Fluids* **23**, 064110.

Matas, J. P., Morris, J. F. & Guazzelli, E. 2003*a* Influence of particles on the transition to turbulence in pipe flow. *Phil. Trans. R. Soc. Lond. A* **361**, 911–919.

Matas, J. P., Morris, J. F. & Guazzelli, E. 2003*b* Transition to turubulence in particulate pipe flow. *Phys. Rev. Lett.* **90**, 014501.

Maxey, M. R. & Riley, J. J. 1983 Equation of motion for a small rigid sphere in a nonuniform flow. *Phys. Fluids* **26**, 883–889.

McCormick, M. E. & Bhattacharyya, R. 1973 Drag reduction of a submersible hull by electrolysis. *Naval Engineers Journal* **85** (2), 11–16.

McLaughlin, J. B. 1991 Inertial migration of a small sphere in linear shear flows. *J. Fluid Mech.* **224**, 262–274.

Mei, R. 1992 An approximate expression for the shear lift force on a spherical particle at finite reynolds number. *Int. J. Multiphase Flow* **18**, 145–147.

Michael, D. H. 1964 The stability of plane Poiseuille flow of a dusty gas. *J. Fluid Mech.* **18**, 19–32.

Reddy, S. C. & Henningson, D. S. 1993 Energy growth in viscous channel flows. *J. Fluid Mech.* **252**, 209–238.

Reddy, S. C., Schmid, P. J., Baggett, J. S. & Henningson, D. S. 1998 On the

stability of streamwise streaks and transition thresholds in plane channel flows. *J. Fluid Mech.* **365**, 269–303.

Rudyak, V., Isakov, E. & Bord, E. 1997 Hydrodynamic stability of the poiseuille flow of dispersed fluid. *J. Aerosol Sc.* **82**, 53–66.

Saffman, P. G. 1962 On the stability of laminar flow of a dusty gas. *J. Fluid Mech.* **13**, 120–128.

Saffman, P. G. 1992 *Vortex Dynamics*. Cambridge, UK: Cambridge Univ. Press.

Schmid, P. J. & Henningson, D. S. 2001 *Stability and transition in shear flows*. Springer.

Sproull, W. T. 1961 Viscosity of Dusty Gases. *Nature* **190**, 976–978.

Tchen, C. M. 1947 Mean value and correlation problems connected with the motion of small particles suspended in a turbulent fluid. PhD thesis, Delft.

Toschi, F. & Bodenschatz, E. 2009 Lagrangian properties of particles in turbulence. *Ann. Rev. of Fluid Mech.* **41**, 375–404.

Trefethen, L. N., Trefethen, A. E., Reddy, S. C. & Driscoll, T. A. 1993 Hydrodynamic stability without eigenvalues. *Science* **261**, 578–584.

Vreman, A. W. 2007 Macroscopic theory of multicomponent flows: Irreversibility and well-posed equations. *Physica D* **225**, 94–111.

Xu, J., Maxey, M. R. & Karniadakis, G. E. 2002 Numerical simulation of turbulent drag reduction using micro-bubbles. *J. Fluid Mech* **468**, 271–281.

Zhao, L. H., Andersson, H. I. & Gillissen, J. J. J. 2010 turbulence modulation and drag reduction by spherical particles. *Phys. Fluids* **22**, 081702.

Paper 3

3

Numerical Simulations of laminar-turbulent transition in particle-laden channel flow

By Joy Klinkenberg[1,2], Gaetano Sardina[2], H.C. de Lange[1] and Luca Brandt[2]

[1]TU/e, Mechanical Engineering, 5600 MB, Eindhoven, The Netherlands

[2]Linné FLOW Centre, KTH Mechanics
SE-100 44 Stockholm, Sweden

Internal Report

Direct Numerical Simulation of a particle-laden channel flow is performed, with particles assumed solid, spherical and heavy. Two-way coupling between fluid and particles is modeled with Stokes drag. The equations describing the fluid flow are solved with an Eulerian mesh and those describing particles are solved in a Lagrangian frame. The numerical code is validated with results from linear optimal growth from previous studies; the optimal growth of streamwise vortices resulting in streamwise streaks is still the most efficient mechanism for disturbance amplification at subcritical conditions as for the case of a single phase fluid.

We consider transition initiated by two initial disturbances well-known in literature, streamwise vortices and oblique waves. The threshold energy for transition is computed for both cases. It is observed that streamwise vortices in combination with an oblique wave as additional initial disturbance, result in a small increase of threshold energy compared to a clean fluid. In addition, the time at which transition occurs clearly increases for disturbances of equal initial energy. The threshold energy in the case of the so-called oblique scenario, increases by a factor about 4 in the presence of particles. The results are explained by considering the reduced amplification of oblique modes in the presence of particles.

The results from these two classical scenarios indicate that, although stability analysis shows hardly any effect on optimal growth, particles do influence secondary instabilities and streak breakdown, thus the non-linear stages of transition, in two different ways. The presence of particles introduced three-dimensional, streamwise-dependent modulations, especially at low concentrations, that may trigger and enhance secondary instabilities of streamwise-independent streaks. On the other hand, particles decrease the amplitude of oblique modes thus delaying transition initiated by their nonlinear interactions as in the oblique scenario.

1. Introduction

Transition from laminar to turbulent flows has been studied extensively in the past. Linear stability analysis is typically considered a first analysis towards understanding transition. This allows determination of critical values of the relevant adimensional parameters above which exponentially growing disturbances exist. However, in many configurations, e.g. shear flows, transition is subcritical and a full nonlinear analysis is needed. In shear flows, it is possible to show that linear mechanisms are responsible for the instantaneous amplification of perturbation energy and therefore a linear non-modal analysis (Schmid & Henningson 2001) can reveal the mechanisms responsible for transition in linearly stable cases. This was the case with the linear lift-up process that was identified as a key process in wall-bounded flows.

Transition leads to an increase of the drag and is therefore often undesirable. One way to influence the transition scenario is by adding small, heavy particles to the flow (Saffman 1962).
Although many fluid flows are seeded with particles, a lot of research still has to be done to understand the influence of particles on the flow, in particular on laminar-turbulent transition. Recent reviews of particle laden turbulent flows are given by Toschi & Bodenschatz (2009) and Balachandar & Eaton (2009).
A particle in a fluid flow is subject to several different interaction forces (Maxey & Riley 1983). First, there is a drag force between the particle and fluid. When particle and fluid have different velocities, a shear force on the interface is present; this interaction can be modeled using Stokes drag. Furthermore, there are history effects, added mass and fluid correction forces. For larger particle volume fraction, also particle-particle interactions have to be taken into account.

In our previous papers (Klinkenberg *et al.* 2011*b*,*a*) stability of flows with either heavy or light particles were investigated. For a flow with heavy particles only Stokes drag is taken into account. For a flow with light particles, added mass and fluid acceleration need also to be included. We found that particles do not influence the transient growth of disturbances in plane channel flow. This suggested that the initial linear stages of transition may not be affected by the presence of particles. However, the numerical simulations by Zhao *et al.* (2010) demonstrate that adding heavy particles reduces the drag of a turbulent channel flow. The latter result indicates that particles have an effect on turbulent structures. Therefore, although particles show no influence in the initial linear stages of transition, they might have an effect on secondary, non-linear, instabilities. The aim of the present paper is therefore to investigate the effect of solid, spherical particles on the evolution of finite-size disturbances leading to turbulent flow.

To investigate the effect of solid spheres, we use Direct Numerical Simulations of a plane Poiseuille flow extended with a model for two-way coupling between the particles and fluid using Stokes drag as interaction force. By means

of numerical simulations, we investigate the behavior of a finite energy perturbation, instead of the infinitesimal small perturbations as in the non-modal analysis. We investigate how the threshold energy for transition, the minimum initial disturbance energy necessary to reach the turbulent state, varies in the presence of heavy particles. This provides information about the non-linear behavior of streaks and it shows whether the secondary instabilities might be damped by the presence of particles.
In relation to transition thresholds several researchers have considered the 'edge of chaos' (Schneider *et al.* 2007). This is the asymptotic state reached by perturbations, neither decaying to a laminar state nor evolving to turbulence. Near the 'edge of chaos', exact coherent structures are found (Nagata 1990; Waleffe 1998, 2001). The 'edge state' has been investigated more recently by e.g. Duguet *et al.* (2010); Schneider *et al.* (2007); Wang *et al.* (2007); Kawahara (2005); Duguet *et al.* (2008*a*,*b*). A review is given by Eckhardt *et al.* (2007).
The exact coherent structures are also investigated for dilute polymer solutions by Stone *et al.* (2002) for a plane Couette flow. They found that for polymer solutions the exact coherent states are a promising method for capturing the essential physics of drag reduction.

In this paper we examine two transition scenarios previously analysed, see e.g. Reddy *et al.* (1998). First we consider transition initiated by streamwise vortices, without any streamwise dependence. Streamwise vortices initiate largest linear transient growth and they are common in many shear flows (Trefethen *et al.* 1993; Reddy & Henningson 1993; Schmid & Henningson 2001). The transition process initiated by these vortices can be summarizes as in (Reddy *et al.* 1998):

$$\text{streamwise vortices} \Rightarrow \text{streamwise streaks} \Rightarrow \text{streak breakdown} \Rightarrow \text{transition}.$$

Because transition cannot take place without streamwise dependent structures,one needs to consider streamwise-dependent perturbations that trigger streak breakdown and transition. Schoppa & Hussain (2002); Cossu *et al.* (2011) show how simple spanwise modulations of the streak can induce a rapid breakdown.
In the second route to turbulence as discussed by Reddy *et al.* (1998), we consider a pair of oblique optimal waves. Each of these waves grow via the transient growth mechanism so that they can nonlinearly interact. From this interaction we get streamwise independent structures, streamwise vortices, that in turn induce streamwise streaks via the lift-up effect. The scenario is thus equal to the previously discussed scenario of streamwise vortices, but with one extra initial step:

$$\text{oblique waves} \Rightarrow \text{streamwise vortices} \Rightarrow$$

$$\Rightarrow \text{streamwise streaks} \Rightarrow \text{streak breakdown} \Rightarrow \text{transition}.$$

This scenario has been extensively investigated in the past for a clean fluid flow, see e.g. Schmid & Henningson (1992); Berlin *et al.* (1994). Note that the oblique scenario is found to be the most efficient way to trigger turbulence

(see also Duguet *et al.* (2010)) and it is identified also in non-linear optimal localized initial conditions (Cherubini *et al.* 2010; Monokrousos *et al.* 2011)

The paper is set up as follows. First we present the governing equations and the details of our the numerical implementation. Secondly we report the results for the two scenarios described above; before that we validate our numerical implementation with the results from linear theory in Klinkenberg *et al.* (2011*b*).

2. Governing equations and implementation

2.1. *Governing Equations*

The equations of motion for the fluid are modeled in an Eulerian grid, whereas the particles are evolved in a Lagrangian framework. The particles are assumed to be solid, spherical and heavy spheres with a diameter smaller than the smallest flow characteristic length scale. By neglecting the gravity, in the hypothesis of heavy particles, the only significant force acting on a single particle is the Stokes drag (Maxey & Riley 1983). The equations in non-dimensional form are:

$$\frac{\partial u_i}{\partial x_i} = 0, \tag{1}$$

$$\frac{\partial u_i}{\partial t} = -\frac{\partial p}{\partial x_i} - u_j \frac{\partial u_i}{\partial x_j} + \frac{1}{R}\frac{\partial^2 u_i}{\partial x_j^2} + \sum_p \frac{f}{SR}(u_{p_i} - u_i)\delta(x_i - x_{p_i}), \tag{2}$$

$$\frac{dx_{p_i}}{dt} = u_{p_i}, \tag{3}$$

$$\frac{du_{p_i}}{dt} = \frac{u_i - u_{p_i}}{SR}, \tag{4}$$

where u_i is the fluid velocity and u_{p_i} the velocity of one particle. In the equations above, δ is the Dirac delta function, f the mass fraction of particles and $SR = \tau_p \frac{U}{L}$ the Stokes number defined using the convective time scale of the flow with L the channel half-width and U the laminar centerline velocity. The particle relaxation is defined as $\tau_p = \frac{2}{9}\frac{r^2}{\nu}\frac{\rho_p}{\rho_f}$, with r the radius of the particle , ρ_p the density of the particle , ρ_f the fluid density and ν the kinematic viscosity.

The Stokes number is a dimensionless relaxation time multiplied by the Reynolds number. The dimensionless relaxation time based on the flow viscous time scale is defined as $S = \frac{\nu\tau_p}{L^2} = \frac{2r^2\rho_p}{9L^2\rho_f}$ and is only a function of particle size and density ratio. When we set the density ratio at $\xi = \rho_f/\rho_p = 0.001$, particles are considered heavy and we can directly relate the size of the particles to the relaxation time. The size of the particles can then be related to the number of particles (N) using the volume fraction (Φ):

$$\Phi = f\xi,$$

$$N = \frac{\Phi}{4/3\pi r^3}.$$

2.2. *Implementation*

The numerical code is a pseudo-spectral solver in which a plane Poiseuille flow is given as base velocity by imposing a constant mass flux. The velocity components are expanded in both x (streamwise) and z (spanwise) direction with Fourier modes and with Chebyshev polynomials in the wall-normal, or y-direction. To advance Equation 2 in time, we use a fourth order Runge-Kutta algorithm. Boundary conditions in x and z are periodic and no-slip is assumed at both walls, $y = \pm 1$. More details about this code are given in Chevalier *et al.* (2007).
The particles are evolved by means of a Lagrangian Solver and are coupled to the Eulerian grid of the fluid flow. The fluid velocities are interpolated from the Eulerian grid onto the particle positions using a tri-linear interpolation. The time advancement of the particle uses the same Runge-Kutta algorithm as the time-advancement of the fluid. The Stokes drag, forcing also the momentum equation, can be extrapolated back onto the Eulerian grid using the same tri-linear scheme of the interpolation. The particle back reaction is calculated in physical space and added to the nonlinear term, before Fourier transformation back into spectral space.
The streamwise and spanwise dimensions of the domain are $L_x = 2\pi$ and $L_z = 2\pi$. The Reynolds number used in all computations is 2000. The resolution used is typically $64 \times 65 \times 64$ for streamwise, wall-normal and spanwise directions respectively. Several resolutions have been used to investigate the convergence of the solution.

A bisection algorithm is used to find the energy threshold (Toh & Itano 2003; Duguet *et al.* 2008*b*, 2010). The criterion for convergence of the energy threshold is the following:

$$2\frac{A_u - A_l}{A_u + A_l} < 1 \cdot 10^{-5},$$

with A_u and A_l the amplitude at which turbulent and laminar flow are observed.

3. Results

In section 3.1 the numerical implementation is validated against the linear stability results in Klinkenberg *et al.* (2011*b*), obtained under the continuum assumption. Second, transition initiated by streamwise-independent counter-rotating streamwise vortices and a weak three-dimensional disturbance is analyzed in section 3.2. We aim to identify the threshold energy of the initial

condition: a lower amplitude will results in laminar flow, while a larger amplitude in a turbulent flow. Finally, results for the oblique scenario are presented in section 3.3.

3.1. *Linear Evolution*

We consider as initial condition a Poiseuille flow with one low-amplitude disturbance of spanwise wavenumber $\beta = 2$ and streamwise wavenumber $\alpha = 0$. This consists of the optimal initial condition yielding the largest energy growth from linear stability theory (this is also the maximum possible amplification over disturbances of different wavenumber). Particles are assumed to have the same initial velocity as the undisturbed base flow and to be uniformly distributed. For low initial amplitude, the disturbance energy goes to zero after a significant transient growth. The linear stability analysis in Klinkenberg *et al.* (2011*b*) shows that particles only affect the time needed to get to the maximum growth, the growth itself is hardly affected. Figure 1(a) shows the results for $SR = 5$ and different values of the mass fraction f. These results shows that we correctly reproduce the linear results in Klinkenberg *et al.* (2011*b*) by direct numerical simulation. The time at which the energy maximum is observed is delayed in time with a factor of $(1 + f)$. This is shown more clearly in Figure 1 (b), where we divided the time by $(1 + f)$.

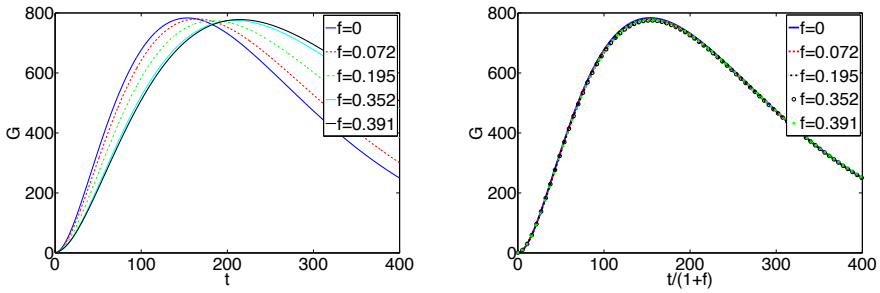

(a) (b)

Figure 1: Transient growth of the perturbation energy with $SR = 5$ and $R = 2000$ versus time. (a) Energy growth for several values of f.(b) Same data with time divided by $(1 + f)$

3.2. *Streak Scenario*

The same perturbation considered above (streamwise-independent vortices) is used here with an additional streamwise-dependent disturbance ($\alpha = 1, \beta = 1$). This is necessary in a monophase fluid to trigger transition and introduce

a three-dimensional velocity field. This oblique mode has an initial energy equal to 1/9 of that pertaining to the $(\alpha = 0, \beta = 2)$-mode. The energy threshold for transition is shown in Figure 2 where we report data for four different numerical resolutions. The thresholds from the different simulations approximately match, just the lowest one $48 \times 65 \times 48$ gives a slightly different result. Therefore results obtained with the mesh-size of $64 \times 65 \times 64$ will be used in the figures presented next. We notice that the energy threshold is not significantly affected by the presence of particles. At small mass fractions the threshold energy is smaller than in a clean fluid flow, whereas larger mass fractions result in a slight increased of the threshold energy.

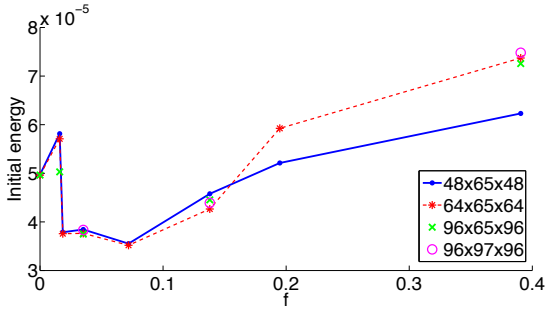

Figure 2: The critical threshold energy as a function of mass fraction particles f, $SR = 5$ and $R = 2000$. Four different resolutions are used to test convergence.

Although the threshold energy is not significantly affected, Figure 3 shows that the time at which transition occurs is altered by the presence of heavy particles. Figure 3 shows the evolution of the integrated wall-normal v- (a) and streamwise u- (b) velocity perturbations for flows with different particle mass fractions. In all cases we kept constant the initial disturbance energy at $6.25 \cdot 10^{-5}$.

Transition follows a similar path in all cases displayed, although the time at which transition is observed (sharp increase of the wall-normal velocity perturbation) is increasing by a factor of 3 or more in the presence of particles; the flow relaminarizes for a mass fraction $f = 0.39$. The particles affect the instability such that at this amplitude the flow does not become turbulent. It is also clear from the figure that the transient growth of the streaks is not affected by the presence of particles, as predicted by linear theory (see Figure 3(b)).

The initial increase of the wall-normal velocity disturbance in Figure 3(a) accounts for the initial weak transient growth of the oblique modes since the in-plane disturbance associated to the $(\alpha = 0, \beta = 2)$ streaky mode is monotonically decreasing. The data clearly indicate that the amplitude of the oblique mode decreases for increasing mass fraction f. This indicates that particles influence the oblique mode such that transition is delayed. To confirm this, we

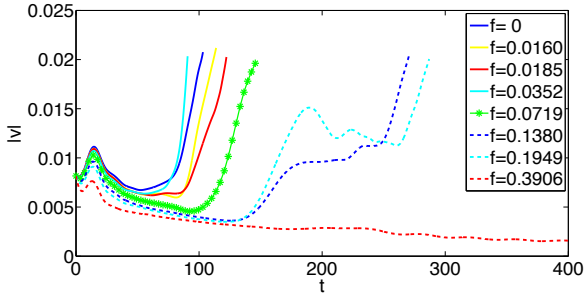

(a)

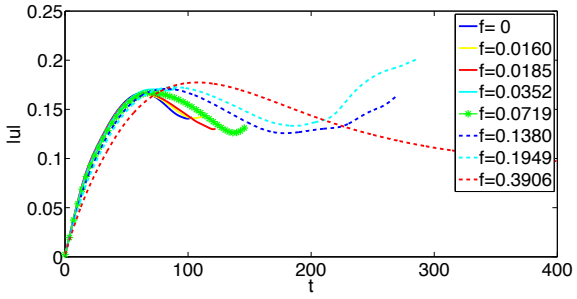

(b)

Figure 3: The v-velocity (a) and u-velocity (b) as a function of time for several mass fractions at $SR = 5$ and $R = 2000$ with an initial perturbation energy of $6.25 \cdot 10^{-5}$.

examine the linear behavior of the oblique mode ($\alpha = 1, \beta = 1$). The linear optimal growth is given in Figure 4 where the largest possible transient energy growth, maximized over the final time at which the disturbance is measured, is displayed versus the particle mass fraction. It is seen that a larger mass fraction decreases the optimal growth significantly. Considering the singular values of the system as representative of the behavior of the system for the evolution of the oblique mode, we can therefore conclude that particles stabilize the oblique mode and this induces a delay of the time at which transition is observed. This is associated to a less effective start of the streak disruption.

In the light of the above discussion, we can now interpret the energy threshold reported in Figure 2. The initial decay of the energy reported for low values of the concentration can be attributed to the forcing from the particles to the fluid. Particles act at isolated locations and therefore induce streamwise modulations of the streaks. This forcing contribute and interact with the oblique mode to induce the streak breakdown. At larger values of f we observe a weak stabilizing effect. On one hand, the amplitude of the oblique mode introduced

initially decreases faster, on the other hand more particles are acting in the flow and their action on the fluid can be assumed to be more homogeneous.

For the scenario considered here, streaks need to reach a sufficient high amplitude so that secondary instabilities can initiate; this may explain the weak dependence of the threshold curves on the mass fraction. The time for transition, however, does depend on the amplitude of the streamwise dependent forcing induced by particles and oblique mode since this determines the initial amplitude of the growing secondary instability mode. Note finally that the threshold curves for transition have usually a fractal or complicated behavior; they are very sensitive to the specific initial condition.

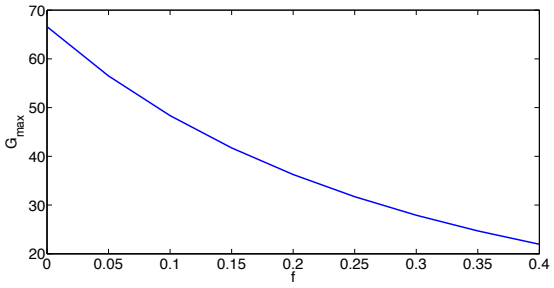

Figure 4: The optimal growth of the oblique mode ($\alpha = 1, \beta = 1$) as a function of mass fraction f using $R = 2000$ and $SR = 5$. The optimal energy gain is maximized over all possible final times

3.3. *Oblique Scenario*

The oblique scenario is initiated by a pair of symmetric oblique waves, ($\alpha = 1, \beta = \pm 1$). These waves interact non-linearly and intiate streaks in the flow with ($\alpha = 0, \beta = 2$) as in the scenario above (Reddy *et al.* 1998). The two oblique waves are both given the same initial energy and again particles are initialized uniformly distributed and with zero disturbance velocity (note that tests where particles have initially the local fluid velocity gave no significant differences in the results).

The threshold energy for transition is displayed in Figure 5 versus the particle mass fraction, where we also compare results obtained with three different resolutions.

As in the previous scenario, the energy initially decreases at low mass fraction and then increases with f, in this case by a factor approximatively 4 for the largest mass fractions considered. As before, we attribute the initial decrease of the energy required to transition to the modulation introduced in the system by the few particles present. Indeed, large scale forcing may be

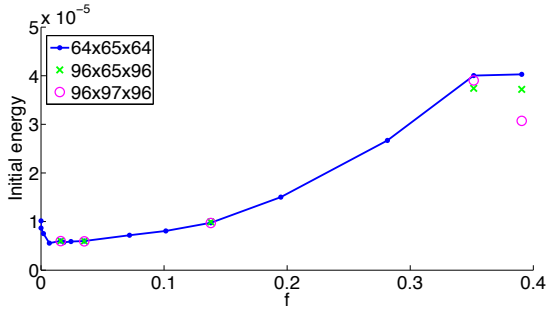

Figure 5: The critical threshold energy of two oblique waves ($\alpha = 1, \beta = \pm 1$)as a function of mass fraction particles f, with $SR = 5$ and $R = 2000$. Three different resolutions are used to test convergence.

more effective than small scale forcing due to lower viscous dissipation at this relatively low value of the Reynolds number. The largest increase observed at large f is related to the decreased amplitude of the oblique modes in the presence of particles, as also discussed above.

The time evolution of the perturbation velocities is reported in Figures 6 and 7, where the initial energy is kept constant at $8 \cdot 10^{-6}$ and $1.8 \cdot 10^{-5}$ respectively. Unlike transition initiated by a pair of counter-rotating streamwise vortices, there is no significant time-delay in the transition. If the particles maintain the energy below the threshold, the flow stays laminar. Figure 6 reveals that for $f \leq 0.36$, transition is induced in spite of the lower amplitude of the oblique modes compared to the single phase flow. This clearly points to the importance of the additional forcing induced by the inertial particles.

In the figures, one can also appreciate the steps involved in the oblique transition: first the amplification of the oblique modes, v perturbation at $t \approx 10$ in Figure 7(a), and later, u perturbation at $t \approx 30$ in Figure 7(b), the emergence of streaky structures. For the case of laminar flow, $f = 0.39$ in Figure 7, the transient growth of the streaks is significantly delayed by the low amplitude of the interacting oblique modes.

4. Discussion and Conclusion

Direct Numerical Simulations of a particle-laden channel flow are performed, with particles assumed heavy, spherical and solid. The interaction between the particles and the fluid is therefore modeled by the Stokes drag as the only interaction term. The fluid flow is computed on a Eulerian mesh with Lagrangian tracking of particles. The interpolation of the fluid velocity at the particle position and of the Stokes drag back to the Eulerian mesh uses a tri-linear scheme. The results are shown to be independent of the numerical resolution.

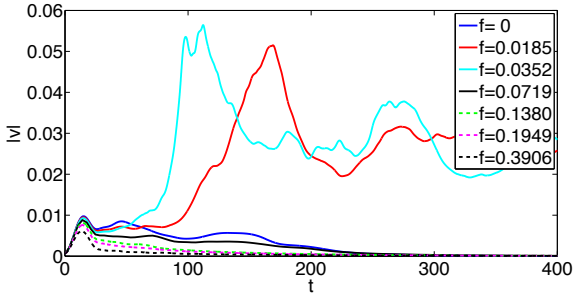

(a)

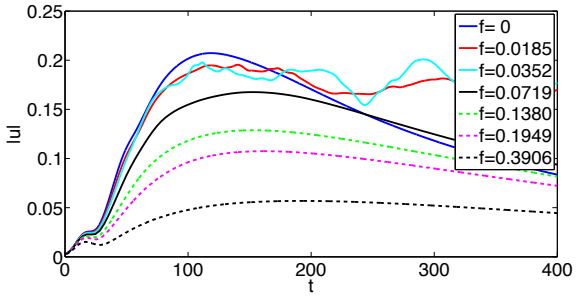

(b)

Figure 6: The v-velocity (a) and u-velocity (b) as a function of time for several mass fractions at $SR = 5$ and $R = 2000$ with an initial perturbation energy of $8 \cdot 10^{-6}$.

We study sub-critical transition in plane channel flow and quantify the effect of particles on the initial energy needed to reach the turbulent regime. Previous studies (Klinkenberg *et al.* 2011*b*) indicate that the linear non-modal lift-up mechanism, responsible for the amplification of streamwise-independent streaks induced by counter-rotating streamwise vortices, is the dominant instability mechanism at sub-critical conditions as for single phase channel flow. This is hardly affected by the presence of particles, unlike modal stability; this was explained by the disparity between the particle relaxation time and the time scales typical of transient growth, at least for values of particle size and density consistent with our model. The aim of the present paper is therefore to assess whether particles influence the nonlinear stages of transition and whether this may have a relation to drag reduction observed in turbulent particle-laden shear flows. It is relevant to recall here that secondary instabilities compete against viscous diffusion of the streak (Schoppa & Hussain 2002), so that streaks need to have sufficiently high amplitudes but also streamwise-dependent modes need time to reach amplitudes at which turbulent breakdown can occur. The time

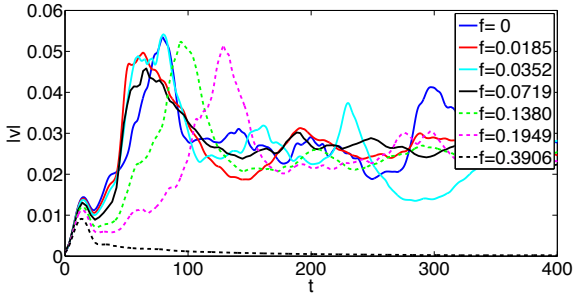

(a)

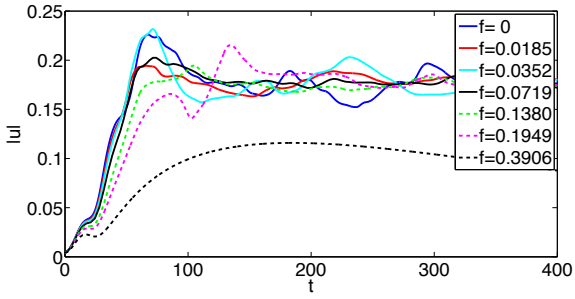

(b)

Figure 7: The v-velocity (a) and u-velocity (b) as a function of time for several mass fractions at $SR = 5$ and $R = 2000$ with an initial perturbation energy of $1.8 \cdot 10^{-5}$.

needed to reach high-enough amplitudes is related to their initial amplitude as well as to the streak amplitude, driving the instability.

We consider two classic transition scenarios: the streak scenario, induced by streamwise vortices and a relatively weak streamwise dependent mode, and oblique transition, induced by a pair of symmetric oblique waves. In the latter, the non-modal growth of streaks is induced by the nonlinear interaction of the two streamwise-dependent modes. This oblique scenario is known to be more effective and require lower initial disturbance energy (Reddy *et al.* 1998; Duguet *et al.* 2010). To appreciate the differences between the two scenarios, the energy threshold for transition is reported in Figure 8, normalized with the value for the corresponding single phase fluid. In both cases, we see a decrease of the energy threshold at very low particle concentrations. This is explained by the fact that in this case streaks and oblique modes are weakly affected by the particles, while these induce additional forcing in the flow that is able to trigger streak secondary instabilities faster. For larger particle mass fraction, we observe an increase of the energy threshold, most pronounced for the oblique

scenario. This is attributed to the stabilizing effect particles have on the oblique modes, an effect quantified by the non-modal analysis of the evolution of these modes reported in Figure 4. This stabilization is more effective in case of oblique transition since it acts directly to hinder the generation of streamwise vortices by nonlinear interactions of these oblique modes. The streak generation is delayed and weakened when the oblique modes decay faster.

In the case of the streak scenario, the streak evolution is basically unaffected by the presence of the particles. Particles act to weaken the oblique mode and therefore delay the transition process. Results obtained for the same initial disturbance amplitude, above the critical threshold, reveal that transition occurs at later times: the secondary instability is initiated with lower amplitudes and requires more time to develop.

One can speculate that the results presented here can have implications for turbulent flows where drag reduction is observed for relatively large mass fraction. In Hamilton *et al.* (1995); Waleffe (1997), a regeneration cycle is proposed to underlie wall-bounded turbulent flows. This consists of three steps: i) generation of streaks induced by streamwise vortices, ii) streak breakdown via secondary instabilities, iii) regeneration of elongated vortices by nonlinear interactions between oblique modes originating at the streak breakdown. In this respect, the present investigation indicates that particles can affect this cycle in two ways. They may be particularly active in the last of these three processes, namely the regeneration of streamwise vortices by nonlinear interactions. Indeed, the first step of the oblique scenario is the most affected in the presence of heavy particles. However, particles also induce a significant time delay on the streak breakdown (stage ii). This time-delay can break the regeneration cycle. As shown in Klinkenberg *et al.* (2011*b*), the streak generation occurs on a time scale too long for particles to have an effect.

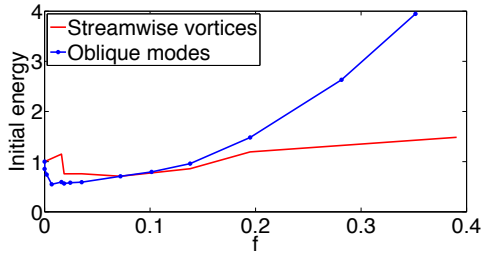

Figure 8: Comparison between the threshold energies for the streamwise vortices and the oblique waves, both normalised with their energy threshold of a clean fluid.

References

Balachandar, S. & Eaton, J. K. 2009 Turbulent Dispersed Multiphase Flow. *Ann. Rev. of Fluid Mech.* **42**, 111–133.

Berlin, S., Lundbladh, A. & Henningson, D. S. 1994 Spatial simulations of oblique transition. *Phys. Fluids* **6**, 1949–1951.

Cherubini, S., De Palma, P., Robinet, J.-C. & Bottaro, A. 2010 Rapid path to transition via nonlinear localized optimal perturbations in a boundary-layer flow. *Phys. Rev. E* **82**, 066302.

Chevalier, M., Schlatter, P., Lundbladh, A. & Henningson, D. S. 2007 A Pseudo-Spectral Solver for Incompressible Boundary Layer Flows. *Tech. Rep* TRITA-MEK 2007:07. Royal Institute of Technology (KTH), Dept. of Mechanics, Stockholm.

Cossu, C., Brandt, L., Bagheri, S. & Henningson, D. S. 2011 Secondary threshold amplitudes for sinuous streak breakdown. *Physics of Fluids* **23** (7), 074103.

Duguet, Y., Brandt, L. & Larsson, B. R. J. 2010 Towards minimal perturbations in transitional plane couette flow. *Phys. Rev. E* **82**, 026316.

Duguet, Y., Pringle, C. C. T. & Kerswell, R. R. 2008*a* Relative periodic orbits in transitional pipe flow. *Physics of Fluids* **20** (11), 114102.

Duguet, Y., Willis, A. P. & Kerswell, R. R. 2008*b* Transition in pipe flow: the saddle structure on the boundary of turbulence. *Journal of Fluid Mechanics* **613**, 255–274.

Eckhardt, B., Schneider, T. M., Hof, B. & Westerweel, J. 2007 Turbulence transition in pipe flow. *Annual Review of Fluid Mechanics* **39**, 447–468.

Hamilton, J. M., Kim, J. & Waleffe, F. 1995 Regeneration mechanisms of near-wall turbulence structures. *J. Fluid Mech.* **287**, 317–348.

Kawahara, G. 2005 Laminarization of minimal plane couette flow: Going beyond the basin of attraction of turbulence. *Physics of Fluids* **17** (4), 041702.

Klinkenberg, J., de Lange, H. C. & Brandt, L. 2011*a* Modal and non-modal stability analysis of a channel flow seeded with light particles. *European Journal of Mechanics B/ Fluids* **submitted**.

Klinkenberg, J., de Lange, H. C. & Brandt, L. 2011*b* Modal and non-modal stability of particle laden channel flow. *Phys. Fluids* **23**, 064110.

Maxey, M. R. & Riley, J. J. 1983 Equation of motion for a small rigid sphere in a nonuniform flow. *Phys. Fluids* **26**, 883–889.

Monokrousos, A., Bottaro, A., Brandt, L., Di Vita, A. & Henningson, D. S. 2011 Nonequilibrium thermodynamics and the optimal path to turbulence in shear flows. *Phys. Rev. Lett.* **106**, 134502.

Nagata, M. 1990 Three-dimensional finite-amplitude solutions in plane couette flow: bifurcation from infinity. *Journal of Fluid Mechanics* **217**, 519–527.

Reddy, S. C. & Henningson, D. S. 1993 Energy growth in viscous channel flows. *J. Fluid Mech.* **252**, 209–238.

Reddy, S. C., Schmid, P. J., Baggett, J. S. & Henningson, D. S. 1998 On stability of streamwise streaks and transition thresholds in plane channel flows. **365**, 269–303.

Saffman, P. G. 1962 On the stability of laminar flow of a dusty gas. *J. Fluid Mech.* **13**, 120–128.

Schmid, P. J. & Henningson, D. S. 1992 A new mechanism for rapid transition involving a pair of oblique waves. *Physics of Fluids* **4**, 1986–1989.

Schmid, P. J. & Henningson, D. S. 2001 *Stability and transition in shear flows*. Springer.

Schneider, T. M., Eckhardt, B. & Yorke, J. A. 2007 Turbulence transition and the edge of chaos in pipe flow. *Phys. Rev. Lett.* **99**, 034502.

Schoppa, W. & Hussain, F. 2002 Coherent structure generation in near-wall turbulence. *Journal of Fluid Mechanics* **453**, 57–108.

Stone, P. A., Waleffe, F. & Graham, M. D. 2002 Toward a structural understanding of turbulent drag reduction: Nonlinear coherent states in viscoelastic shear flows. *Phys. Rev. Lett.* **89**, 208301.

Toh, S. & Itano, T. 2003 A periodic-like solution in channel flow. *Journal of Fluid Mechanics* **481**, 67–76.

Toschi, F. & Bodenschatz, E. 2009 Lagrangian properties of particles in turbulence. *Ann. Rev. of Fluid Mech.* **41**, 375–404.

Trefethen, L. N., Trefethen, A. E., Reddy, S. C. & Driscoll, T. A. 1993 Hydrodynamic stability without eigenvalues. *Science* **261**, 578–584.

Waleffe, F. 1997 On a self-sustaining process in shear flows. *Phys. Fluids* **9**, 883–900.

Waleffe, F. 1998 Three-dimensional coherent states in plane shear flows. *Phys. Rev. Lett.* **81**, 4140–4143.

Waleffe, F. 2001 Exact coherent structures in channel flow. *Journal of Fluid Mechanics* **435**, 93–102.

Wang, J., Gibson, J. & Waleffe, F. 2007 Lower branch coherent states in shear flows: Transition and control. *Phys. Rev. Lett.* **98**, 204501.

Zhao, L. H., Andersson, H. I. & Gillissen, J. J. J. 2010 turbulence modulation and drag reduction by spherical particles. *Phys. Fluids* **22**, 081702.